

KINETIC AND THERMODYNAMIC FACTORS GOVERN
DNA CONDENSATE SIZE AND MORPHOLOGY

A Dissertation
Presented to
The Academic Faculty

By

Christine C. Conwell

In Partial Fulfillment
Of the Requirements for the Degree
Doctor of Philosophy in Chemistry

Georgia Institute of Technology

March 2004

KINETIC AND THERMODYNAMIC FACTORS GOVERN DNA
CONDENSATE SIZE AND MORPHOLOGY

Approved by:

Dr. Nicholas V. Hud, Advisor

Dr. James C. Powers

Dr. L. Andrew Lyon

Dr. Loren D. Williams

Dr. Mark R. Prausnitz

Date Approved 3/26/04

DEDICATION

I would like to dedicate this thesis to my parents Richard and Justine Conwell. Thank you for believing in me and constantly supporting me in all that I have done. Dad—thanks for always reminding me that *What doesn't kill you makes you stronger!* They are words I have learned to live by each day and have passed on to others. I would also like to dedicate it to my sisters, Reene and Colleen for encouraging me even though our experiences in life have taken us down different paths.

ACKNOWLEDGEMENTS

I would like to thank Dr. Nicholas Hud for taking a chance by accepting me as his first student. I have learned so much from you, not only about science but also about being creative, patient and persistent. Thank you for taking the time to teach me (the molecular biologist) to think like a real biophysical chemist!

I would like to thank the many friends and colleagues that I have had the pleasure of knowing during my time at Georgia Tech. To Tumpa Sarkar, Ozgul Persil, Heather Bean and Cathy Santai, thank you for your companionship and making sure there was never a dull moment in the lab! I would also like to thank Igor Vilfan, Swapan Jain, Matjaz Polak, Mary Daula and Lili Harvey for their constant support and for always being here to remind me that I love what I am doing!!

I would like to thank Yolande Berta for all of her help teaching me how to use and troubleshoot the TEM. Thank you for being so patient every time I had to knock on your door to tell you that the camera broke.....again.

And last but certainly not least, I would like to thank David for being here for me through the last 5 years. Thank you for constantly supporting me and encouraging me. Thank you for all the many times you have been there to pick up the pieces!!

TABLE OF CONTENTS

Dedication	ii
Acknowledgements	iii
Table of Figures	vi
Table of Schemes	viii
List of Abbreviations	ix
Summary	x
Chapter 1 Introduction	1
Chapter 2 A Quantitative Study of Static Curvature and Ionic Strength Effects on DNA Toroid Dimensions	25
2.1 Experimental Procedures	26
2.2 Results and Discussion	28
2.3 Concluding Remarks	46
Chapter 3 MgCl₂ Enhances Cluster Formation by Nanoscale Toroidal DNA Condensates	50
3.1 Experimental Procedures	51
3.2 Results and Discussion	52
Chapter 4 Evidence That Both Kinetic and Thermodynamic Factors Govern DNA Toroid Dimensions	60
4.1 Experimental Procedures	62
4.2 Results	64
4.3 Discussion	73
4.4 Concluding Remarks	82

Chapter 5	Characterization of ssDNA condensation	87
5.1	Experimental Procedures	88
5.2	Results	94
5.3	Discussion	107
5.4	Concluding Remarks	113
Chapter 6	High Mobility Group (HMG) Proteins Alter the Path of DNA Condensation	118
6.1	Experimental Procedures	120
6.2	Results	123
6.3	Discussion	135
Chapter 7	Brief Discussion of Temperature, Topology and Mixed DNA Populations on DNA Condensation	146
7.1	Variations in Temperature Affect DNA Toroid Size	147
7.2	DNA Topology Influences Condensate Size and Morphology	154
7.3	Condensation of Mixtures of DNA With and Without Static Curvature	158
7.4	Condensation of Fragmented Plasmid DNA	162
Chapter 8	Implications of DNA Condensation on the Development of Gene Delivery Systems	167
	Vita	170

LIST OF FIGURES

Figure 2.1	Transmission electron micrographs (TEM) of toroids produced by the condensation of DNA with hexamine cobalt (III) under a variety of conditions.	31
Figure 2.2	A plot of toroid diameter versus toroid thickness for all DNA toroids measured.	34
Figure 2.3	Histograms of toroid diameters and toroid thickness measurements for DNA condensates under various solution conditions.	36
Figure 2.4	Histograms of toroid hole diameters for <i>3kbDNA</i> condensed in three different salt solutions.	39
Figure 2.5	Plots of energy potential as a function of toroid cross-sectional area for <i>3kbDNA</i> condensed in various salt solutions.	45
Figure 3.1	Transmission Electron Microscope (TEM) images of linear <i>3kb DNA</i> condensed with hexamine cobalt (III) in the presence of $MgCl_2$.	53
Figure 3.2	Histograms of toroid outer diameter for toroids formed in presence of three different salt conditions.	56
Figure 3.3	Histograms of toroid outer diameter for toroids formed in presence of three different salt conditions.	57
Figure 4.1	Transmission electron microscopy (TEM) images of DNA condensates formed at $22^{\circ}C$ by the addition of hexamine cobalt chloride.	66
Figure 4.2	TEM images of DNA condensed at $22^{\circ}C$ by the addition of $200 \mu M$ hexamine cobalt chloride, followed by dilution with either dH_2O or a $MgCl_2$ solution.	68
Figure 4.3	TEM images of DNA condensates formed at $37^{\circ}C$ by the addition of hexamine cobalt chloride.	70
Figure 4.4	TEM images of condensates produced at $37^{\circ}C$ by the addition of $200 \mu M$ hexamine cobalt chloride to DNA, followed by dilution with either $MgCl_2$ or dH_2O .	72

Figure 4.5	Models for the condensation of DNA by hexammine cobalt(III) under various conditions.	74
Figure 5.1	Verification of ssDNA isolation by gel electrophoresis and atomic force microscopy.	97
Figure 5.2	Transmission electron microscopy (TEM) images of ssDNA condensates produced with various condensing agents.	99
Figure 5.3	TEM images of dsDNA condensates produced with various condensing agents.	100
Figure 5.4	TEM images of ssDNA condensate with pLL ₅₀ under several solution conditions.	102
Figure 5.5	TEM images of ssDNA condensed with various concentrations of poly-L-lysine.	105
Figure 5.6	Histogram of particle diameters from ssDNA condensed with poly-L-lysine.	107
Figure 6.1	Transmission electron microscopy (TEM) images of supercoiled and linear pBluescript SK II- (<i>3kbDNA</i>) DNA condensates.	126
Figure 6.2	Histogram of DNA condensate morphologies (rod vs. toroid) for various DNA samples and condensation conditions.	128
Figure 6.3	TEM images of DNA condensates formed by the condensation of linear plasmid DNA containing varying amounts of static curvature (<i>Atract15</i> and <i>Atract30</i>).	129
Figure 6.4	TEM images of <i>3kbDNA</i> condensed with hexammine cobalt chloride in the presence of varying concentrations of nuclear extract.	133
Figure 6.5	TEM image of <i>Atract30</i> condensed with hexammine cobalt chloride in the presence of increased concentrations of nuclear extract.	134
Figure 6.6	TEM images of linear <i>3kbDNA</i> condensed with hexammine cobalt chloride with increasing concentrations of sample buffer.	135
Figure 6.7	Schematic diagrams of DNA condensation in the presence and absence of nuclear extract.	138
Figure 7.1	TEM images of <i>3kbDNA</i> condensed at 4, 22, and 38°C	150

Figure 7.2	Scatter plot of toroid diameter and thickness for DNA condensed at 4, 22, 38°C	151
Figure 7.3	TEM images of linear, relaxed circular, and supercoiled <i>3kbDNA</i> condensed with hexamine cobalt chloride	157
Figure 7.4	TEM images of <i>Atract30: 3kbDNA</i> mixtures condensed with hexamine cobalt chloride	161

LIST OF SCHEMES

Scheme 1.1	Definition of toroid diameter and thickness.	32
Scheme 1.2	Toroid nucleation and growth with equal inward and outward growth from the nucleation loop.	37
Scheme 1.3	Toroid nucleation and growth with preferential growth outward from the nucleation loop during the latter stages of toroid growth.	41
Scheme 1.4	Toroid nucleation and growth with annealing to larger nucleation loop sizes during the early stages of formation, and preferential outward growth during the latter stages of toroid formation.	42
Scheme 6.1	Schematic representation of the topologies of plasmid DNA used for condensation experiments.	124

TABLE OF ABBREVIATIONS

TEM	Transmission Electron Microscopy
AFM	Atomic Force Microscopy

SUMMARY

It is well known that multivalent cations can cause DNA to condense from solution to form high-density nanometer scale particles. However, several fundamental questions concerning the phenomenon of DNA condensation remain unanswered. DNA condensation *in vitro* has been of interest for many years as a model of naturally occurring DNA packaging (e.g. chromatin, sperm head and virus capsid packing). More recently, DNA condensation has been of interest in optimizing artificial gene delivery, where packaging genes to an optimal size is essential to developing efficient uptake and delivery systems. The research presented in this dissertation provides an in depth biophysical study of the factors that control DNA condensate size and morphology. Millimolar changes in the ionic strength of the solution were found to alter the size of toroidal condensates. Variations in the order of addition of the counterions also significantly changed the size and morphology of the condensates. Studies were also performed to investigate the effects of static curvature and increased DNA flexibility on DNA condensation. These include the addition of static bending by sequence directed curvature, dynamic bending through protein-DNA interactions and reducing DNA persistence length by condensing single-stranded DNA. Several new models of DNA condensation are proposed based on the experimental data presented in this thesis.

CHAPTER 1

OVERVIEW OF DNA CONDENSATION

DNA condensation is the process in which an extended DNA molecule is compacted into a discrete particle. Condensation of DNA is distinguished from aggregation as condensates are of finite size with ordered DNA packing (1). A complete explanation of DNA condensation would have broad implications from biology to polymer physics.

Understanding mechanism for the compaction of genomic DNA *in vivo* was the focus of most early studies of DNA condensation (2-5). In replicating cells, transcription requires chromatin to be unraveled and repacked efficiently as a part of the cell cycle (6). DNA condensation approaches the limits of molecular compaction in non-replicating cells where transcription is inactive (7). In particular, the packaging of DNA into viruses and sperm has attracted much attention, as genomic DNA is compacted on the order of 10^4 - 10^6 fold for encapsulation into the volume of the virus capsid or sperm head (1, 8, 9). More recently, the significance of understanding the factors that contribute to DNA condensation has been recognized in studies of gene delivery. Studies have indicated that the size of the gene delivery vector is directly correlated to the efficiency of uptake into the cells (i.e., larger vectors have decreased transfection) (10-12); thus, compacting the gene(s) of interest into discrete particles is essential to the optimization of gene delivery systems.

1.1 Experimental Studies of DNA Condensation *in vivo*

Early studies of DNA condensation *in vivo* sought to determine the morphology of DNA compacted in virus capsids and sperm heads (2-5, 13, 14). Lysis of T2 and T7 bacteriophage capsids revealed that DNA was compacted into toroidal structures (5, 15). Richards et al. observed that the condensed DNA was not kinked, but was wound with uniform curvature (5). Based on the observation of toroidal structures, the “ball of string” and “concentric spool” models for DNA packaging *in vivo* were proposed. In the “ball of string” model, DNA is wound around a circular path at any radius and with no particular order. The concentric spool model, on the other hand, DNA is proposed to wind in concentric circles along a single axis. X-ray diffraction studies of bacteriophage DNA supported the close-pack ordered structure proposed in the concentric spool model (2). The model for coaxial spooling of DNA has since been modified several times, most recently by Cerritelli et al., whose cryo-EM images distinctly show multiple concentric rings of compacted DNA within a bacteriophage capsid (2-4, 13).

1.2 Experimental Studies of DNA Condensation *in vitro*: Condensing Agent and Ionic Strength Effects

Model systems have been developed *in vitro* to understand the factors that contribute to the condensation of DNA in biological systems. Nearly three decades ago it was discovered that multivalent cations (3^+ or greater) condense DNA *in vitro* into toroidal structures similar in size to those ejected from bacteriophage capsids (5, 15-17). Toroidal condensates were produced in the presence of polyamines (spermidine $^{3+}$ and spermine $^{4+}$), the inorganic cation (hexammine cobalt $^{3+}$) and cationic peptides (polylysine and

protamine) (9, 14, 17-22). Divalent cations, however, do not produce condensates from an aqueous solution (19, 23).

Wilson and Bloomfield condensed DNA with various concentrations of condensing agent in the presence of mono- and divalent cations (23). As concentrations of condensing agent were increased, they monitored the collapse of DNA in solution by light scattering experiments. The charge neutralization of the anionic DNA polymers was estimated based on Manning's counterion condensation theory. Briefly, Manning modeled DNA as a stiff anionic polymer and predicted that the quantity of phosphate charge neutralized by solutions of mono-, di- and trivalent cations would be 76%, 88% and 92%, respectively (24). Based on experimental observations and calculations of the total charge neutralized, Wilson estimated that a *minimum* of 89-90% of the phosphate charged must be neutralized in order to initiate the collapse of DNA into a compact structure. Once condensation is initiated, other contributions such as ion bridging may further reduce the charge of the DNA molecules in a condensed state (23).

Most studies of DNA condensation have employed condensing agents with a 3⁺ or greater charge per molecule to neutralize DNA phosphate charge, as it was predicted that optimal charge neutralization required for collapse could not be accomplished by mono- or divalent cations (9, 17-19, 23). However, there are a few exceptions to this assumption. According to Manning's counterion condensation theory, the charge density of the DNA polymer in solution is a function of the dielectric constant, which allows for a specific cationic contribution to DNA charge neutralization to increase or decrease with the nature of the solution. By decreasing the dielectric constant of the solution, more cations can associate with DNA in solution. Experimentally this was demonstrated in a

mixture of 50% methanol, where the divalent cation, Mg^{2+} , was shown to initiate condensation of DNA in solution (20, 23). Arscott et al. further investigated the effects of alcohols on condensation and verified that a lower dielectric constant of the solution increased association of the cations with the DNA (i.e., concentrations of condensing agent necessary to commence condensation was decreased) (25). Furthermore, the divalent cation, Mn^{2+} , was shown to condense supercoiled DNA. Mn^{2+} has been shown to have affinity for binding DNA bases over the phosphates, which can lead to some distortion of the helical structure of DNA (26). Association of Mn^{2+} can promote destabilization of the helix, leading to collapse of DNA molecules, particularly those with a large amount of superhelical stress (27).

Under most circumstances mono- and divalent cations cannot initiate condensation; however, their presence in solution directly affects the condensation reactions. Increasing the concentration of counterions in solution from millimolar to molar quantities has been shown to reduce the condensation of DNA. It has been proposed that competition between the condensing agent and the high concentration of counterions decreases the amount of condensing agent associated at the surface of the DNA, thereby reducing the overall charge neutralization of the anionic polymer (18, 23). Competition between the cations occurs for DNA binding, and as the concentrations of counterions increases in solution, the amount of condensation is reduced (18, 23, 28-30). These studies demonstrated that the concentrations of condensing agent must be increased to maintain conditions favorable for the condensation of DNA. It was proposed based on this data that the concentration of condensing agent must be optimized according to the concentration of counterions in solution for efficient condensation of

DNA. Large increases in mono- and divalent cations have been shown to hinder and reverse condensation by competing with the condensing agent for association with DNA. These effects must also be investigated at low ionic strength (i.e., millimolar changes in cation concentration) to determine the influence of competition on DNA condensate formation (26, 31-34).

1.3 Experimental Studies of DNA Condensation: DNA Length and Secondary Structural Effects

Toroidal condensates formed by polyamines and hexamine cobalt chloride have been reported to be similar in size (17, 18). Furthermore, toroidal condensates produced by DNA ranging in length from 400 bp to approximately 50,000 bp resulted in particles of roughly the same dimensions (18). A review by Bloomfield provided data from several more recent studies of DNA of various lengths and found that most of the toroidal structures averaged a diameter of approximately 100 nm (1). This implies that the size of the toroid is determined by the quantity of DNA packaged as opposed to the length of the DNA that is incorporated into the structure (i.e., a toroid may contain several short DNA or a few long DNA molecules).

The topology of plasmid DNA (i.e., supercoiled, linear or relaxed circle) has been shown to affect the morphology of DNA condensates (27, 35, 36). Böttcher et al. condensed all three forms of plasmid DNA with spermine, and then compared the resulting condensates (35). They observed the toroidal condensates for all topologies of the DNA, but the supercoiled and linear DNA displayed an increased propensity for aggregation. The variation in the condensate structure and aggregation was attributed to

the “intermediate flexibility” of the relaxed DNA as compared to the highly constrained supercoiled and very flexible linear DNA (35).

Further studies of supercoiled DNA suggest that the topological constraints caused by the winding of the DNA influence the ability of the DNA to condense into compact structures. Condensation of supercoiled DNA causes an increase in the torsional free energy of the molecule (37). It has been predicted that the radius of the toroid formed by the supercoiled DNA will therefore be less than that of linear or relaxed circular DNA, which was experimentally supported by the results of Arscott et al. (36). The ability of the supercoiled DNA to bend to a smaller radius than linear DNA implies that the topology of the DNA allows for bending to occur with reduced energetic barriers. An increased propensity for bending over smaller lengths of DNA may also explain the increased formation of rods in a preparation of supercoiled DNA condensates.

DNA secondary/tertiary structure may also be altered by the introduction of sequence directed curvature. Regions of static bending can be induced into DNA through the insertion of specific sequences that are known to cause helical distortions leading to DNA bending, specifically A-tract sequences. An A-tract sequence is defined as a series of 4-8 consecutive adenines, which induce a bend of 12-21° into the helix of DNA (38, 39). Shen et al. inserted a series of 60 phased A-tract repeats into standard plasmid DNA (40). The bend introduced into the DNA topology was expected to produce a minimum of 720° of curvature, or 2 static loops into the DNA structure. Preliminary studies indicated that the toroids produce by DNA containing the A-tract sequences were in fact smaller in diameter than those formed by the same plasmid lacking the insert (40). More detailed

studies of A-tract effects are necessary to determine the extent in which this sequence directed curvature influences toroid formation.

Another means of altering the secondary structural elements of DNA is through protein-DNA interactions. Histone proteins have been recognized for their ability compact DNA into a beads-on-a-string structure. This involves inducing a bending of the helical axis by 47° for each turn of the duplex, which is much greater than is predicted to occur for DNA free in solution based on calculations of persistence length (41, 42). Other proteins have also been found to induce bends into the secondary structure of DNA, including HU, integration host factor (IHF), and high mobility group proteins (HMG). The function of these proteins is to induce a high degree of bending in the DNA to aid in a cellular function, such as transcription, recombination, and chromatin packing (41, 43-46). By introducing a defect in the secondary structure of DNA (i.e., helix), these proteins tag the DNA for recognition by other cellular proteins, which initiate the aforementioned processes.

High mobility group proteins have recently peaked interested due to their innate ability to bend DNA *in vivo* (41, 43-53). Proteins in this family are believed to induce a bend of $60-120^\circ$ into the DNA helix (48, 49, 54). It was predicted that the introduction of this degree of bending would promote DNA curvature under otherwise unfavorable conditions. To examine this hypothesis, ligation circularization studies were performed, which demonstrated the significance of the HMG-induced dynamic bending. Oligonucleotides exposed to the nuclear extract and HMG proteins tended to circularize at much shorter lengths than those not exposed to the protein, as a result of the bending introduced by the protein binding (43, 44). While the exact function of HMG proteins has

yet to be determined, they have been shown to play a role in transcription activation, recombination, replication, chromatin packing and nucleosome assembly (41). It has been proposed that the function of the HMG proteins is as a DNA chaperone, where their function is solely to bend DNA (41). Additionally, most of the many of the proteins in this family bind any DNA sequence or topology (44). The ability of high mobility proteins to induce a high degree of dynamic bending and assist in chromatin packing *in vivo* provides great promise for the application of these proteins for *in vitro* condensation. Further experimentation is necessary to determine the exact contribution of HMG proteins to DNA condensation.

1.4 Models of Toroid Formation Based on Experimental Studies

Toroid formation is a nucleation and growth process (55, 56). Several studies have indicated that the formation of a stable toroid begins with the nucleation of a proto-toroid structure (1, 55). There are two possible mechanisms for initiation of nucleation loop formation: the nucleation of an intramolecular proto-toroid or the intermolecular nucleation of the structure by dimer formation. In order for either of these structures to successfully nucleate toroid formation, there must be a minimal attractive potential between the packed strands, which must be greater than competing energetic terms that favor DNA remaining as an extended polymer in solution. While it is not clear precisely which mechanism initiates toroid formation, it is understood that toroid nucleation and further growth requires a minimum number of contacts between neighboring DNA strands (1). If enough successful contacts formed, either via several interstrand or few intrastrand interactions, the toroid will nucleate and grow. The formation of the contacts

is essentially independent of the length of the DNA, which is supported by the aforementioned studies of DNA length and toroid size (1, 18). Failure to stabilize the proto-toroid in this manner will lead to unsuccessful nucleation. DNA from unsuccessfully nucleated toroids is released back into solution and either attaches to another stable proto-toroid or eventually makes the minimal contacts necessary for successful nucleation. It is expected that the spontaneous formation of the nucleation loop is the rate-limiting step in this process, as both bending energy and persistence length constraints must be overcome (55). The persistence length of DNA is defined as the distance beyond which the helical axis vectors of two DNA segments are uncorrelated. For B-DNA, the persistence length has been calculated to be approximately 150 bp (42). Studies have suggested that toroid nucleation and growth are two distinct processes that are controlled by different energetic contributions to the condensation process. Several models have been proposed to describe these processes.

The spool model for DNA condensation was proposed in early studies of DNA packaging in bacteriophage capsids (2, 4, 5, 13). One major weakness of this model was that it required DNA to bend to very small radii, below the persistence length of DNA, in order to account for the small toroid inner diameters of approximately 15 nm (1). Bending of the DNA below the persistence length requires a substantial energetic contribution, and therefore would not be favorable.

The constant radius of curvature model was developed as an alternative mechanism for toroid formation, which considered that the DNA must not be bent below the radius of curvature allowed by the persistence length (55). In this model, a toroid loop of a constant radius initiates the formation of the toroid. Growth proceeds as similar loops

of DNA are deposited around the initial loop at gradually increasing radii from the nucleation site (55).

Both of these models have been overshadowed by a more recent model of toroid structure based on cryo-EM images of DNA toroids. From these images, distinct strands of DNA can be deciphered and the packing of DNA in the toroid is clearly visible (57). The distance between DNA strands on the surface of the toroid was measured and found to be in excellent agreement with the radial spacing of strands in a hexagonal lattice. While hexagonal packing was clearly present within the toroidal structures, there were regions that were found to contain nonhexagonal packing. These nonhexagonal packed regions were attributed to crossovers of DNA strands within the toroid. DNA packaging was modeled in patterns that resembled crystal growth with screw disorders, where crossovers in the packing may occur but the DNA only breaks the structure to the outside of the toroid, never wrapping through the center of the structure. The computer modeled toroids resulting from these varied paths of DNA packaging were closely examined for their surface features. As was observed in many of the toroids imaged by cryo-EM, the model toroids contained crossovers in the DNA packaging contained regions of local disorder (i.e., nonhexagonal packing) on the surfaces of the particles (57). Thus, this model provides a well-defined mechanism for DNA toroid packaging that simultaneously explains the regions of local disorder, the possibility for crossovers in DNA packaging and accounts for the observation that toroid diameter is smaller during early stages of toroid growth (55, 56).

1.5 Theoretical Studies of DNA Condensation

In the last decade, there has been a surge of theoretical investigations of DNA condensation. Most of these studies have focused on exploring either the thermodynamic or the kinetic factors that are thought to contribute to the process of DNA condensation (1, 37, 58-67). Far fewer experimental studies have proposed detailed physical explanations for the kinetic and thermodynamic factors that govern condensate size and morphology (36, 56, 68, 69). While much progress has been made in terms of deciphering the forces that control the process of DNA condensation, there is still much to learn regarding the individual energetic contributions on DNA condensation under various conditions.

DNA condensation results from of several thermodynamic contributions including: DNA bending, the entropy and enthalpy associated with the addition of condensing agent to solution, hydration of the polymer and electrostatic interactions. In general, these contributions can be described by the following equation (37):

$$\Delta G_{\text{tot}} = \Delta G_{\text{bend}} + \Delta G_{\text{mix}} + \Delta G_{\text{elec}} + \Delta G_{\text{fluct}} + \Delta G_{\text{hyd}}$$

These free energies can provide positive or negative contributions to the total free energy, and the sign of this contribution is largely dependent on the solution conditions of the reaction.

Bending Energy: The free energy associated with the bending of DNA is directly related to the length of the DNA and the radius of curvature. If the radius of curvature is larger than approximately 50 nm in diameter, the energy required to bend the DNA should be

minimal, as under these conditions DNA is not bent below the persistence length (42). Solution conditions may affect the persistence length of DNA. The flexibility of the DNA increases in the presence of monovalent concentrations of >10 mM or divalent concentrations > 0.1 mM (42, 70). Since the formation of DNA toroids is largely dependent on the spontaneous nucleation of a loop within the DNA, overcoming the energetic barrier associated with bending DNA is essential to initiating toroid growth. Under most circumstances, the bending of DNA requires energy from the system, leading to a positive ΔG_{bend} (1). It is possible to eliminate the positive ΔG_{bend} contribution by inherent bending in the DNA (i.e., sequence directed curvature) or by exposing the DNA to condensing agents that distort the helix and induce helical bending (e.g., high mobility group proteins) (37).

While toroids are the most frequent condensate morphology observed *in vitro*, rod structures are also observed. Bending of the DNA to form rods involves abrupt kinking in the DNA structure, whereas in toroids there is a continuous bending of the DNA. It has been proposed that the continuous bending of the toroidal DNA and the occasional kinking of DNA in rods have a free energy requirement for bending that is of the same order of magnitude (1). Thus, this estimation of bending energies implies that the observation of predominantly toroidal structures resulting from condensate reactions is largely regulated by the components of the solution or the kinetics of formation not promoting kinking or helical distortions that would favor rod morphologies, as opposed to large differences in bending energies.

The Free Energy of Mixing: As DNA is condensed, it undergoes a coil to globule transition. The compaction of the DNA into a tightly packed particle requires rearrangement of polymer and solvent interactions. Initially, when the condensing agent is added to the solution, water molecules and cations of lower valency (e.g. mono- and divalent cations) are displaced by the condensing agent, which has a higher affinity for the DNA surface. Furthermore, as the collapse of the DNA occurs, additional layers of solvent are expelled so that the DNA strands are able to pack into the hexagonal arrangement observed. The release of cations and solvent molecules provides a favorable entropic contribution to condensation.

Electrostatic Energy: The electrostatic contribution may be the most significant repulsive term contributing to DNA condensation. For DNA molecules to interact closely with each other, the anionic charge produced by the phosphate backbone must be shielded by positive counterions in the solution. Although monovalent ions contribute to charge shielding, divalent cations have been shown to allow DNA molecules to have definite interactions with each other (31-34). As was shown in experimental studies, the minimal amount of phosphate charge neutralization (89-90%) required to promote close interactions between strands to initiate condensation is most often accomplished through the addition of cations with a charge of +3 or greater (9, 17-20, 23, 25, 36, 55-57, 68, 69, 71-73).

In addition to the reduction of the repulsive charges between DNA molecules, ion correlation effects must also be considered. Theoretical studies of correlation fluctuations between paired counterions have led to the development of several theories regarding

the role of ion fluctuations in DNA condensation (1, 61, 63, 74). These theories take into account not only the charge screening at the surface of the charged polymer, but also considers the correlations of the counterions, unlike previous theories (24). Understanding the ion correlation interactions between the condensing agent, counterions and DNA in solution are essential to interpreting electrostatic contributions to DNA condensation.

Competition for cation binding to the DNA surface must also be considered, as the addition of condensing agent leads to the displacement of ions near the surface of the DNA. A theoretical formalism developed by Rouzina and Bloomfield allow for the calculation of the surface charge of the polymer based on a system containing two counterions (e.g., a monovalent cation and a trivalent condensing agent) (65, 66). Their calculations consider both the charge on the cation as well as the concentration in solution. The effects proposed by this theory are supported by previous studies showing competition between the condensing agent and counterions in solution (18). Using the formalism developed in this theoretical study, it is possible to predict the surface neutralization of DNA phosphate charge for various solution conditions containing several species of cations. This theory explains the physical origin of the experimental observations that high concentrations of mono- and divalent cations can effectively compete with the condensing agent for the surface of the DNA, thereby reducing the overall charge neutralization possible under those conditions (65, 66).

Finally, the electrostatic contributions to determining the size of condensates must be considered. Wilson and Bloomfield determined that ~90% of DNA charge must be neutralized for condensation to be initiated (23). This allows for up to 10% of the

negative charge *per DNA molecule* to remain, although some portion of this charge is likely compensated through ion correlation interactions and bridging between cations as the DNA collapses (23). As a toroid grows, any remaining uncompensated phosphate charge would lead to the accumulation of a net negative charge on the DNA condensates. It has been proposed that the toroid will eventually reach a point at which the net negative charge on the condensate causes further growth of the toroid to be energetically unfavorable, thereby limiting toroid growth (37, 62, 75). This “undercharging” limit has been suggested to determine the optimal size of condensates. The extent to which undercharging contributes to determining toroid size has not yet been verified experimentally.

Overcharging of DNA condensates has also been proposed. Overcharging requires the condensate to acquire a net *positive* charge. Although theoretically possible, experimental studies of double-stranded DNA have failed to provide evidence overcharging occurs at any concentration of cation in solution (28-30, 37, 61-63, 75-77). Further investigations are necessary to understand the present disagreement between the theory and experimental results concerning overcharging.

Hydration Forces: Hydration forces are due to the reconfiguration of water molecules around the surface of the DNA. Water molecules are displaced and rearranged as the condensing agent binds and the DNA collapses into the globule form. Hydration forces have been analyzed using osmotic stress measurements (78). These hydration forces tend to fluctuate between attractive and repulsive, depending on the solution conditions. Repulsions are predicted to occur due to the disruption of the ordered water layer that is

generally maintained at the surface of uncondensed DNA in solution. The disruption of these DNA-bound waters creates an entropically favorable situation. If the water molecules are able to create “water bridges” between the helices or bind with counterions in solution, the effect will generally be favorable towards condensation (37, 78).

As mentioned above, the initiation of nucleation by the formation of the nucleation loop is a kinetically driven process, largely dependent upon the fluctuations of DNA in solution. Theoretical calculations and simulations have also investigated the potential that kinetic contributions predominantly control DNA condensation. Ha and Liu have proposed that bundle growth (e.g., bundle of DNA strands within a toroid) must first overcome an energetic barrier to nucleate, but also must also overcome kinetic barriers to growth, which prohibit bundle growth to an infinite size (58). Bundle growth is determined by the angle in which the molecule approaches the bundle. If the molecule is nearly parallel to the bundle, the interaction is attractive and the molecule is added to the bundle. However, if the molecule approaches the bundle at a large angle (i.e., perpendicular to the bundle), then the interaction would be repulsive. This theory is largely based on the effects of charge-fluctuations between ions. As the molecule-bundle distance increases, the interactions become weaker, making growth less favorable. Conditions of the reaction, including temperature and ionic strength are predicted to affect bundle growth. Calculations have also suggested that as the bundle size increases, the energy barrier of incorporating additional molecules to the bundle increases, further limiting bundle size.

Simulations by Stevens also indicate a substantial kinetic contribution to the ultimate limit of bundle size (64). Unlike Ha and Liu’s model of bundle growth, in the

simulations by Stevens, molecules are proposed to aggregate rather quickly into bundles but are not required to approach the bundle at a specific orientation. Molecules may align themselves once incorporated into the bundle; however this process is slow due to the strong interactions with other molecules in the bundle. This strong binding of DNA molecules within a bundle also makes the movement of a molecule from one bundle to another extremely slow compared to the initial aggregation (64). The stability of the bundles is largely attributed to the association of a multivalent cation between two monomers in the bundle, suggesting the significance of ion fluctuations to this model of bundle formation.

A recent study by Nguyen and Shklovskii investigated the effects of ion correlations and coulombic barriers on the kinetics of condensate formation (62). They proposed a two-stage mechanism for particle growth. Initially, the condensate increases in size (i.e., undercharging). As the condensates grow, the coulombic interactions within the particles become increasingly repulsive. Eventually, this barrier limits particle growth. In the second stage, the less stable condensate begins to desorb DNA molecules from their surface. The free DNA will then attach to a stable condensate, leading to further growth of the particle (62). This model is also directly affected by variations in the ionic strength of the solution, which substantially alter the interactions and associations expected to occur between components of the system.

1.6 Thermodynamic vs. Kinetic Contributions to Toroid Growth

While there are numerous theories regarding potential thermodynamic and kinetic contributions to DNA condensation, few studies have thoroughly considered both effects

in detail. The weakness of most theories investigating DNA condensation is that each calculation or simulation typically neglects one component; the thermodynamic theories have often disregarded kinetic effects and vice versa. As was previously noted in a review by Bloomfield, although current experimental and theoretical studies are providing useful information towards the understanding of the factors that govern DNA condensation, the problems presented by this process are not likely to be quickly solved (8).

References

1. Bloomfield, V. A. (1991) *Biopolymers* 31, 1471-1481.
2. Earnshaw, W., and Harrison, S. (1977) *Nature* 268, 598-602.
3. Earnshaw, W. C., King, J., Harrison, S. C., and Eiserling, F. A. (1978) *Cell* 14, 559-568.
4. Harrison, S. C. (1983) *Journal of Molecular Biology* 171, 577-580.
5. Richards, K. E., Williams, R. C., and Calendar, R. (1973) *Journal of Molecular Biology* 190, 255-259.
6. Holmes, V. F., and Cozzarelli, N. R. (2000) *Proceedings of the National Academy of Sciences of the United States of America* 97, 1322-1324.
7. Allen, M., Lee, J., Lee, C., and Balhorn, R. (1996) *Molecular Reproduction and Development* 45, 87-92.
8. Bloomfield, V. (1996) *Current Opinion in Structural Biology* 6, 334-341.
9. Gosule, L. C., and Schellman, J. A. (1976) *Nature* 259, 333-335.
10. Molas, M., Bartrons, J. C., and Perales, J. C. (2002) *Biochimica et Biophysica Acta* 1572, 37-44.
11. Mahato, R., Smith, L., and Rolland, A. (1999) in *Advances in Genetics* pp 95-155, Academic Press, New York.
12. Rolland, A. (1998) *Critical Reviews in Therapeutic Drug Carrier Systems* 15, 143-198.
13. Cerritelli, M., Cheng, N., Rosenberg, A., McPherson, C., Booy, F., and Steven, A. (1997) *Cell* 91, 271-280.

14. Hud, N. V., Allen, M. J., Downing, K. H., Lee, J., and Balhorn, R. (1993) *Biochemical and Biophysical Research Communications* 193, 1347-1354.
15. Klimenko, S., Tikchonenko, T., and Andreev, V. (1967) *Journal of Molecular Biology*. 23, 523-533.
16. Bloomfield, V. A., Crothers, D. M., and Tinoco, I. (2000) *Nucleic Acids: Structures, Properties and Functions*, University Science Books, Sausalito, CA.
17. Chatteraj, D. K., Gosule, L. C., and Schellman, J. A. (1978) *Journal of Molecular Biology* 121, 327-337.
18. Widom, J., and Baldwin, R. L. (1980) *Journal of Molecular Biology* 144, 431-453.
19. Gosule, L. C., and Schellman, J. A. (1978) *Journal of Molecular Biology* 121, 311-326.
20. Schellman, J. A., and Parthasarathy, N. (1984) *Journal of Molecular Biology* 175, 313-329.
21. Golan, R., Pietrasanta, L., Hsieh, W., and Hansma, H. (1999) *Biochemistry* 38, 14069-14076.
22. Hansma, H. G., Golan, R., Hsieh, W., Lollo, C. P., Mullen-Ley, P., and Kwoh, D. (1998) *Nucleic Acids Research* 26, 2481-2487.
23. Wilson, R. W., and Bloomfield, V. A. (1979) *Biochemistry* 18, 2192-2196.
24. Manning, G. S. (1978) *Quarterly Reviews of Biophysics* 11, 179-246.
25. Arscott, P. G., Ma, C., Wenner, J. R., and Bloomfield, V. A. (1995) *Biopolymers* 36, 345-364.
26. Knoll, D. A., Fried, M. G., and Bloomfield, V. A. (1988) in *DNA and its drug complexes* (Sarma, R. H., and Sarma, M. H., Eds.) pp 123-145, Adenine Press, Albany, NY.

27. Ma, C., and Bloomfield, V. A. (1994) *Biophysical Journal* 67, 1678-1681.
28. de Fructos, M., Raspaud, E., Leforstier, A., and Livolant, F. (2001) *Biophysical Journal* 81, 1127-1132.
29. Raspaud, E., Chaperon, I., Leforstier, A., and Livolant, F. (1999) *Biophysical Journal* 77, 1547-1555.
30. Raspaud, E., Olvera de la Cruz, M., Sikorav, J.-L., and Livolant, F. (1998) *Biophysical Journal* 74, 381-393.
31. Revet, B., and Fourcade, A. (1998) *Nucleic Acids Research* 26, 2092-2097.
32. Dahlgren, P. R., and Lyubchenko, Y. L. (2002) *Biochemistry* 41, 11372-11378.
33. Zinchenko, A. A., Sergeyev, V. G., Yamabe, K., Murata, S., and Yoshikawa, K. (2004) *Chembiochem* 5, 360-368.
34. Kornyshev, A. A. (1999) *Physical Review Letters* 82, 4138-4141.
35. Böttcher, C., Endisch, C., Fuhrhop, J. H., Catterall, C., and Eaton, M. (1998) *Journal of the American Chemical Society* 120, 12-17.
36. Arscott, P. G., Li, A.-Z., and Bloomfield, V. A. (1990) *Biopolymers* 30, 619-630.
37. Bloomfield, V. (1998) *Biopolymers* 44, 269-282.
38. Koo, H. S., Drak, J., Rice, J. A., and Crothers, D. M. (1990) *Biochemistry* 29, 4227-4234.
39. Rivetti, C., Walker, C., and Bustamante, C. (1998) *Journal of Molecular Biology* 280, 41-59.
40. Shen, M., Downing, K., Balhorn, R., and Hud, N. (2000) *Journal of the American Chemical Society* 122, 4833-4834.

41. Travers, A. A., Ner, S. S., and Churchill, M. E. (1994) *Cell* 77, 167-169.
42. Hagerman, P. J. (1988) *Annual Review of Biophysical Chemistry* 17, 265-286.
43. Paull, T. T., Haykinson, M. J., and Johnson, R. C. (1993) *Genes and Development* 7, 1521-1534.
44. Ross, E. D., Hardwidge, P. R., and Maher, L. J. (2001) *Molecular and Cellular Biology* 21, 6598-6605.
45. MacAlpine, D. M., Perlman, P. S., and Butow, R. A. (1998) *Proceedings of the National Academy of Sciences of the United States of America* 95, 6739-6743.
46. Alam, T. I., Kanki, T., Muta, T., Ukaji, K., Abe, Y., Nakayama, H., Takio, K., Hamasaki, N., and Kang, D. (2003) *Nucleic Acids Research* 31, 1640-1645.
47. Love, J. J., Li, X., Case, D. A., Giese, K., Grosschedl, R., and Wright, P. E. (1995) *Nature* 376, 791-795.
48. Tang, L., J., L., Katz, D. S., and Feng, J. (2000) *Biochemistry* 39, 3052-3060.
49. Werner, M. H., Huth, J. R., Gronenborn, A. M., and Clore, G. M. (1995) *Cell* 81, 705-714.
50. Ellwood, K. B., Yen, Y. M., Johnson, R. C., and Carey, M. (2000) *Molecular and Cellular Biology* 20, 4359-4370.
51. Schlierf, B., Ludwig, A., Klenovsek, K., and Wegner, M. (2002) *Nucleic Acids Research* 30, 5509-5516.
52. Webb, M., Payet, D., Lee, K. B., Travers, A. A., and Thomas, J. O. (2001) *Journal of Molecular Biology* 309, 79-88.
53. Yie, J., Liang, S., Merika, M., and Thanos, D. (1997) *Molecular and Cellular Biology* 17, 3649-3662.

54. Love, J. J., Li, X., Case, D. A., Giese, K., Grosschedl, R., and Wright, P. E. (1995) *Nature (London)* 376, 791-795.
55. Hud, N. V., Downing, K. H., and Balhorn, R. (1995) *Proceedings of the National Academy of Sciences of the United States of America* 92, 3581-3585.
56. Yoshikawa, K., and Matsuzawa, Y. (1996) *Journal of the American Chemical Society* 118, 929-930.
57. Hud, N. V., and Downing, K. H. (2001) *Proceedings of the National Academy of Sciences of the United States of America* 98, 14925-14930.
58. Ha, B. Y., and Liu, A. J. (1999) *Europhysics Letters* 46, 624-630.
59. Sakaue, T., and Yoshikawa, K. (2002) *Journal of Chemical Physics* 117, 6323-6330.
60. Noguchi, N., and Yoshikawa, K. (2000) *Journal of Chemical Physics* 113, 854-862.
61. Nguyen, T. T., Rouzina, I., and Shklovskii, B. I. (2000) *Journal of Chemical Physics* 112, 2562-2568.
62. Nguyen, T. T., and Shklovskii, B. I. (2002) *Physical Review E* 65, 031409-1-031409-7.
63. Shklovskii, B. I. (1999) *Physical Review E* 60, 5802-5811.
64. Stevens, M. J. (1999) *Physical Review Letters* 82, 101-104.
65. Rouzina, I., and Bloomfield, V. A. (1996) *Journal of Physical Chemistry* 100, 4292-4304.
66. Rouzina, I., and Bloomfield, V. A. (1997) *Biophysical Chemistry* 64, 139-155.
67. Rouzina, I., and Bloomfield, V. (1996) *Journal of Physical Chemistry* 100, 9977-9989.

68. Vasilevskaya, V. V., Khokhlov, A. R., Kidoaki, S., and Yoshikawa, K. (1997) *Biopolymers* 41, 51-60.
69. He, S., Arscott, P. G., and Bloomfield, V. A. (2000) *Biopolymers* 53, 329-341.
70. Lu, Y., Weers, B., and Stellwagen, N. C. (2002) *Biopolymers* 61, 261-275.
71. Yoshikawa, Y., Yoshikawa, K., and Kanbe, T. (1999) *Langmuir* 15, 4085-4088.
72. Trubetskoy, V. S., Loomis, A., Hagstrom, J. E., Budker, V. G., and Wolff, J. A. (1999) *Nucleic Acids Research* 27, 3090-3095.
73. Allison, S. A., Herr, J. C., and Schurr, J. M. (1981) *Biopolymers* 20, 469-488.
74. Olvera de la Cruz, M., Belloni, L., Delsanti, M., Dalbiez, J. P., Spalla, O., and Drifford, M. (1995) *Journal of Chemical Physics* 103, 5781-5791.
75. Gelbart, W. M., Bruinsma, R. F., Pincus, P. A., and Parsegian, V. A. (2000) *Physics Today* 53, 38-44.
76. Park, S. Y., Bruinsma, R. F., and Gelbart, W. M. (1999) *Europhysics Letters* 46, 454-460.
77. Mateescu, E. M., Jeppensen, C., and Pincus, P. (1999) *Europhysics Letters* 46, 493-498.
78. Rau, D., and Parsegian, V. (1992) *Biophysical Journal* 61, 260-271.

CHAPTER 2

A QUANTITATIVE STUDY OF STATIC CURVATURE AND IONIC STRENGTH EFFECTS ON DNA TOROID DIMENSIONS

More than twenty-five years ago it was discovered that multivalent cations cause DNA to collapse from solution into toroid-shaped condensates (1). These structures have typically been reported to measure around 100 nm in outside diameter with a 30 nm hole, however, the generation of substantially larger toroids has also been reported (2, 3). Toroidal DNA condensates have been reported to be the morphology of DNA packaged within some bacterial phages and vertebrate sperm cells (4-8). Thus, the DNA toroid is a morphology used by nature for the high-density packing of genomes. The condensation of DNA for artificial gene delivery has also utilized toroids (9, 10). However, researchers have yet to develop a method to package DNA that produces particles as homogeneous, both in terms of size and shape, as is achieved by natural packing systems.

A considerable number of theoretical studies have sought to explain why DNA toroids and other condensate morphologies (e.g. rods) favor a particular size. These theories include growth limits based upon the buildup of uncompensated electrostatic repulsions, the accumulation of packing defects and kinetic barriers to DNA strand association in solution (11-17). All of these theoretical studies agree that DNA toroids should favor a particular size. However, the validity of such theories has been difficult to assess due to the fact that most experimental studies have only presented measurements

for toroids collected for a single solution condition. Additionally, variations between the experimental protocols of different laboratories also make it difficult to appreciate how toroid size depends on solution conditions.

The focus of this chapter is a systematic study of how static loops and salt affect the dimensions of toroids generated by the condensation of DNA with hexamine cobalt (III). We demonstrate that static curvature reduces toroid dimensions and that toroid dimensions increase with added salt. The number of toroids measured has allowed the determination of statistically significant shifts in average toroid dimensions that result from changes in salt concentrations as small as 2.5 mM NaCl. Analysis of toroid diameter versus toroid thickness for varying solution conditions supports a model for toroid growth that includes two parts; a nucleation stage and a multistranded growth stage. Changes in toroid diameter and thickness with salt also demonstrate that toroid nucleation and growth are affected differently by ionic strength.

2.1 Experimental Procedures

DNA Preparation. Bluescript II SK- plasmid DNA (Stratagene) was grown in DH5a (Life Technologies) and isolated using the Qiagen Maxi Prep kit. The DNA was eluted in 1× TE (10 mM Tris, pH 7.8, 1 mM EDTA) and linearized by digestion with the restriction enzyme Hind III (New England Biolabs). Restriction digests were generally performed using 5 to 10 µg of DNA in a 100 µl reaction mixture, and allowed to incubate for 2-4 hours. Buffer and salts introduced for the restriction digest reaction were removed by rinsing the DNA at least five times with 0.25× TE using a Microcon YM-30 spin column (Millipore). Removal of any excess salts is very important as variations in ionic

strength can alter the results of the condensation reaction. Approximately 400 μ l of buffer was added to the Microcon YM-30 membrane, and then the \sim 100 μ l restriction digest was thoroughly mixed with the buffer. Between rinses and before elution, the buffer was mixed by pipetting on the column. After the final rinse, DNA was resuspended from the spin column membrane to a final concentration of 20 μ g/ml in 0.25 \times TE. DNA concentrations were verified spectrophotometrically. A modified Bluescript II SK- containing extensive sequence-directed curvature was also used in this study. This plasmid, previously reported by Shen *et al.*, (18) contains four tandem repeats of the following A-tract containing sequence: 5'-ATCCATCGACC(AAAAAACGGGCAAAAAACGGC)₇AAAAAAGCAGTGGAAG-3'. This plasmid was grown in Sure2 Supercompetent cells (Stratagene), then isolated and prepared as described above.

To examine the effects of ionic strength and cation species on DNA condensation, three stock solutions were prepared of the linearized Bluescript II SK- plasmid DNA: a low salt stock solution in 1 \times TE, a 15 mM NaCl stock solution and a 7.5 mM MgCl₂ stock solution. All three stock solutions contained 17 μ g/ml DNA in 1 \times TE. The buffer concentration was brought to 1 \times TE by adding several microliters of 7.8 \times TE to the DNA samples. Preparations with salt concentrations between the low salt and the NaCl or MgCl₂ stock solutions were prepared by mixing specific ratios of the low salt stock solution with the NaCl or MgCl₂ stock solutions, respectively.

DNA Condensate Preparation and Imaging. DNA condensates were prepared by mixing a DNA sample solution with an equal volume of a hexammine cobalt chloride (Sigma)

solution to yield a condensation reaction mixture 8.5 $\mu\text{g/ml}$ in DNA, 100 μM in hexammine cobalt chloride and 0.5 \times in the salt/buffer of the DNA sample. Condensate reaction mixtures were allowed to equilibrate for 5 minutes and then deposited on carbon-coated grids (Ted Pella). Samples were pipetted repeatedly to mix for condensation and again before deposition onto the grids. Additionally, the grids were covered with a Petri dish to prevent excess evaporation. After 10 minutes on the grids, 2% uranyl acetate (Ted Pella) was added momentarily to the condensate mixtures, the grids were then rinsed in 95% ethanol and air-dried. The DNA condensates were recorded on film using a JEOL-100C transmission electron microscope (TEM) at $\times 100,000$ magnification. The TEM negatives were scanned at 300 pixels/inch and Canvas graphics program was used to measure the outer diameter and thickness of individual DNA toroids. The lines representing the toroid diameters and thicknesses were copied to a new Canvas file and saved in .eps format. This file was read using the “*Read Coordinates*” program written by Nick Hud, which allowed the data to be opened and analyzed in Microsoft Excel.

2.2 Results and Discussion

We have studied the condensation of a linear 2961 bp DNA, and a slightly longer DNA that contains extensive sequence-directed curvature, under a range of salt conditions. The 2961 bp DNA [abbreviated *3kbDNA*] is a bacterial plasmid linearized by cutting at a single site with a restriction enzyme. The second DNA (*19*) is the same bacterial plasmid with an additional 720 bp insert. The sequence of this insert contains sixty A-tracts of the form d(AAAAAA) that are phased with respect to the helical twist of

DNA in order to maximize long range axial bending of the DNA (Experimental Procedures). A single A-tract produces a bend in the DNA helical axis of approximately 13° (20). Thus, the sixty phased A-tracts in the 720 bp insert of *Atract60* are expected to produce a cumulative axial bend of around 780° , or two static DNA loops. Linearization of the circular *Atract60* plasmid by enzymatic cutting at a single site near the 720 bp insert produced a linear 3.7 kb DNA with the two static loops near one end.

Salt and Static Curvature Effect Toroid Dimensions. DNA condensation *in vitro* by multivalent cations follows a nucleation-growth process (17, 21). The nucleation event for DNA condensation into toroidal particles has been proposed to be the spontaneous formation of a DNA loop along the polymer in solution (22). The introduction of two static loops provides *Atract60* with a "built-in" site for toroid nucleation, which is expected to be kinetically favored for nucleation over loops that transiently form due to random polymer fluctuations (18). Condensation of *Atract60* by the addition of the trivalent inorganic cation hexamine cobalt (III) produces smaller toroids than those formed by *3kbDNA*, under the same "low salt" solution conditions of 0.5×TE buffer, pH 7.8 (Figures 2.1A & B). Toroids produced by *Atract60* condensation have a mean outer diameter of 68 nm, whereas *3kbDNA* condenses into toroids with a mean outer diameter of 80 nm. Because the static loops of *Atract60* are on average smaller than loops that are expected to spontaneously form along linear DNA at room temperature, i.e. 30-40 nm versus approximately 50 nm (*vide infra*), these results demonstrate that the size of the initial nucleation loop in toroid formation is a principal factor in determining the overall size of toroidal DNA condensates.

The effects of increasing ionic strength on the condensation of *3kbDNA* were also investigated. Millimolar increases in NaCl concentration to *3kbDNA* DNA samples, initially in a low salt solution, produce significantly larger toroids upon condensation by hexamine cobalt (III). For example, *3kbDNA* toroids formed in the presence of 2.5mM NaCl have a mean outer diameter of 90 nm, as compared to 80 nm with no added salt (Figures 2.1B & C). This shift in mean outer diameter is primarily due to the presence of considerably larger toroids, along with toroids similar in size to those in the low salt sample (Figure 2.1C). When the NaCl concentration is increased further to 3.75 mM the mean outer diameter increases an additional 20% to 118 nm, with essentially all toroids being of the larger size (Figure 2.1E). At approximately 4.5 mM NaCl, fiber-like condensates are formed instead of toroids (data not shown).

The effects of divalent cations on DNA toroid dimensions were studied by the addition of MgCl₂ to the *3kbDNA* solution prior to condensation with hexamine cobalt (III). Toroidal condensates produced from a DNA solution 1.75 mM in MgCl₂ are comparable in outer diameter to those of a sample 3.75 mM in NaCl (Figures 2.1D & E). At 1.75 mM MgCl₂ the ionic strength of the sample is approximately the same as that of the 3.75 mM NaCl sample, if the chelating affect of the 0.5 mM EDTA is taken into account. This observation suggests that the increase in toroid size at 3.75 mM NaCl and 1.75 mM MgCl₂ is purely an effect of ionic strength and not dependent on cationic species. However, one notable difference between these two preparations is an increased aggregation of toroids in the MgCl₂ sample (Figure 2.1E). At 2.5 mM MgCl₂ the mean

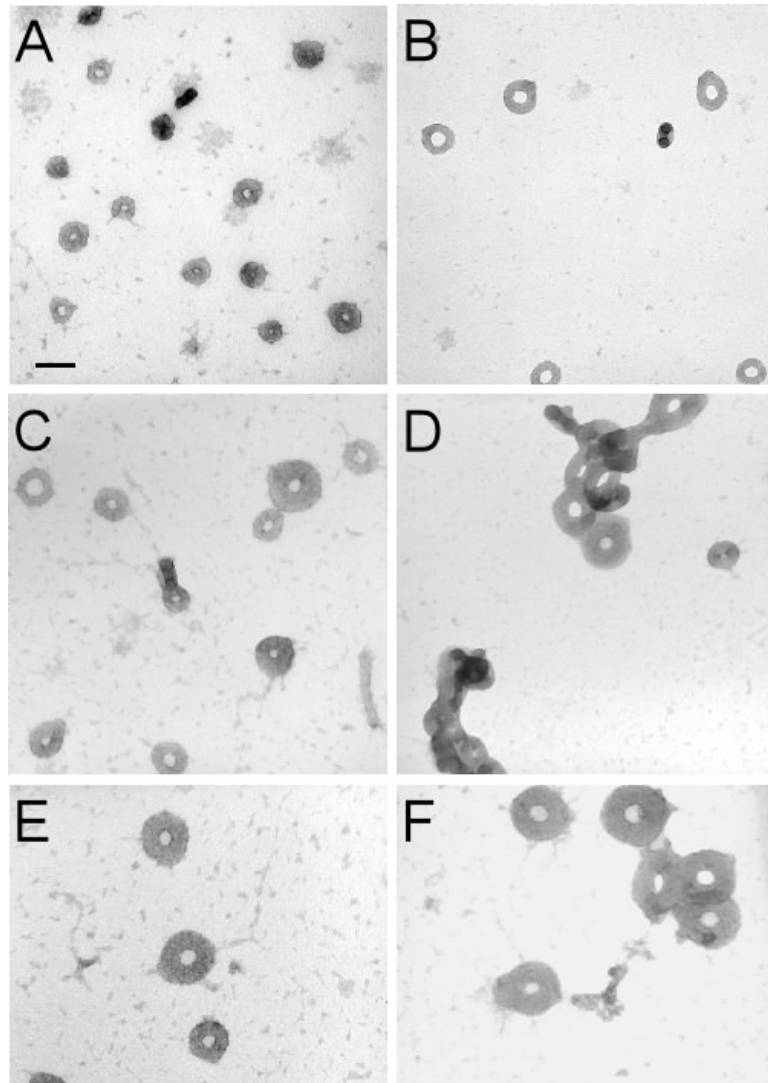
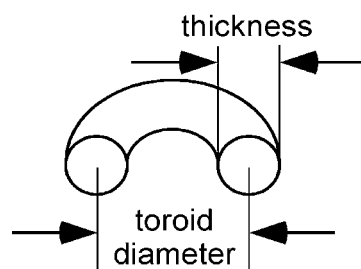


Figure 2.1. Transmission electron micrographs (TEM) of toroids produced by the condensation of DNA with hexamine cobalt (III) under a variety of conditions. (A) *Atract60* condensed in the low salt buffer (0.5×TE: 5 mM Tris, 0.5 mM EDTA). *Atract60* is a linear 3681 bp DNA with extensive sequence-directed curvature near one end. (B) *3kbDNA* condensed in the low salt buffer. *3kbDNA* is a linear 2961 bp plasmid DNA. (C) *3kbDNA* condensed in 2.5 mM NaCl, 0.5×TE. (D) *3kbDNA* condensed in 3.75 mM NaCl, 0.5×TE. (E) *3kbDNA* condensed in 1.75mM MgCl₂, 0.5×TE. (F) *3kbDNA* condensed in 2.5 mM MgCl₂, 0.5×TE. All samples were 8.5 μg/mL in DNA and 100 μM hexamine cobalt chloride. (Scale bar is 100nm. All micrographs are shown at the same magnification.)

outer diameter of *3kbDNA* toroids increased to 158 nm, which is twice the size of the low salt condensates (Figure 2.1F). At MgCl_2 concentrations above 2.5 mM fiber-like DNA condensates become the dominant morphology, similar to what is observed with increasing NaCl concentrations. However, for MgCl_2 the transition to fiber-like condensates occurs at an ionic strength that is approximately two times the ionic strength at which the same transition occurs for samples with added NaCl.

Toroid Diameter and Thickness Are Not Strictly Coupled. A systematic comparison of toroids produced by the condensation of *3kbDNA* and *Atract60* provides substantial insights into the process of toroid formation. In Figure 2.2 the toroid diameter of each

DNA condensate measured in this study is plotted with respect to its thickness. Here *toroid diameter* refers to the average of the outer diameter and the hole (i.e. inner) diameter for a given toroid (Scheme 2.1). Toroid outer diameters and hole diameters have typically been reported



Scheme 2.1: Definition of toroid diameter and thickness

in studies of DNA toroids (2, 11, 23, 24). However, we have found that analysis of the toroid diameter and toroid thickness is potentially more useful for understanding the process of DNA toroid formation.

Toroids produced by the condensation of *3kbDNA* in the low salt buffer have a mean toroid diameter of 55 nm and a mean thickness of 25 nm (Figure 2.3). If we approximate the cross-section of DNA toroids as circular, then a simple volume calculation based upon diameter and thickness measurements indicates that 98% of the low salt *3kbDNA* toroids contain from 6 to 32 *3kbDNA* molecules per toroid. Thus,

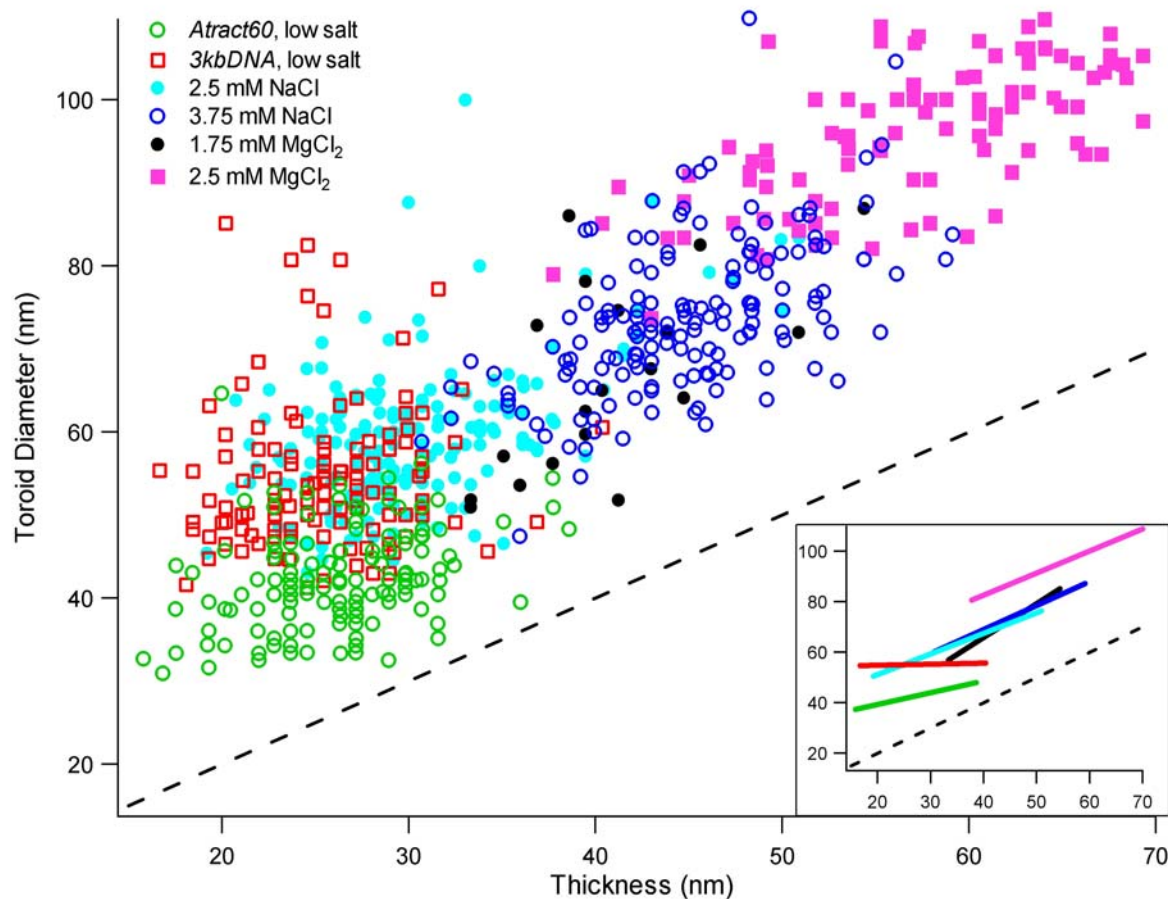


Figure 2.2. A plot of toroid diameter versus toroid thickness for all DNA toroids measured. Toroid diameter is defined as an arithmetic mean of the outside diameter of the toroid and the diameter of the toroid hole. Toroid thickness is defined as a difference between toroid outside diameter and the diameter of the toroid hole. The dashed line represents the position in the plot where toroid diameter is equal to toroid thickness. Toroid data points that fall along this line would have a hole diameter of zero (observed as spheroids). All data sets with added salt were for condensates of *3kbDNA*. (Insert) A plot of linear best-fit lines for the toroid diameter versus toroid thickness data sets. Line colors in the inserted plot correspond to data legend in the larger plot.

during formation a growing toroid must add DNA molecules until toroid growth becomes limited either by a kinetic factor (e.g. no free DNA remains in solution) or a thermodynamic factor (e.g. an equilibrium state for optimal toroid thickness is reached).

If during DNA toroid formation the thickness of a toroid increases equally outward and inward from the nucleation loop, then the toroid diameter will remain equal to the diameter of the nucleation loop. Under the conditions of our studies (i.e. ionic strength >1 mM) the most probable size of loops that spontaneously form along a DNA polymer is approximately 50 nm in diameter (22). This is very close to the measured mean toroid diameter of 55 nm for the low salt *3kbDNA* toroids, which supports the proposal that toroid diameter is largely determined by nucleation loop diameter and that growth in toroid thickness proceeds equally outward and inward from the nucleation loop (22, 25).

Condensation of *Atract60* in the low salt buffer produces toroids with a mean toroid diameter of 42 nm, which is the smallest reported in this study (Figures 2.2 & 2.3). This reduced mean diameter of *Atract60* toroids is a direct result of the static loops in *Atract60*, since the conditions of condensation were identical to those of the low salt *3kbDNA* condensation. If we assume equal outward and inward growth for *Atract60* toroids from the static nucleation loops, then the sixty A-tracts in this DNA produce loops approximately 42 nm in diameter. This would imply that each A-tract contributes an axial bend of around 11° to the overall curvature of the 720 bp insert, an angle that is not unreasonable considering the previously determined value of 13° for a single A-tract bend (20). This correlation between *Atract60* mean toroid diameter and the expected size of A-tract loops provides further support that, in our low salt buffer, toroid diameter is

determined by the nucleation loop and toroid growth proceeds both outward and inward from the nucleation loop(s).

The mean thickness of *Atract60* and *3kbDNA* toroids is essentially the same at 26 nm and 25 nm, respectively (Figures 2.2 & 2.3). Thus, reducing toroid size by providing smaller static loops for nucleation does not change toroid thickness. This result provides definitive evidence that toroid thickness is independent of nucleation loop size. Another manifestation of the fact that toroid thickness is independent of nucleation loop size/toroid diameter is the zero slope of a linear fit of the low salt *3kbDNA* toroid diameter versus toroid thickness data (Figure 2.2 insert). If toroid thickness was coupled to toroid diameter for this data set, a non-zero slope would be expected.

It is possible that our estimate of the axial bend per A-tract of approximately 11° is less than the reported value of 13° because these bends are actually not as pronounced in our particular experimental conditions. However, there are other plausible explanations. Due to the extremely small radius of curvature of the *Atract60* holes (Figure 2.1A), the bending energy of DNA wound near the hole of *Atract60* toroids is expected to be significantly greater than DNA wound around the outside of these toroids (26, 27). Thus, it is possible that for *Atract60* toroids growth is altered slightly such that DNA deposition is biased more towards outward growth than inward growth from the static nucleation loops. This would result in a mean toroid diameter of *Atract60* toroids that is larger than the actual size of the nucleation loops, and hence an underestimation of the actual bend per A-tract. This would also explain the positive slope observed for the linear fit of the *Atract60* toroid diameter versus toroid thickness data (Figure 2.2 insert). A second possibility is that a systematic bias has been introduced into our *Atract60* data

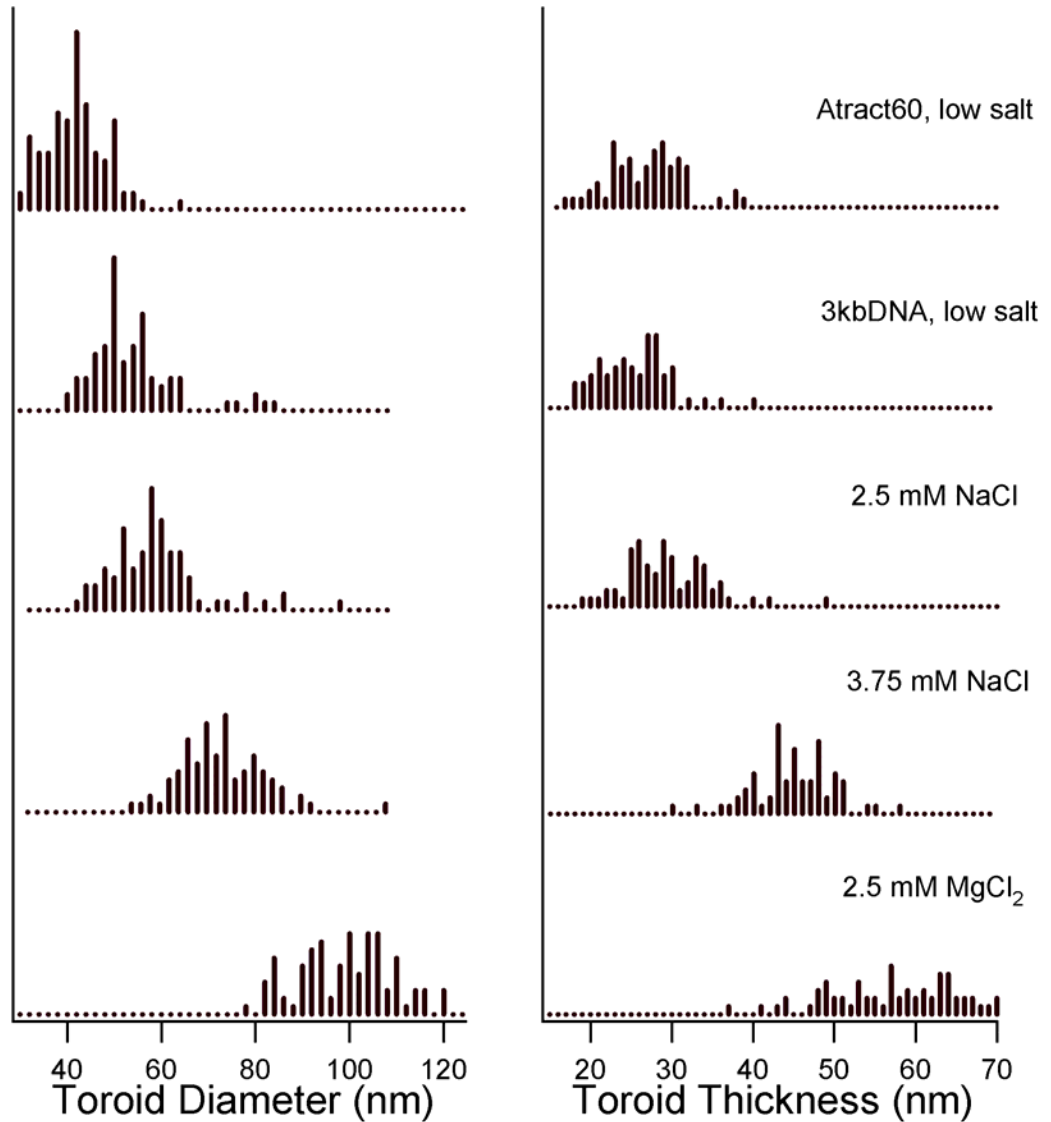
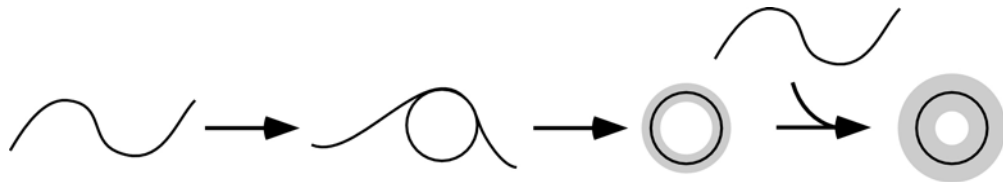


Figure 2.3. Histograms of toroid diameters and toroid thickness measurements for DNA condensates under various solution conditions. DNA and salt conditions for toroid diameter data sets correspond to those given to the right of the graph for the toroid thickness data. All data sets with added salt were for condensates of *3kbDNA*.

that artificially increased the observed mean toroid diameter. In the present study, measurements were only collected for toroids with a clearly defined hole. If a significant percentage of *Atract60* toroids grow to a thickness that obscures their hole, the exclusion of these DNA particles from our data set would artificially increase the mean toroid diameter (reducing the apparent axial bend per A-tract), and cause a positive slope in the linear fit to the *Atract60* data set.

Analysis of toroid diameter and thickness for toroids produced by the condensation of *3kbDNA* in low salt solutions support the following model for toroid



Scheme 2.2: Toroid nucleation and growth with equal inward and outward growth from the nucleation loop. The black circle on the proto-toroid (second from right) and the fully grown toroid (right) illustrates the size of the nucleation loop.

growth (Scheme 2.2). The first step in toroid formation is the spontaneous formation of a DNA loop along a *3kbDNA* polymer. This loop acts as the nucleation site for condensation upon which the remainder of the DNA polymer condenses, forming a proto-toroid. Additional *3kbDNA* polymers condense onto the proto-toroid, which increases the thickness of the growing toroid. The DNA wraps around the toroid such that the toroid grows both outward and inward, keeping the toroid diameter relatively constant. The toroid continues to grow in this manner until it reaches a limiting thickness. For *Atract60* toroids, this model is slightly altered since the initial state of the DNA

polymer contains static loops, allowing *Atract60* to bypass the nucleation step in toroid formation.

Increased Ionic Strength Alters Toroid Growth. The mean toroid diameter and mean thickness of *3kbDNA* condensates increase with ionic strength. For a *3kbDNA* sample in 2.5 mM NaCl this shift is appreciable, although there is still a significant amount of overlap for both toroid diameter and thickness measurements with the low salt measurements (Figures 2.2 & 2.3). At 3.75mM NaCl and 1.75mM MgCl₂, both diameter and thickness measurements are substantially offset from the low salt data (Figures 2.2 & 2.3). The mean toroid diameters measured for the 2.5 mM and 3.75 mM NaCl samples are 59 nm and 74 nm, respectively, whereas the mean toroid diameter of the low salt sample is 55 nm. The 1.75 mM MgCl₂ data is similar to the 3.75 mM NaCl data (approximately equal ionic strength), except that fewer data points were collected due to toroid aggregation in the 1.75 mM MgCl₂ sample. With increasing ionic strength, an increase in the slope of a linear fit of toroid diameter versus toroid thickness data is also observed; a slope of 0.8 is observed for the 2.5 mM NaCl *3kbDNA* sample and a slope of 0.9 for the 3.75 mM NaCl *3kbDNA* sample (Figure 2.2 insert).

The relatively equal offset of the *3kbDNA* toroid data from for the dashed line in Figure 2.2, for all but the highest MgCl₂ concentration sample, indicates a close similarity in the distribution of toroid hole diameters for these various salt conditions. This is more easily appreciated by a direct comparison of the hole diameters of the low salt buffer toroids with the hole diameters of the 3.75 mM NaCl toroids (Figure 2.4). From the histograms presented in Figure 4 it is clear that the distributions of the hole diameters are

essentially the same, even though the toroid diameters and thickness for the same two samples are significantly different (Figure 2.3). Similar distributions (i.e. approx. equal mean and std. deviation) are also seen for the 2.5 mM NaCl and 1.75 mM MgCl₂ samples. This suggests that the hole diameter of a toroid is less sensitive to changes in the ionic strength than toroid diameter, toroid thickness or toroid outer diameter.

Above approximately 1 mM monovalent cation concentration the persistence length of DNA does not vary for higher salt concentrations (19, 28, 29). Thus, the average size of the loops that spontaneously form along a *3kbDNA* should be approximately the same for all solution conditions of this study, given that the 0.5× TE buffer alone is over 2 mM in monovalent cations. If the nucleation loop is the same for the toroid samples with the same hole size (Figure 2.4), then the observed change in toroid diameter must be due to growth being more favored outward than inward from the nucleation loop. This proposal is supported by the positive slopes of the linear best-fit lines to the toroid diameter versus toroid thickness data (Figure 2.2). Additional support is given by the increase in mean thickness of *3kbDNA* toroids of the 3.75 mM NaCl sample from the low salt data. The difference in mean toroid thickness between these two samples is 18 nm, which is also the observed difference in the mean toroid diameter. This is exactly as expected if the mean nucleation loop size for the 3.75 mM NaCl sample is equal to that of the low salt sample. However, DNA added onto the 3.75 mM NaCl toroids beyond that of low salt toroid growth is added exclusively to the outside of the toroid.

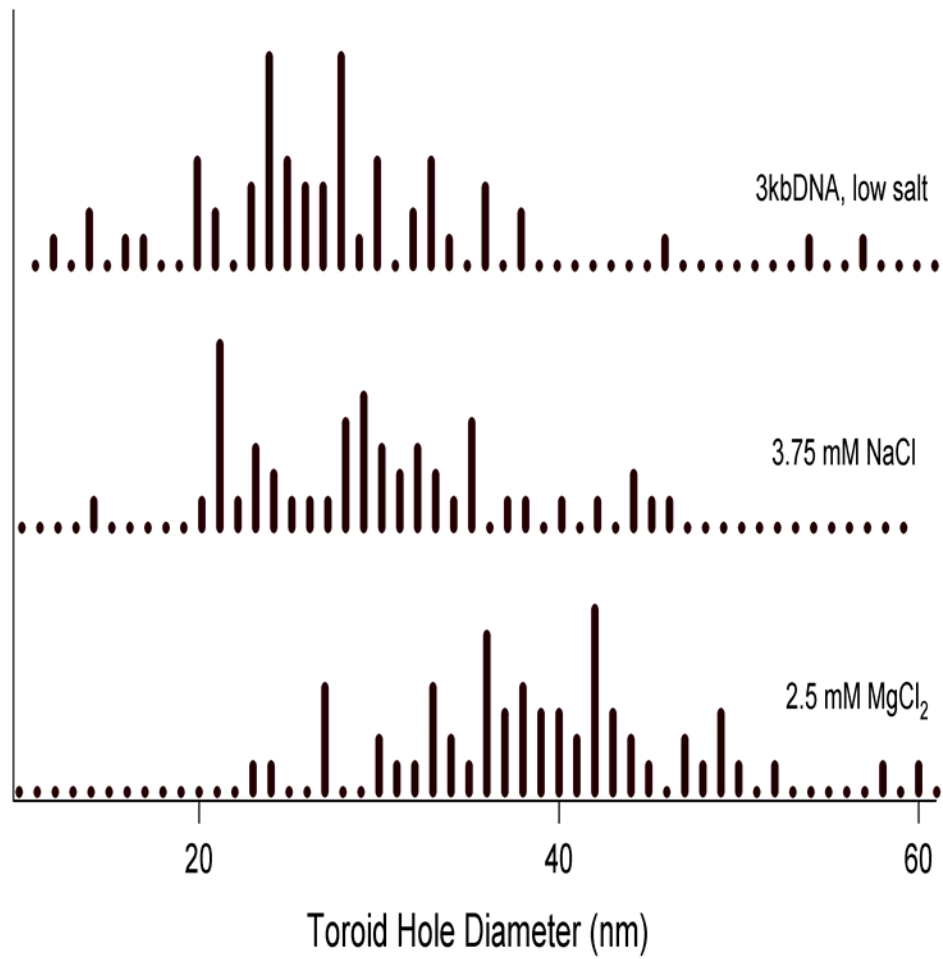
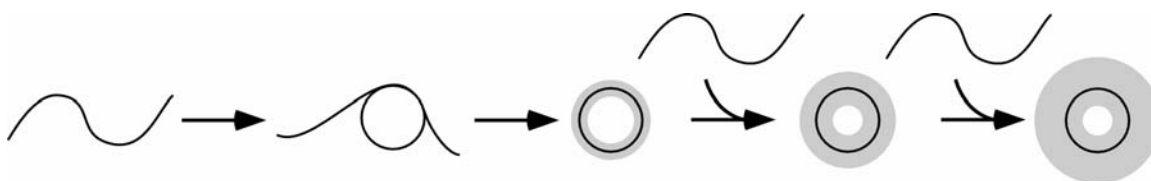


Figure 2.4. Histograms of toroid hole diameters for *3kbDNA* condensed in three different salt solutions.

Based upon the observation that mean toroid diameter and mean toroid thickness increase while mean hole diameter remains constant, a second model of toroid growth emerges for our intermediate ionic strength conditions (Scheme 2.3). Nucleation occurs and toroid growth follows the same preliminary growth pathway as the low salt model presented above. However, in the presence of additional ions, there is a secondary growth that results in the addition of DNA exclusively to the outside of the toroid.



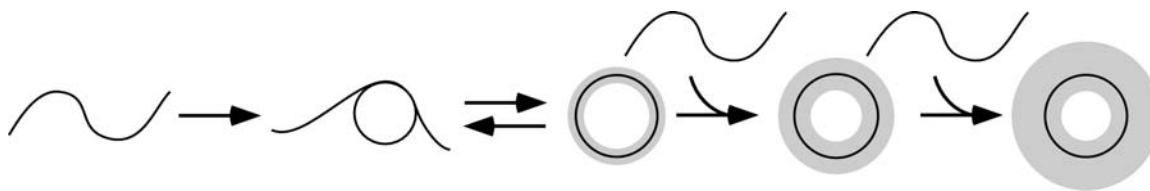
Scheme 2.3: Toroid nucleation and growth with preferential growth outward from the nucleation loop during the latter stages of toroid growth

2.5 mM MgCl₂ Causes a Greater Increase in Toroid Diameter than Toroid Thickness. Condensation of *3kbDNA* in 2.5 mM MgCl₂ produced toroids with a mean toroid diameter of 99 nm, which is nearly twice the 55 nm mean toroid diameter of the low salt preparation. The mean thickness of toroids produced in the presence of 2.5 mM MgCl₂, 59 nm, is also considerably larger than the mean thickness of any other toroid preparation of the present study (Figures 2.2 & 2.3). As the MgCl₂ concentration of the DNA solution was increased above 2.5 mM the condensation process underwent a transition where toroids were replaced by fiber-like condensates as the dominant structure (data not shown).

The linear fit of toroid diameter versus thickness for the 2.5mM MgCl₂ data has a slope of 0.9, which is the same as the slope of the 3.75 mM NaCl data. This positive

correlation is again indicative of toroid diameter and thickness being coupled, and can be understood as a result of preferential outward growth in toroid thickness from the nucleation loop. However, the position of the 2.5 mM MgCl₂ best fit line is further removed from the dashed line in Figure 2 than the best-fit lines for all other data sets (Figure 2.2 inset). The shift in this line indicates a greater change in mean toroid diameter than in mean toroid thickness for the 2.5 mM MgCl₂, with respect to the intermediate salt concentration data. This cannot be explained as being the result of a further bias toward outward growth as described in Scheme III, because in that event the 2.5 mM MgCl₂ data points would be expected to move along the line of the 3.7 mM NaCl data. The easiest way to appreciate the effect of this unequal shift in toroid diameter versus toroid thickness for the 2.5 mM MgCl₂ toroids is that these toroids have larger holes than the other *3kbDNA* samples (Figure 2.4). The models presented thus far for toroid formation do not explain this result for the 2.5 mM MgCl₂ sample.

The increase in the off-set of the 2.5 mM MgCl₂ toroid diameter/thickness data from the dashed line in Figure 2.2 could be explained by an increase in nucleation loop size. However, the size of loops that spontaneously form along the DNA polymer should not be appreciably affected by the relatively small increase in ionic strength between the 2.5 mM MgCl₂ sample and the 1.75 mM MgCl₂ sample, as previous reports have shown that with increasing divalent cation concentrations the persistence length of DNA changes only minimally once divalent cation concentration is greater than 0.1 mM. As an alternative explanation, we propose that an annealing process occurs in the presence of 2.5 mM MgCl₂ in which larger loops are selected from the ensemble of loops sizes that form spontaneously during the initial stage of condensation (Scheme 2.4). This may



Scheme 2.4: Toroid nucleation and growth with annealing to larger nucleation loop sizes during the early stages of formation, and preferential outward growth during the latter stages of toroid formation.

occur by the following two mechanisms. The first possibility is that in 2.5 mM MgCl_2 competition between Mg^{2+} and hexamine cobalt (III) for interaction with DNA reduces the DNA-DNA association energy such that proto-toroids formed by the condensation of a single DNA polymer are near the edge of stability, and proto-toroids formed with relatively small loops have too much bending energy to persist long enough to the go onto the next stage of toroid growth. The breakup of the smaller (i.e. higher energy) proto-toroids would produce a bias towards toroids nucleated from larger loops. A second possibility, suggested by computer simulations of DNA condensation (30), is that during toroid nucleation the DNA in the first loops of the proto-toroid slide past one another to reduce bending strain in the condensed DNA and thereby increase their diameters, and ultimately the diameters of full-grown toroids. It is not possible from the current study to determine which mode of toroid diameter size increase is more likely, and it is possible that both mechanisms are active.

Toroid Thickness Limits as a Function of Salt. Several theories have been put forth as attempts to explain why toroids and other DNA condensate morphologies grow to a particular size (11, 13, 14, 16, 19). A common target of these theories has been to

determine the origin of a limitation on DNA bundle size, or thickness/number of windings in the case of toroids. We have shown that toroid nucleation loop size can be understood in terms of DNA flexibility or static curvature. However, the origin of a limit on toroid thickness is more obscure. Examples of thermodynamic models for the physical limits on toroid growth include the model of Bloomfield in which a net buildup of uncompensated negative charge in the DNA of a toroid produces an electrostatic repulsion (11), and the more recent model of Ray and Manning predicts that pair potentials of DNA molecules with associated counter ions will depend on distance in such a way that an optimum bundle size results from the balance of short-range attractive interactions and long-range repulsive interactions between polyanions (16). Liu and co-workers have also argued for a kinetic origin for the source of a limitation on DNA bundle thickness (15). It has been difficult to fully assess the relative validity of these theories due to the lack of systematic studies of toroid size as a function of a fundamental physical parameter. Here we have shown a clear correlation exists between ionic strength and toroid thickness, which could be useful in this regard.

Theoretical models for the origins of limitations to DNA condensate bundle size or toroid thickness have typically developed a relationship between an energy term and the cross-sectional area of a DNA condensate rather than thickness *per se*. If we make the approximation that the toroids of this study have circular cross-sections, we can calculate the cross-sectional areas of toroids based upon their thickness measurements. Histograms of approximate cross-sectional area were generated in this manner and then fit with a continuous function to produce idealized cross-sectional area distributions. From these distributions, the energy potential curves were calculated using the Boltzman equation

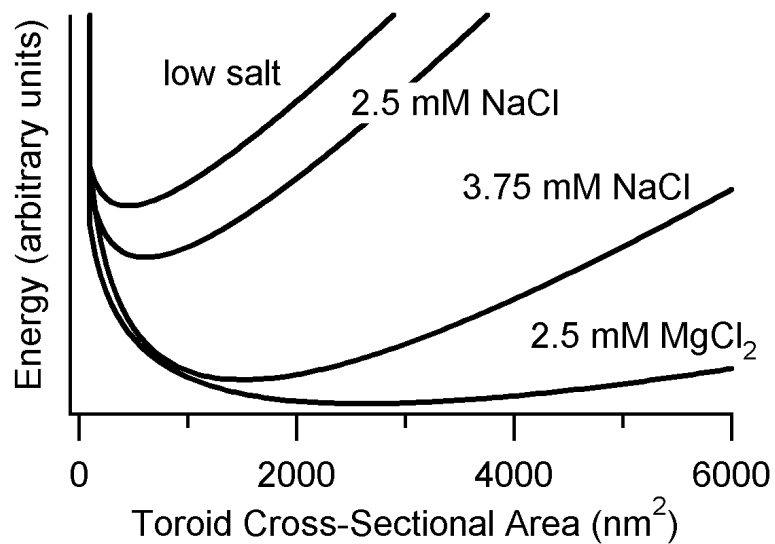


Figure 2.5. Plots of energy potential as a function of toroid cross-sectional area for *3kbDNA* condensed in various salt solutions. Probability distributions of toroid cross-sectional areas were calculated using data shown in Figure 3 and by assuming a circular cross-section for toroids. The resulting distributions were fit with asymmetrical χ^2 distribution functions and converted to potential energy curves using the Boltzman equation. The vertical energy scale for all curves is the same, however, units are not given because the absolute energy, and energy difference between curves could not be determined.

(Figure 2.5). These energy potential curves illustrate how the shape and the minimum of the toroid cross-sectional area potential change with added salt. It may be fruitful to test present and future theoretical models of DNA toroid growth limits and DNA condensate bundle size for quantitative agreement with these potential energy curves.

2.3 Concluding Remarks

We have demonstrated that both nucleation loop size and solution conditions (e.g. ionic strength) play significant roles in determining DNA toroid dimensions. We have also presented models that suggest how toroid nucleation and growth are affected by ionic strength. The data presented here should prove to be of value as a test for future theories for the physical origin of limitations on DNA toroid formation and growth. Finally, our results illustrate that by using static structures and specific solution conditions, the diameter and thickness of toroidal DNA condensates produced *in vitro* can be controlled continuously over a range of values that extends at least a factor of two.

References

1. Gosule, L. C., and Schellman, J. A. (1976) *Nature* 259, 333-335.
2. Allison, S. A., Herr, J. C., and Schurr, J. M. (1981) *Biopolymers* 20, 469-488.
3. Yoshikawa, Y., Yoshikawa, K., and Kanbe, T. (1999) *Langmuir* 15, 4085-4088.
4. Richards, K. E., Williams, R. C., and Calendar, R. (1973) *Journal of Molecular Biology* 190, 255-259.
5. Klimenko, S., Tikchonenko, T., and Andreev, V. (1967) *Journal of Molecular Biology* 23, 523-533.
6. Hud, N. V., Allen, M. J., Downing, K. H., Lee, J., and Balhorn, R. (1993) *Biochemical and Biophysical Research Communications* 193, 1347-1354.
7. Hud, N. (1995) *Biophysical Journal* 69, 1355-1362.
8. Earnshaw, W. C., King, J., Harrison, S. C., and Eiserling, F. A. (1978) *Cell* 14, 559-568.
9. Wagner, E., Cotten, M., Foisner, R., and Birnstiel, M. (1991) *Proceedings of the National Academy of Science* 88, 4255-4259.
10. Kwoh, D., Coffin, C. C., Lollo, C. P., Jovenal, J., Banaszczyk, M. G., Mullen, P., Phillips, A., Amini, A., Fabrycki, J., Bartholomew, R., Brostoff, S. W., and Carlo, D. J. (1999) *Biochimica et Biophysica Acta* 1444, 171-190.
11. Bloomfield, V. A. (1991) *Biopolymers* 31, 1471-1481.
12. Ubbink, J., and Odjik, T. (1995) *Biophysical Journal* 68, 54-61.
13. Vasilevskaya, V. V., Khokhlov, A. R., Kidoaki, S., and Yoshikawa, K. (1997) *Biopolymers* 41, 51-60.

14. Park, S. Y., Harries, D., and Gelbart, W. M. (1998) *Biophysical Journal* 75, 714-720.
15. Ha, B. Y., and Liu, A. J. (1999) *Europhysics Letters* 46, 624-630.
16. Ray, J., and Manning, G. S. (2000) *Macromolecules* 33, 2901-2908.
17. Sakaue, T., and Yoshikawa, K. (2002) *Journal of Chemical Physics* 117, 6323-6330.
18. Shen, M., Downing, K., Balhorn, R., and Hud, N. (2000) *Journal of the American Chemical Society* 122, 4833-4834.
19. Lu, Y., Weers, B., and Stellwagen, N. C. (2002) *Biopolymers* 61, 261-275.
20. Rivetti, C., Walker, C., and Bustamante, C. (1998) *Journal of Molecular Biology* 280, 41-59.
21. Baumann, C. G., Bloomfield, V. A., Smith, S. B., Bustamante, C., and Wang, M. D. (2000) *Biophysical Journal* 78, 1965-1978.
22. Hud, N. V., Downing, K. H., and Balhorn, R. (1995) *Proceedings of the National Academy of Sciences of the United States of America* 92, 3581-3585.
23. Widom, J., and Baldwin, R. L. (1980) *Journal of Molecular Biology* 144, 431-453.
24. Arscott, P. G., Li, A.-Z., and Bloomfield, V. A. (1990) *Biopolymers* 30, 619-630.
25. Hud, N. V., and Downing, K. H. (2001) *Proceedings of the National Academy of Sciences of the United States of America* 98, 14925-14930.
26. Schurr, J. M., and Schmitz, K. M. (1986) *Annual Review of Physical Chemistry* 37, 271-305.
27. Bloomfield, V. A., Crothers, D. M., and Tinoco, I., Jr. (2000) *Physical Chemistry of Nucleic Acids*, Harper and Row, New York.

28. Porschke, D. (1986) *Journal of Biomolecular Structure and Dynamics* 4, 373-389.
29. Hagerman, P. J. (1988) *Annual Review of Biophysical Chemistry* 17, 265-286.
30. Noguchi, N., and Yoshikawa, K. (2000) *Journal of Chemical Physics* 113, 854-862.

CHAPTER 3

MgCl₂ ENHANCES CLUSTER FORMATION BY NANOSCALE TOROIDIAL DNA CONDENSATES

As described in the previous chapter, understanding the factors that control the size of DNA condensates, specifically toroids, has been of interest in both experimental and theoretical studies of DNA condensation (1-4). Studies presented in Chapter 2 provide evidence that variations in ionic strength of the condensate solution can lead a 2-fold increase in the size of toroidal condensates (5). In this chapter, we will further investigate the effects of changes in ionic strength on the morphology and degree of aggregation of DNA toroids. We show that toroid formation from DNA solutions containing MgCl₂ is distinct from that observed for DNA solutions containing only monovalent cations. In particular, MgCl₂ causes significant changes in toroid size and cluster formation by toroids, as observed by transmission electron microscopy (TEM). A comparison of toroid dimensions from several preparations reveals that, at equal ionic strength, toroids formed in the presence of divalent cations are of similar size to those of monovalent cations, although cluster formation is much greater in the case of divalent cations.

3.1 Experimental Procedures

DNA Preparation. A 2961 bp plasmid, Bluescript II SK-, was grown in DH5 α cells (Life Technologies). The plasmid DNA was isolated and purified using the Qiagen Maxi Prep kit. The endonuclease Hind III (New England Biolabs) was used to linearize the plasmid by digestion at a single site. Buffers and salts introduced for the restriction digest were removed by rinsing the DNA at least 5 times with 0.25 \times TE using Microcon YM-30 spin columns (Amicon). The DNA was eluted from the column in 0.25 \times TE and diluted to a concentration of 20 μ g/ml. Concentrations were verified by spectrophotometrically.

Three stock solutions were prepared of the linear Bluescript II SK- plasmid DNA: a low salt solution in 1 \times TE (10 mM Tris base, pH 7.8, 1 mM EDTA), a 15 mM NaCl solution and a 7.5 mM MgCl₂ solution. The final solutions all contained 17 μ g/ml DNA in 1 \times TE. Intermediate salt concentrations were prepared by mixing the low salt solution with either the NaCl stock solution or the MgCl₂ stock solution in specific ratios.

DNA Condensation. DNA was condensed in the presence of an equal volume of hexamine cobalt (III) chloride (Sigma). The solution was mixed thoroughly. Final condensate solutions contained 8.5 μ g/ml of DNA and 0.5 \times the salt/buffer of the original DNA sample, as well as 100 μ M of hexamine cobalt (III). Condensation mixtures were allowed to react for 5 minutes.

Electron Microscopy Sample Preparations and Analysis. Five microliters of the reaction mixture was deposited on carbon-coated grids (Ted Pella) and allowed to settle for 10 minutes. The grids were stained with 2% uranyl acetate (Ted Pella), rinsed in 95%

ethanol and air-dried. Data was collected using the JEOL-100C transmission electron microscope (TEM) at a magnification of 100,000 \times . Negatives were scanned at 300 pixels/inch and analyzed using a graphics program, which allowed for toroid dimensions to be measured and recorded.

3.2 Results and Discussion

A linear 3kb bacterial plasmid DNA was condensed with hexamine cobalt (III) under several salt conditions (Experimental Procedures). The condensates produced for samples containing a range of MgCl₂ concentrations were closely examined by TEM to investigate the possible effects of divalent cations on the condensation process. As shown in Figure 3.1, DNA condensed by hexamine cobalt (III) in the presence of MgCl₂ from 1.0 mM to 2.5 mM produces toroidal condensates around 100 nm in outer diameter. The outer diameter of a toroid was measured as the distance between the outer edges of a toroid for a line that passes through the toroid center. Most toroids are associated into small clusters for samples containing 1.0 mM MgCl₂, with very few single toroids observed in such preparations. At 1.75 mM MgCl₂ toroids are also clustered and appear to be larger in outer diameter than the 1.0 mM MgCl₂ toroids. It is difficult to determine quantitatively the change in toroid size between 1.0 mM and 1.75 mM MgCl₂ due to the degree of aggregation. However, there does appear to be a difference in either the morphology of the clusters of these two samples, or in the way in which the clusters attach to the EM grids. At 1.75 mM MgCl₂, contacts between toroids of a cluster appears to be predominantly between flanking toroids in a 2D assembly of toroids, whereas in the

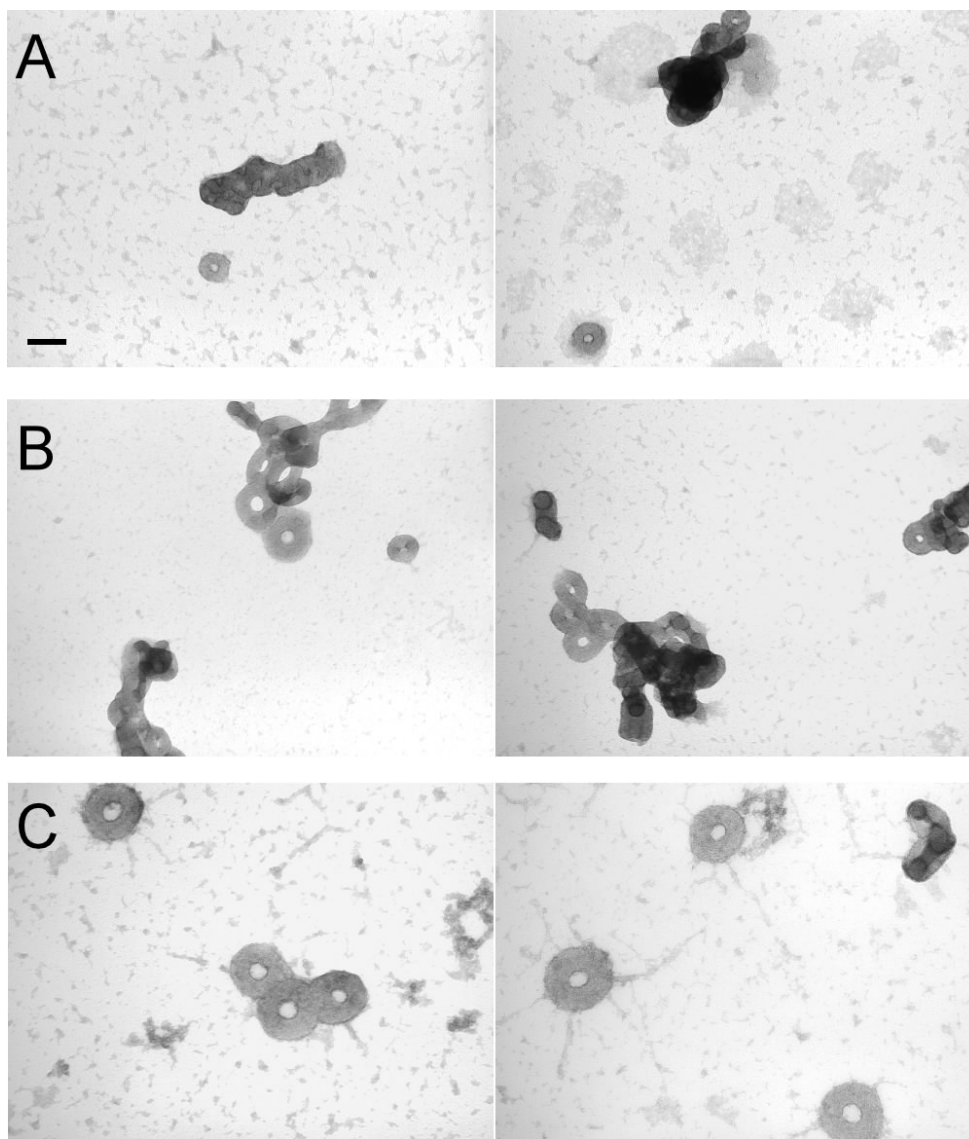


Figure 3.1. Transmission Electron Microscope (TEM) images of linear 3kb DNA condensed with hexamine cobalt (III) in the presence of MgCl_2 . Buffers for all DNA solutions were $0.5\times$ TE (5 mM Tris, pH 7.8, 0.5 mM EDTA), plus added MgCl_2 . (A) DNA condensates formed in the presence of 1.0 mM MgCl_2 . (B) Condensates formed in the presence of 1.75 mM MgCl_2 . (C) DNA condensates formed in the presence of 2.5 mM MgCl_2 . For all samples the DNA concentration was $8.5 \mu\text{g/ml}$, and hexamine cobalt (III) concentration was $100 \mu\text{M}$. All images are shown at the same magnification. Scale bar is 100 nm.

1.0 mM MgCl₂ sample toroids more often appear to be stacked upon each other in a 3D arrangement (Figures 3.1A and B).

A further increase in MgCl₂ concentration to 2.5 mM produces a shift in toroid size from the lower MgCl₂ concentration samples, which can be readily appreciated in the TEM images (Figure 3.1C). As another means of comparison, in Figure 3.2 histograms of toroid outer diameter are compared for toroids prepared in the presence of 1.75 mM MgCl₂ and 2.5 mM MgCl₂, respectively. The average outer diameter of DNA toroids increased approximately 50 nm, from 107 nm to 158 nm, with the increase in MgCl₂ concentration from 1.75 mM to 2.5 mM MgCl₂. In addition to increased outer diameters, a decrease in aggregation was observed. Single toroids were the primary structures in the 2.5 mM MgCl₂ condensate preparations, although some small clusters of toroids were still present. Another difference in the 2.5 mM MgCl₂ sample condensate preparation was that small fiber-like DNA structures were seen protruding from the outsides of toroids (Figure 3.1C). This could indicate that the DNA of toroids produced in the presence of 2.5 mM MgCl₂ is not fully condensed. When the MgCl₂ concentration of the DNA condensation reaction was increased above 3 mM, toroids were no longer observed to be the dominant condensate structure. The condensed DNA that was observed on the TEM grids for the 2.5 mM MgCl₂ preparations was part of fiber-like network of DNA (data not shown).

In order to determine if the observed effects of MgCl₂ on DNA condensation are primarily the result of ionic strength, as opposed to cation species, DNA condensates were also prepared in the presence of NaCl at various concentrations, including

concentrations that correspond to the ionic strength of the MgCl_2 samples (Experimental Procedures).

Toroids formed in the NaCl solution are very similar in outer diameter to those formed under equal ionic strength MgCl_2 conditions (Figure 3.2). Furthermore, for both NaCl and MgCl_2 samples, DNA toroid outer diameters increase with ionic strength (Figures 3.1 and 3.3). However, condensates prepared in the presence of MgCl_2 are much more prone to cluster formation than condensates formed in the presence of NaCl . For example, a DNA solution containing 3.75 mM NaCl is approximately equal in ionic strength to the 1.75 mM MgCl_2 sample (when the chelating effect of the 0.5 mM EDTA is taken into account), yet the formation of clusters in the latter sample is clearly more pronounced (Figures 3.1 and 3.3). Thus, the difference observed in cluster formation (i.e. aggregation) by toroidal condensates formed in the presence of these two different cations is principally an effect of the specific cation species, rather than ionic strength.

We have shown that the size of toroids formed by the condensation of DNA in the presence of NaCl and MgCl_2 , respectively, is similar for solutions of equal ionic strength. However, cluster formation and aggregation by DNA toroids is greatly enhanced in the presence of Mg^{2+} . Previous studies have shown that divalent cations in aqueous solution at room temperature are not capable of condensing DNA into high-density nanoscale structures (2, 6, 7). Nevertheless, the higher charge density of Mg^{2+} is expected to increase the local concentration of cations around DNA in solution, due to the valency dependence of counter ion condensation around a polyvalent ion (i.e. DNA) (8). Although Mg^{2+} cannot neutralize the negative charge of DNA to the point where condensation occurs, divalent cations could be providing additional shielding between

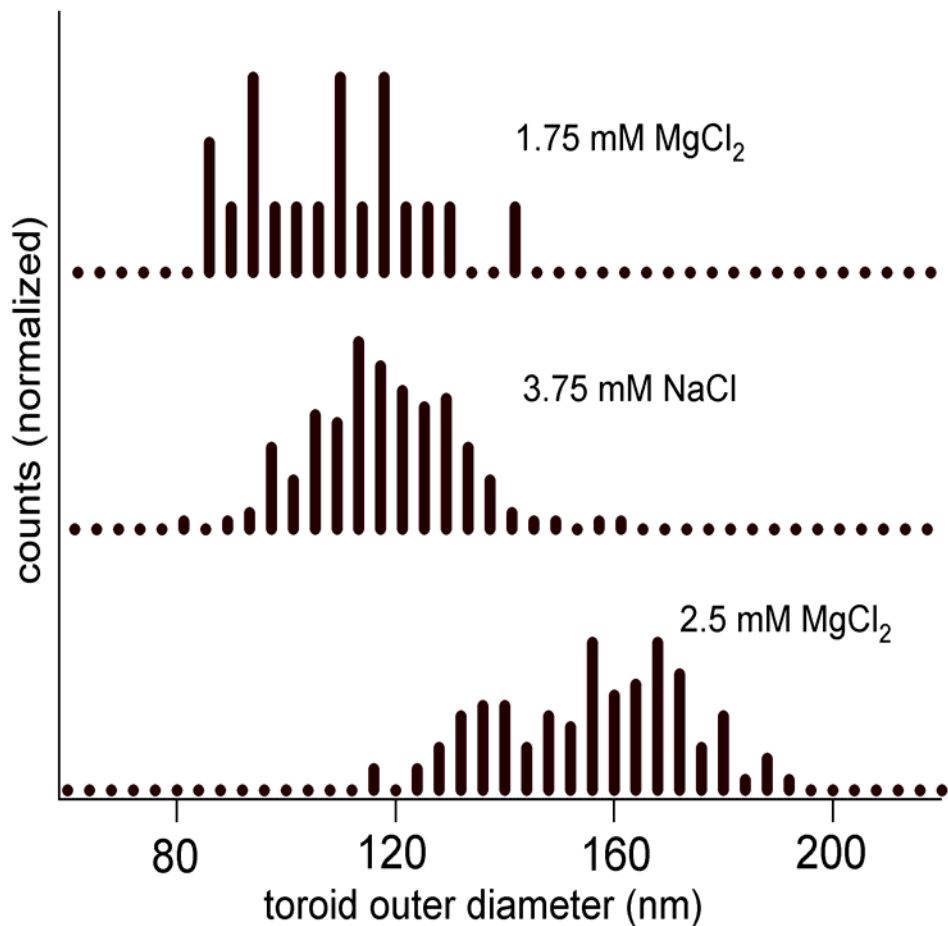


Figure 3.2. Histograms of toroid outer diameter for toroids formed in presence of three different salt conditions. All condensation reactions had final concentrations of 8.5 $\mu\text{g/ml}$ DNA and 100 μM hexamine cobalt (III) in 0.5 \times TE, additional salts present during DNA condensation for the particular samples are indicated to the right of the histograms.

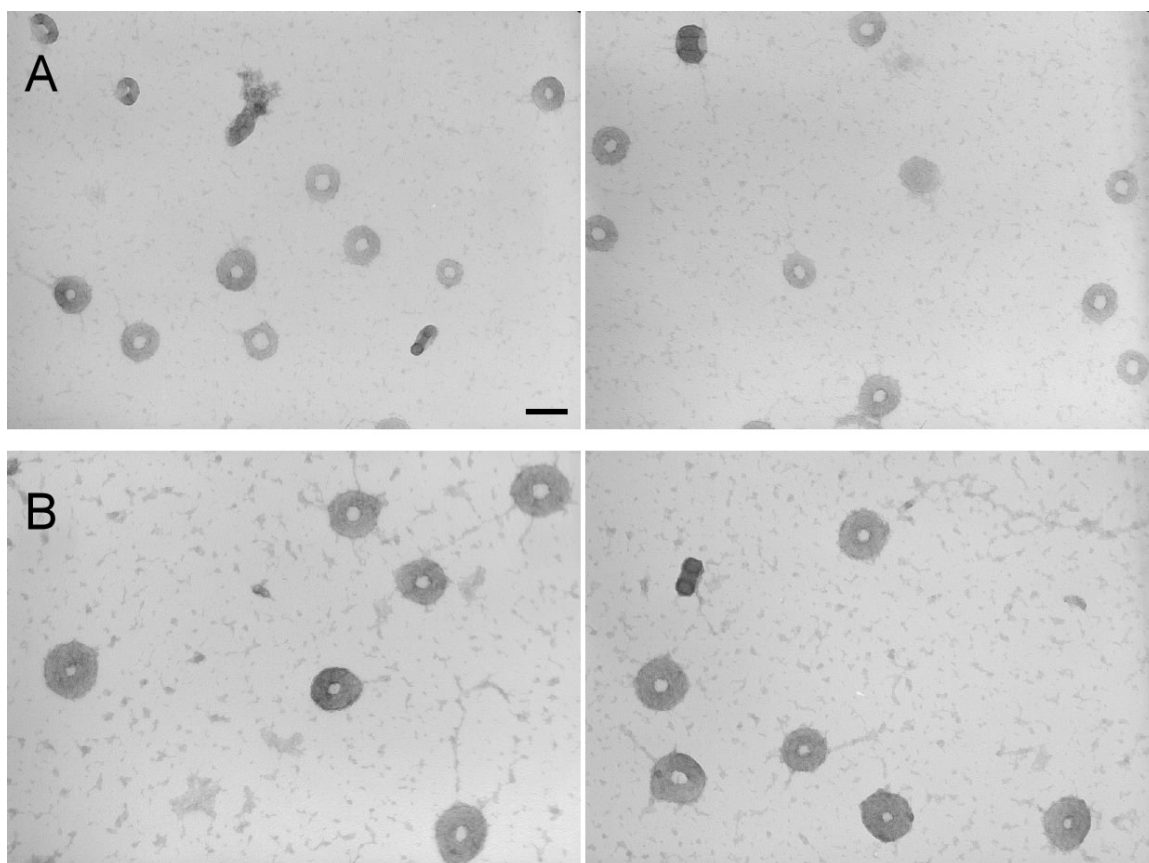


Figure 3.3. TEM images of toroids formed in the presence of NaCl at ionic strengths similar to the MgCl₂ preparations. 8.5 μg/ml of linear plasmid DNA was condensed with an equal volume of 100 μM hexamine cobalt (III) in 0.5×TE. (A) Toroids formed when DNA was condensed in the presence of 2.5 mM NaCl. (B) Toroids formed when DNA was condensed in the presence of 3.75 mM NaCl. The 3.75 mM NaCl sample is approximately equal in ionic strength to the 1.75 mM MgCl₂ sample, when the chelating effect of the EDTA is considered. Scale bar is 100nm.

DNA molecules during condensation. This may facilitate the aggregation of fully formed DNA toroids. Alternatively, Mg^{2+} may allow DNA molecules to become more entangled during the toroid formation process, which then leads the formation of toroids that share DNA strands, and thus appear as clusters (9, 10).

These results suggest a complex interplay between the condensing agent and other cations in a condensation reaction. Further investigation is necessary to determine how exactly DNA condensation is affected by variations in solution conditions. Understanding effects of ionic strength on condensates is important not only for gaining an understanding of *in vivo* condensation, but also for optimizing condensation for gene delivery under physiological conditions.

References

1. Bloomfield, V. A. (1991) *Biopolymers* 31, 1471-1481.
2. Bloomfield, V. (1996) *Current Opinion in Structural Biology* 6, 334-341.
3. Park, S. Y., Harries, D., and Gelbart, W. M. (1998) *Biophysical Journal* 75, 714-720.
4. Nguyen, T. T., and Shklovskii, B. I. (2002) *Physical Review E* 65, 031409-1-031409-7.
5. Conwell, C. C., Vilfan, I. D., and Hud, N. V. (2003) *Proceedings of the National Academy of Sciences of the United States of America* 100, 9296-9301.
6. Widom, J., and Baldwin, R. L. (1980) *Journal of Molecular Biology* 144, 431-453.
7. Bloomfield, V. (1997) *Biopolymers* 44, 269-282.
8. Manning, G. S. (1978) *Quarterly Reviews of Biophysics* 11, 179-246.
9. Revet, B., and Fourcade, A. (1998) *Nucleic Acids Research* 26, 2092-2097.
10. Dahlgren, P. R., and Lyubchenko, Y. L. (2002) *Biochemistry* 41, 11372-11378.

CHAPTER 4

EVIDENCE THAT BOTH KINETIC AND THERMODYNAMIC FACTORS GOVERN DNA TOROID DIMENSIONS

Over the past several years theoreticians have provided an in depth view of the attractive potential that causes DNA to condense in the presence of multivalent cations (1-3). However, uncovering the factors that govern DNA toroid size (i.e. thickness and diameter) has proven to be particularly challenging, especially because both thermodynamic and kinetic factors can contribute to limits on toroid growth. Under conditions of DNA condensation where there remains a free exchange of DNA strands between individual particles, the condensed DNA will eventually reach a thermodynamic equilibrium. In this situation, the size of DNA condensates should ultimately be determined by the buildup of a net electrostatic charge on each particle that is due to imperfect charge compensation between DNA and bound multivalent cations (4-12). However, under conditions where condensed DNA strands are not free to exchange between particles once condensation has initiated, particle size can be governed by the kinetics of condensation, which can in turn depend on salt conditions and DNA concentration (13-15).

We recently demonstrated that DNA toroid size increases substantially if the NaCl concentration in a DNA solution is increased from 1 to 10 mM, prior to condensation with hexamine cobalt(III) (15). At low ionic strengths, condensates produced in the presence of MgCl₂ showed an increase in toroid size similar to the

increase observed in samples containing NaCl at approximately the same ionic strength. We observed a further increase in mean toroid diameter for samples containing higher concentrations of MgCl₂ that could not be attributed solely to ionic strength, as a solution containing NaCl at the same ionic strength did not exhibit the same increase (15). Thus, at very low ionic strength, monovalent and divalent cations can have a similar influence on the formation of toroidal condensates. However, as ionic strength increases, cation valency also becomes an important parameter in determining condensate size. To the best of our knowledge, no other studies have systematically investigated the effects of salt concentrations below 10 mM on the formation of DNA toroids. It is somewhat surprising that such a fundamental parameter of DNA condensation was not previously investigated in detail, particularly since we have found millimolar changes in ionic strength to have a profound effect on the size of DNA condensates. Understanding the effects of ionic strength and cation valency on DNA condensation is important for the preparation of DNA for gene delivery, as DNA particles are typically exposed to various salt conditions as they are condensed, encapsulated and incorporated into cells. Additionally, such studies are valuable for elucidating the factors that govern toroid size under commonly used laboratory protocols for DNA condensation.

To further investigate the effects of Mg(II) on DNA condensation, we prepared a series of DNA condensation reactions in which the order of MgCl₂ addition was varied. These condensation reactions were carried out at both 22 and 37°C. The effects of sample dilution after condensation were also explored to determine how varying the absolute, but not relative, concentration of different cations in the solution affects the integrity of DNA condensates. Transmission electron microscopy studies reveal the extent to which

variations in the condensate structures are affected by the presence of Mg(II), particularly whether Mg(II) is associated with the DNA prior to condensation or if it is added to the DNA concurrently with hexamine cobalt(III). Analyses of the observed effects of Mg(II) on particle size and morphology have allowed the development of models for the process of DNA toroid formation that illustrate how both kinetic and thermodynamic factors can determine toroid size.

4.1 Experimental Procedures

DNA Preparation. Bluescript II SK- plasmid DNA (Stratagene, La Jolla, CA) was isolated from the *E. coli* cell line DH5 α (Life Technologies, Carlsbad, CA) using the Qiagen Maxi Prep kit (Valencia, CA). The DNA was eluted in 1 \times TE (10 mM Tris base, pH 7.8, 1 mM EDTA). All DNA used was linearized by the restriction endonuclease *Hind* III (New England Biolabs, Beverly, MA), which singly cuts Bluescript II SK-. The DNA was rinsed through Microcon YM-30 spin columns (Millipore, Bedford, MA) at least five times with 0.25 \times TE to remove the buffer and salt from the restriction digest. The DNA was eluted from the spin column membrane to a final concentration of 20 μ g/ml in 0.25 \times TE. Concentrations of DNA were verified spectrophotometrically. The DNA was prepared as two stock solutions: a low salt solution in 1 \times TE, and solution containing 7.5 mM MgCl₂ in 1 \times TE.

Preparation of Condensation Solutions. DNA in solution was condensed by mixing with an equal volume of 200 μ M hexamine cobalt chloride (Sigma, St. Louis, MO). Condensates were prepared such that MgCl₂ was introduced at three different stages of

the condensation process: 1) DNA in solution with 3.5 mM MgCl₂ was condensed with hexamine cobalt chloride (pre-association of Mg(II)); 2) DNA was condensed with a hexamine cobalt chloride solution that contained 3.5 mM MgCl₂ (concurrent addition of MgCl₂); and 3) MgCl₂ was added after the DNA was condensed with hexamine cobalt chloride in the absence of MgCl₂ (low salt conditions). In all cases, DNA was allowed to condense for 5 minutes after mixing with the hexamine cobalt chloride solution. An aliquot was removed from the condensation reaction for examination by transmission electron microscopy (TEM). The remaining solution was diluted two-fold with dH₂O, for samples in which MgCl₂ was already present, or with 1.75 mM MgCl₂ for the DNA condensates prepared in the absence of MgCl₂. These samples were allowed to equilibrate for an additional 10 minutes after dilution. The three diluted condensate solutions were identical in composition, at 5 µg/ml DNA, 50 µM hexamine cobalt chloride, and 0.87 mM MgCl₂.

Transmission Electron Microscopy (TEM). Condensation mixtures were deposited on carbon coated EM grids (Ted Pella, Redding, CA) and allowed to settle for 10 minutes. EM grids were stained by the addition of 2% uranyl acetate (Ted Pella) directly to the grid, then rinsed in 95% ethanol and air-dried. Condensation reactions and grid preparations were performed at 22 and 37°C. Images of the condensates were collected on film using a JEOL-100C transmission electron microscope. All images were collected at 100,000× magnification.

4.2 Results

Condensation is directly affected by the presence of MgCl_2 . The morphology, size and degree of aggregation of DNA condensates were examined as a function MgCl_2 being added at different points during the condensation process. Under the first experimental conditions, a linear 3 kb DNA was condensed by hexamine cobalt chloride in the absence of MgCl_2 . Condensates were produced by mixing a 20 $\mu\text{g/ml}$ DNA solution in a low salt buffer (1 \times TE, pH 7.8) with an equal volume of 200 μM hexamine cobalt chloride. These conditions will be referred to as “low salt” condensation. The majority of the particles observed by TEM were well-defined toroids, although rods were occasionally observed (Figure 4.1A). The toroids in these preparations have a mean outside diameter of 77 nm and a hole diameter of 21 nm. These measurements are typical of toroids produced by the condensation of DNA from a low salt solution (15, 16).

In the second protocol, a 20 $\mu\text{g/ml}$ DNA solution containing MgCl_2 (3.5 mM MgCl_2 ; 1 \times TE, pH 7.8) was mixed with an equal volume of 200 μM hexamine cobalt chloride. This condensation reaction produced toroidal structures that were predominately associated within small aggregates, typically containing three to ten toroids (Figure 4.1B). Additionally, toroids within these aggregates appear larger than those observed in the low salt preparation that contained no divalent cations.

In the third condensation protocol, low salt DNA was condensed by mixing with an equal volume of solution containing both 200 μM hexamine cobalt chloride and 3.5 mM MgCl_2 . The resulting condensates were toroid-like structures, but were dissimilar from any DNA toroids we had previously observed. These “super toroids”, as we will

refer to these particular condensates, were approximately three times larger than toroids observed under low salt conditions and often had angular features that are not generally observed in toroidal DNA structures; some even exhibit five distinct edges and a pentagonal shape (Figure 4.1C). TEM images also revealed variations in the intensity of the super toroids, suggesting that DNA packing was not uniform throughout these particles. To the best of our knowledge, such structures have not been previously reported.

In order to determine which differences between the low salt condensates (Figure 1A) and the condensates prepared in the presence of MgCl_2 (Figures 4.1B and 4.1C) are due to equilibrium versus non-equilibrium effects of MgCl_2 on DNA condensation, the three condensation reactions described above were diluted with either an equal volume of 1.75 mM MgCl_2 (for the low salt sample) or dH_2O (for the samples containing MgCl_2) so that the final composition of all three samples were identical (Experimental Procedures). The thickness and outside diameter of the toroids prepared in the absence of MgCl_2 (i.e. low salt toroidal condensates) increased slightly upon the addition of MgCl_2 (mean thickness of 28 nm and mean diameter of 78 nm increased to 32 nm and 90 nm, respectively) (Figure 4.2A). An increase in toroid aggregation was also observed. Although many of the toroids within these small aggregates remained as distinct toroids, it was evident that there were some regions where the DNA strands of the toroids were intertwined with each other (Figure 4.2A), similar to those produced when MgCl_2 was pre-associated with DNA (Figure 4.1B).

The samples containing MgCl_2 at the time of DNA condensation, either pre-associated with DNA (Figure 4.1B) or added concurrently with hexamine cobalt

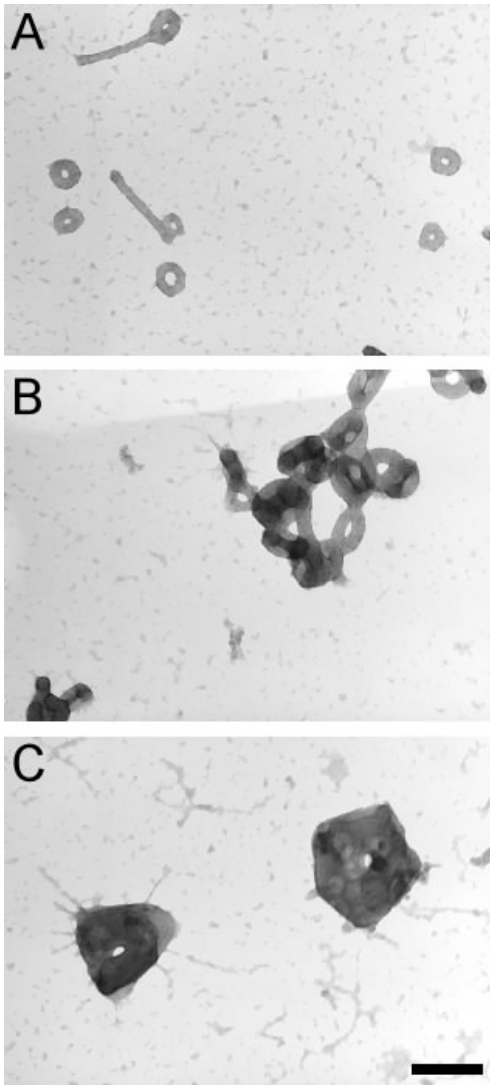


Figure 4.1. Transmission electron microscopy (TEM) images of DNA condensates formed at 22°C by the addition of hexamine cobalt chloride. (A) DNA condensed from a low salt solution (1× TE) by mixing with 200 μM hexamine cobalt chloride. (B) DNA condensed from a solution of 3.5 mM MgCl₂, 1× TE by mixing with 200 μM hexamine cobalt chloride. (C) DNA condensed from a low salt solution by mixing with 200 μM hexamine cobalt chloride, 3.5 mM MgCl₂. DNA was linearized pBluescript II SK- at a final concentration of 10 μg/ml. Scale bar is 200nm.

chloride (Figure 4.1C), were diluted with dH₂O to produce solutions identical in chemical composition to the low salt condensates after dilution with a MgCl₂ solution. A comparison between the condensates of Figure 4.1B with those of Figure 4.2B, as well as those of Figure 4.1C with those of Figure 4.2C, illustrates the effect of diluting hexamine cobalt(III) and Mg(II) by a factor of two, after DNA has been condensed. The similarities between the same samples before and after dilution indicate that condensate size and morphology were essentially unchanged by dilution.

The DNA condensates shown in Figure 4.2 are from three solutions of identical chemical composition. Thus, any differences observed between these DNA condensates are purely the result of the *order* in which Mg(II) was added to each sample with respect to hexamine cobalt(III). It is clear from these images that the overall morphology and particle size of DNA condensates is largely determined by a non-equilibrium process, which is substantially altered by the presence of Mg(II).

It is important to note that the DNA used in the present study was linearized by *Hind* III, an endonuclease that produces a staggered cut with a four base overhang (i.e. sticky ends). Previous studies have shown that divalent cations increase the association of sticky ends in solution, and thereby enhance the formation of DNA concatamers (17, 18). To investigate the possibility that concatenation by end association causes toroid aggregation in samples pre-associated with Mg(II), the same DNA used in this study was linearized with the blunt-end cutting endonuclease *Sca* I (New England Biolabs) and then condensed using protocols identical to the pre-associated Mg(II) sample. The toroids produced by these experiments closely resembled those produced by DNA cut with *Hind*

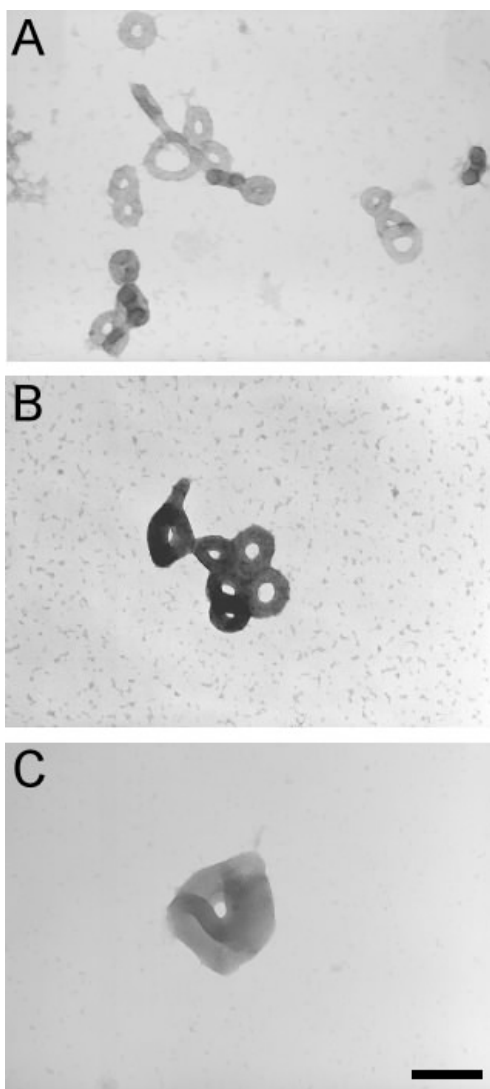


Figure 4.2. TEM images of DNA condensed at 22°C by the addition of 200 μM hexammine cobalt chloride, followed by dilution with either dH_2O or a MgCl_2 solution. (A) DNA condensates produced under low salt conditions (1 \times TE) followed by dilution with an equal volume of 1.75 mM MgCl_2 . (B) DNA condensed from a solution of 3.5 mM MgCl_2 , 1 \times TE by mixing with hexammine cobalt chloride, followed by dilution with an equal volume of dH_2O . (C) DNA condensed from a low salt solution by mixing with hexammine cobalt chloride, 3.5 mM MgCl_2 , followed by dilution with an equal volume of dH_2O . Scale bar is 200 nm.

III (data not shown). Thus, the aggregation of toroids produced by the condensation of *Hind* III-digested DNA cannot be attributed to the presence of sticky ends.

A Small Temperature Increase Can Alter Condensate Size and Morphology. To gain additional insight into the origin of Mg(II) effects on DNA condensation, the condensation reactions described above were also performed at 37°C. Toroids formed under low salt conditions at 37°C are similar to the low salt toroids formed at 22°C in that the vast majority of toroids observed were single toroids (Figure 4.3A). However, toroids formed under low salt conditions at 37°C are thicker than those formed at 22°C (mean thickness of 35 nm vs. 28 nm), and have a larger outside diameter (mean diameter of 87 nm vs. 77 nm) (Figure 4.3A).

An equal volume of 1.75 mM MgCl₂ was added to the low salt condensates formed at 37°C, with all solutions being constantly maintained at 37°C, to bring the reaction mixture to the same chemical composition as the diluted DNA condensate solutions prepared at 22°C. This addition of divalent cations, along with sample dilution, did not alter the size of the condensates significantly and no additional aggregation was observed (Figure 4.4A). These results differ from those at 22°C, where variations in particle size and degree of aggregation were observed upon the addition of MgCl₂ (Figure 4.2A).

Small aggregates of toroids were almost exclusively observed when DNA pre-associated with Mg(II) was condensed at 37°C (Figure 4.3B), as was the case for DNA condensation by the same protocol at 22°C (Figure 4.1B). However, the DNA of toroids produced at 37°C was not as well condensed as the DNA of toroids produced at 22°C. All

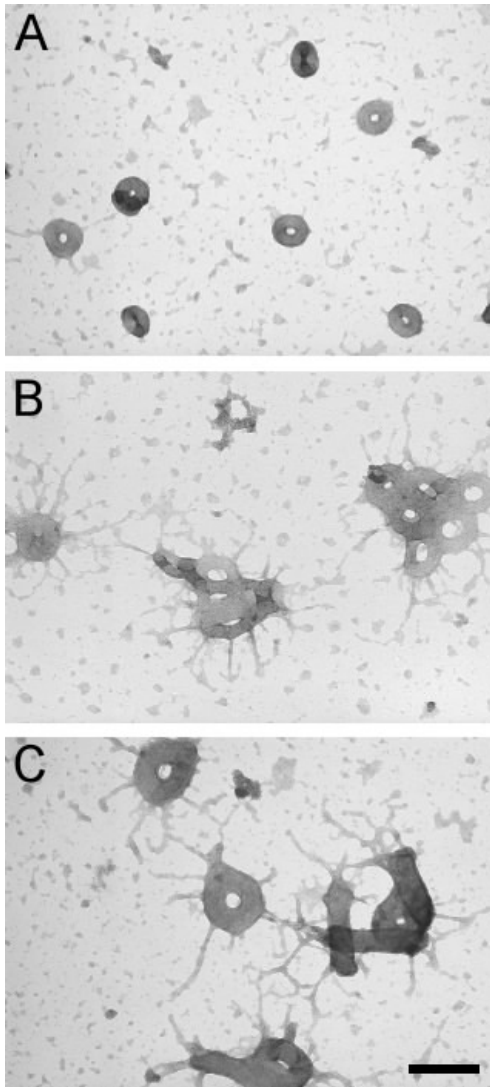


Figure 4.3. TEM images of DNA condensates formed at 37°C by the addition of hexammine cobalt chloride. (A) DNA condensed from a low salt solution (1× TE: 10 mM Tris, 1.0 mM EDTA) by mixing with 200 μM hexammine cobalt chloride. (B) DNA condensed from a solution of 3.5 mM MgCl₂, 1× TE by mixing with 200 μM hexammine cobalt chloride. (C) DNA condensed from a low salt solution by mixing with 200 μM hexammine cobalt chloride, 3.5 mM MgCl₂. Scale bar is 200 nm.

toroids formed at 37°C from DNA pre-associated with Mg(II) have DNA fibrils extending in a radial fashion (Figure 4.3B). This less- condensed state of DNA is a combined result of an increase in temperature and the presence of Mg(II) during condensation, as toroids formed at 37°C in the absence of Mg(II) (Figure 4.3A) or toroids formed at 22°C in the presence of Mg(II) (Figure 4.1B) did not exhibit appreciable DNA fibrils.

A two-fold dilution with dH₂O produced a dramatic change in the DNA condensates formed at 37°C from DNA pre-associated with Mg(II) (Figure 4.4B). The DNA fibrils protruding from toroids in these samples completely disappear upon dilution (Figure 4.4B). However, toroids remain locked in small aggregates. These observations suggest that the DNA fibrils extending from toroids, prior to dilution, condense onto toroids upon sample dilution (Figure 4.2B).

The effects of increased temperature were most obvious for condensates produced when DNA in the low salt buffer was condensed by the concurrent addition of hexamine cobalt chloride and MgCl₂ at 37°C (Figure 4.3C). The condensates produced by this protocol at 37°C were more typical than the super toroids produced by the same protocol at 22°C (Figure 4.1C). The TEM images also revealed a marked increase in the quantity of DNA fibrils protruding from these toroids (Figure 4.3C), which were essentially absent from the super toroids produced at 22°C (Figure 4.1C). The appearance of fibrils when DNA was condensed at 37°C by the concurrent addition of hexamine cobalt chloride and MgCl₂ again indicates that both Mg(II) and increased temperature contribute to the appearance of DNA fibrils.

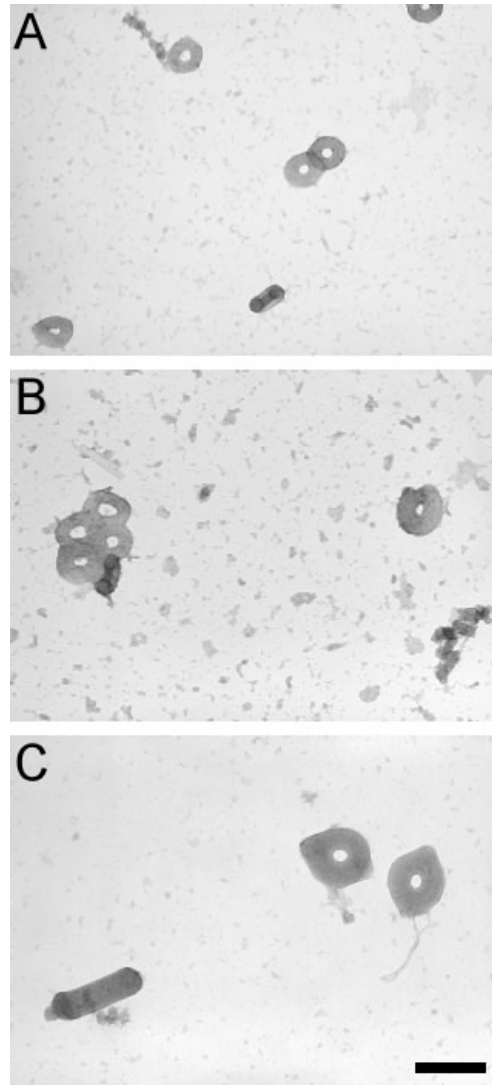


Figure 4.4. TEM images of condensates produced at 37°C by the addition of 200 μM hexamine cobalt chloride to DNA, followed by dilution with either MgCl_2 or dH_2O . (A) Toroids observed from the low salt condensate mixture when diluted with an equal volume of 1.75 mM MgCl_2 . (B) Toroids from condensation of the DNA, 3.5 mM MgCl_2 mix diluted with an equal volume of dH_2O . (C) Toroids condensed from the low salt DNA and the hexamine cobalt chloride, 3.5 mM MgCl_2 mixture. Scale bar is 200 nm.

The DNA of condensates formed at 37°C by the concurrent addition of hexamine cobalt chloride and MgCl₂, followed by dilution with an equal volume of dH₂O, were more completely condensed as indicated by the disappearance of fibrils that extended from toroids prior to dilution (Figures 4.3C and 4.4C). This observation also suggests that dilution facilitates the incorporation of fibrils onto toroids. Condensates produced by the concurrent addition of hexamine cobalt chloride and MgCl₂ remained as individual toroids upon dilution with dH₂O, and were appreciably larger in outer diameter and thickness (Figure 4.4C) than the aggregated toroids produced by the condensation of DNA pre-associated with Mg(II) (Figure 4.4B). Additionally, toroids produced by the concurrent addition of hexamine cobalt chloride and MgCl₂ are less circular than those produced by pre-association with Mg(II), and appear to be pinched at two points approximately 180° from each other (Figure 4.4C). Toroids with these features occurred frequently in our preparations when hexamine cobalt chloride and MgCl₂ were added simultaneously to the low salt DNA at 37°C.

4.3 Discussion

DNA toroid formation is known to be a nucleation-growth phenomenon (15, 19, 20). This implies that toroid size can be governed by both kinetic and thermodynamic factors. If toroid nucleation is rapid (i.e. occurs simultaneously throughout the solution) and association of DNA strands onto a growing toroid is always favorable (e.g. regardless of toroid size), then toroid size will be initially determined by the kinetics of condensation (Figure 4.5A) (21). That is, nucleated toroids will only stop growing when all DNA in the solution is condensed. The more frequently toroid nucleation occurs

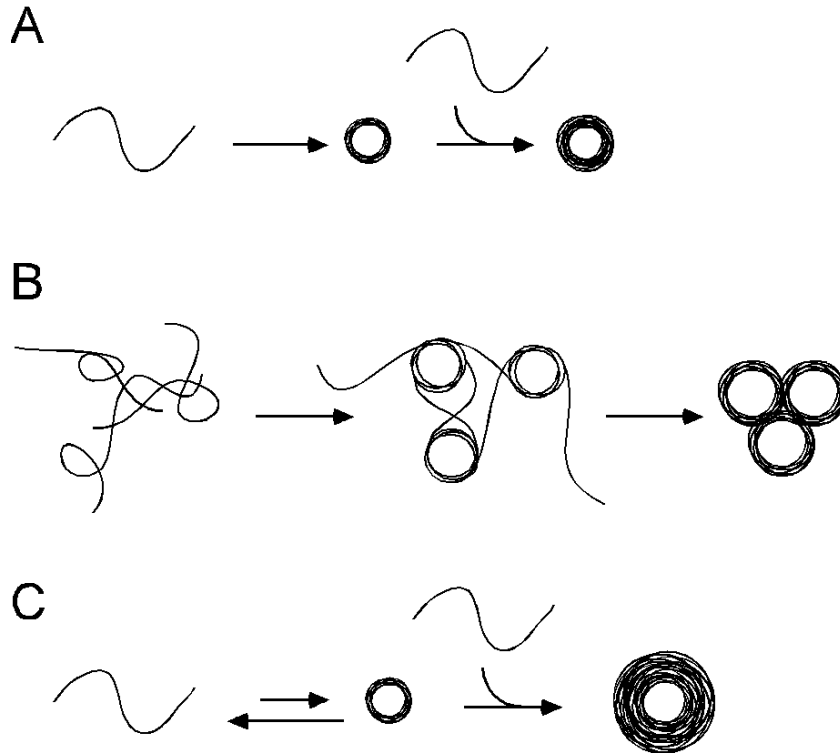


Figure 4.5. Models for the condensation of DNA by hexamine cobalt(III) under various conditions. (A) DNA condensation by a nucleation-growth pathway. DNA is well dispersed in solution and spontaneously forms nucleation loops that are stabilized by the addition of hexamine cobalt (III). The toroid continues to grow until free DNA is depleted from solution. DNA condensation under low salt conditions is expected to follow this pathway. (B) DNA condensation with pre-associated Mg(II). Intra- and intermolecular helix-helix contacts are stabilized by the presence of Mg(II). Upon addition of hexamine cobalt chloride, both forms of helix-helix contacts nucleate DNA condensation, leading to aggregation. (C) DNA condensation from a low salt solution by the concurrent addition of hexamine cobalt chloride and MgCl₂. Without Mg(II) pre-association, DNA is well dispersed in the low salt buffer. Competition between Mg(II) and hexamine cobalt(III) for association with DNA reduces the stability of nucleated toroids. The fewer successfully nucleated toroids grow larger in comparison to condensation in the absence of Mg(II).

within a solution, the smaller the resulting toroids. If DNA strands do not exchange with solution once they have been condensed into toroids, then toroid size will be solely determined by the kinetics of nucleation and growth and the condensed DNA may not represent a minimum energy state.

Under most solution conditions, a net electrostatic charge is expected to accumulate on a DNA toroid as it increases in size because the negative charges of DNA within the toroid will not be perfectly compensated by associated cations (i.e. undercharging) (3-6, 11, 12, 22, 23). If toroid nucleation is slow compared to toroid growth, then the net negative charge of an individual toroid could eventually reach a point at which it is energetically unfavorable for additional DNA to add to the toroid, even though uncondensed DNA remains in solution. In this case undercharging would be the primary physical parameter governing toroid size (24). Even under conditions where the condensation of DNA onto a growing toroid is energetically favorable, undercharging could significantly slow the kinetics of DNA deposition onto the growing toroids and thereby regulate toroid size (11). Under such conditions, toroid size would be governed by both thermodynamic factors and the kinetics of toroid nucleation and growth. If DNA strands remain in equilibrium exchange with solution after their initial condensation into toroids, then the repartitioning of DNA between individual toroids would eventually result in the existence of toroids with dimensions that are under thermodynamic control (11). At very high multivalent cation concentrations it is also theoretically possible that the charges of DNA can be over compensated by multivalent cations such that a net positive charge accumulates on DNA condensate particles (i.e. overcharging), which should likewise lead to a limit on condensate dimensions (3-6, 11, 12, 22, 23). However,

overcharging has only been observed experimentally for double stranded DNA while associated within nucleosome core particles (8, 10).

Low Salt Toroid Size is Kinetically Determined. If toroid size in our low salt DNA solution was limited by undercharging, then undercharging would limit growth at an even earlier stage of toroid formation in the condensation reactions that contain MgCl_2 due to competition between Mg(II) and hexamine cobalt(III) for association with DNA (25, 26). However, it was observed that the toroids of preparations containing MgCl_2 are significantly larger than those of the low salt preparations (Figure 4.1). Thus, DNA undercharging *cannot* be the size-determining factor for the low salt toroids. DNA overcharging can also be ruled out as a limit to toroid growth because the conditions of all condensation reactions of the present study are far from the realm of conditions necessary for overcharging to occur (8, 10). Thus, the size of low salt toroids must be kinetically determined; otherwise the low salt toroids would grow to be at least as large as toroids in the condensation reactions that contained MgCl_2 .

The formation of super toroids by the concurrent addition of MgCl_2 and hexamine cobalt chloride to low salt DNA can be attributed to an alteration in the kinetics of toroid growth by Mg(II) (21). The presence of Mg(II) during the initiation of DNA condensation will reduce the frequency of toroid nucleation because the competition between Mg(II) and hexamine cobalt(III) for DNA will weaken the helix-helix associations that are promoted by hexamine cobalt(III) (25, 26). For certain concentrations of MgCl_2 and hexamine cobalt chloride (e.g. those selected for this study), successful toroid nucleation may only occur when several DNA molecules

simultaneously condense to form a proto-toroid with the minimum number of helix-helix contacts necessary for stability in the presence of Mg(II) (24). With less frequent nucleation, free DNA would be available in solution for a longer time after the initiation of condensation, which would allow the fewer toroids formed to grow to the size of super toroids (Figure 4.5C). This same explanation applies to the positive correlation we have reported between toroid size and NaCl concentration, (15) although the effect is not as dramatic in the case of monovalent cations. It is possible that super toroid size is ultimately limited by undercharging. This possibility is discussed further below in regards to the 37°C data.

The fact that super toroids have holes of similar size to the low salt toroids suggests that super toroids may be nucleated by proto-toroids similar in size to the low salt toroids (Figure 4.1). Unfortunately, it is currently not possible to measure the size of DNA toroids as a function of time during the onset of condensation because the initial stages of condensation are too rapid to obtain toroid size information at nanometer resolution by solution based techniques, such as light scattering (27, 28).

DNA Preorganization by Mg(II) Causes Toroid Aggregation by Altering Nucleation Structures. The addition of MgCl₂ to DNA prior to condensation resulted in the production of toroid aggregates (Figure 4.1B), in contrast to the predominance of single toroids observed when MgCl₂ was not present or was added concurrently with hexamine cobalt chloride (Figures 4.1A and C). The presence of an alternative nucleation structure for DNA samples with pre-associated Mg(II) explains this observation. It has been previously demonstrated that divalent cations promote DNA

helix-helix contacts in solution, (29-33) but not to the extent necessary for condensation. Consequently, the addition of MgCl_2 to DNA samples prior to condensation would be expected to promote an appreciable number of intramolecular helix-helix contacts (e.g. DNA loops) and intermolecular helix-helix contacts along 3 kb DNA (Figure 4.5B). Upon the addition of hexamine cobalt chloride, these pre-formed structures would act as nucleation sites for DNA condensation (19, 34). Mg(II) -stabilized DNA loops would nucleate toroid formation, whereas Mg(II) -stabilized intermolecular helix-helix contacts could result in the co-condensation of DNA strands onto different toroids at different points along their lengths. Thus, the existence of pre-condensation helix-helix contacts would promote the rapid formation of intertwined toroids, ultimately producing networks of toroids that are impossible to separate without complete decondensation of the DNA (Figure 4.5B). We propose that this is the origin of the toroid aggregates observed upon the condensation of DNA with pre-associated Mg(II) .

If the concurrent addition of MgCl_2 with hexamine cobalt chloride can produce super toroids (Figure 4.5C), then we must question why DNA samples with pre-associated Mg(II) produces significantly smaller toroids. This can also be explained as a result of the kinetic path taken during DNA condensation. As we mentioned above, the pre-association of Mg(II) with DNA will lead to the formation of intra- and intermolecular helix-helix contacts (Figure 4.5B). These contacts could cause the formation of toroidal aggregates to be rapid compared to the rate of strand rearrangement that would be necessary for the production of super toroids. In other words, the pre-association of Mg(II) leads to the formation of intertwined toroids that act as kinetic traps, which makes the formation of super toroids extremely rare. Two additional

observations support this explanation. First, we have observed a single super toroid amid an EM grid of smaller, aggregated toroids from a condensation reaction of DNA pre-associated with Mg(II) (data not shown). This is consistent with a kinetic component contributing to the origin of aggregate formation. Second, when higher concentrations of MgCl₂ are pre-incubated with DNA, the toroids produced upon condensation are not aggregated (15). This observation would support an increase in competition between Mg(II) and hexamine cobalt(III) allowing DNA in the early stages of condensation to pass over the kinetic barriers presented by entangled structures and to rearrange into (presumably) more efficiently packed single toroids.

Polymer Exchange Between Toroids is Limited. Adding MgCl₂ to the low salt toroid preparation increased the average outer diameter of toroids by 13 nm (i.e. from 77 to 90 nm), and caused a substantial increase in toroid aggregation (Figure 4.2A). Both of these changes can be explained by DNA strand exchange occurring between toroids after the addition of MgCl₂. The release of DNA from some toroids upon the introduction of MgCl₂ could lead to complete decondensation of some (particularly smaller) toroids, thereby reintroducing free DNA into solution that subsequently contributes to the growth and stabilization of other toroids. Similarly, aggregation could come about by the equilibrium exchange of DNA strands between toroids, which causes some toroids to become associated by strand sharing. In any case, the changes resulting from the addition of MgCl₂ to the low salt condensates represent a shift in the size and degree of aggregation closer to that observed when Mg(II) is pre-associated with DNA (Figure 4.2B). However, it is clear that the DNA strands of toroids are not entirely free to

exchange with solution, as the addition of MgCl_2 to low salt toroids (Figure 4.2A) does not result in toroid growth to the same size or aggregation state as those formed in the presence of MgCl_2 (Figures 4.2B and C). These combined results again illustrate that toroid size can be highly dependent on the path taken by DNA during condensation.

Comparison of DNA condensed at different temperatures illustrates both thermodynamic and kinetic limits to toroid growth. DNA condensation has been shown to be a result of dynamic correlations between multivalent cations that are associated with DNA strands in close proximity (1-3). This attractive potential decreases with increasing temperature (3, 13, 35-38). Thus, under conditions where toroid size is primarily limited by thermodynamic factors, toroid size would be expected to decrease with increasing temperature. On the other hand, if toroid size is primarily limited by the kinetics of growth, then toroid size should initially increase with increasing temperature because toroid nucleation will be less favored at higher temperatures. We have observed that the concurrent addition of MgCl_2 and hexammine cobalt chloride to DNA at 37°C produces single toroids that are considerably smaller and greater in number than the super toroids produced by the same condensation protocol at 22°C (Figure 4.3C). This observation indicates that at 37°C toroid size is limited by a thermodynamic parameter (i.e. undercharging), rather than the kinetics of nucleation and growth.

Our conclusion that the size of low salt toroids is kinetically determined is also consistent with our observation that low salt toroids produced at 37°C are larger (mean diameter 87 nm, mean thickness 35 nm) than those produced under low salt conditions at 22°C (mean diameter 77 nm, mean thickness 28 nm) (Figures 4.1A and 4.3A). Thus, under the low salt conditions, the reduction in DNA helix-helix attraction potential upon

raising the temperature from 22 to 37°C must reduce the probability of toroid nucleation enough to allow successfully nucleated toroids at 37°C to grow measurably larger than those produced at 22°C.

When the temperature of condensation was increased to 37°C abundant DNA fibrils were observed protruding from the toroids produced by the condensation of DNA in the presence of MgCl₂ (Figures 4.3B and C). We propose that these fibrils result from uncondensed loops of DNA that protrude from the surfaces of toroids in solution, and that these loops collapse into fibrils upon preparation of EM grids. This proposal is based upon two previous reports. First, atomic force microscopy (AFM) studies of DNA condensates in solution have revealed DNA loops protruding from a more condensed core particle under conditions where DNA condensation was incomplete (39). Second, a previous study by cryo-TEM has demonstrated that staining with uranyl acetate facilitates DNA condensation (40). Thus, it is reasonable that if a toroidal condensate has loops of DNA protruding from its surface when deposited on an EM grid, then the subsequent addition of uranyl acetate (and rinsing by ethanol) would cause these loops to condense into fibrils. These loops may appear because toroids prepared at 37°C are at their maximum limit of growth due to undercharging, and DNA strands added to those toroids during the final stage of growth remain only partially condensed. If this is truly the case, then the DNA condensates produced in the presence of MgCl₂ at 37°C are governed by both kinetic and thermodynamic factors, as condensation under purely thermodynamic control would be expected to allow the partially condensed DNA to release into solution and form slightly smaller toroids with completely condensed DNA.

Upon dilution with water, fibrils extending from condensates prepared in the presence of Mg(II) at 37°C (Figures 4.3B and C) are no longer observed, as all DNA particles appear to be fully condensed with clearly defined edges (Figures 4.4B and C). This observation provides additional support for our hypothesis that at 37°C the fibrils are indicative of some DNA associated with each toroid remaining partially uncondensed. Based upon the formalism derived by Rouzina and Bloomfield to calculate the surface concentration of cations around DNA as a function of cation valence and bulk concentration, (25, 26) dilution by a factor of two of the condensation reactions in this study would appreciably increase the DNA charge neutralized by trivalent hexamine cobalt(III) over divalent Mg(II), even though the relative concentration of these cations in solution remains constant. Thus, sample dilution would be expected to enhance DNA condensation, which causes the DNA loops to condense onto the toroids in an ordered fashion prior to EM grid preparation.

4.4 Conclusions

The results presented here demonstrate that the size of DNA toroids can be governed by both thermodynamic and kinetic factors. Under our low salt conditions we have concluded that toroid size is primarily limited by the kinetics of toroid nucleation and growth. Understanding the size and morphology of DNA condensates prepared in the presence of MgCl₂, on the other hand, requires the consideration of both kinetic and thermodynamic factors. When MgCl₂ is added to DNA prior to condensation, Mg(II)-stabilized helix-helix contacts provide a means to kinetically trap DNA into aggregate structures that are unable to rearrange into what are presumably lower energy structures.

The influence of these kinetic traps in limiting toroid size is illustrated by the observation that the concurrent addition of MgCl_2 and hexamine cobalt chloride allows the formation of super toroids. The dominance of thermodynamic limits on toroid size when MgCl_2 and hexamine cobalt chloride are added concurrently to DNA is supported by the fact that toroids decrease in size if the temperature is increased at the time of condensation. We have also demonstrated that DNA strand exchange between toroids can be very limited, as three condensate samples that only differ in regards to the step at which MgCl_2 is added maintain very different condensate structures. All together our results clearly illustrate that DNA condensates are not likely, in many cases, to represent equilibrium structures.

References

1. Bloomfield, V. (1996) *Current Opinion in Structural Biology* 6, 334-341.
2. Strey, H. H., Podgornik, R., Rau, D. C., and Parsegian, V. A. (1998) *Current Opinion in Structural Biology* 8, 309-313.
3. Gelbart, W. M., Bruinsma, R. F., Pincus, P. A., and Parsegian, V. A. (2000) *Physics Today* 53, 38-44.
4. Park, S. Y., Bruinsma, R. F., and Gelbart, W. M. (1999) *Europhysics Letters* 46, 454-460.
5. Shklovskii, B. I. (1999) *Physical Review E* 60, 5802-5811.
6. Nguyen, T. T., Rouzina, I., and Shklovskii, B. I. (2000) *Journal of Chemical Physics* 112, 2562-2568.
7. Raspaud, E., Olvera de la Cruz, M., Sikorav, J.-L., and Livolant, F. (1998) *Biophysical Journal* 74, 381-393.
8. Raspaud, E., Chaperon, I., Leforstier, A., and Livolant, F. (1999) *Biophysical Journal* 77, 1547-1555.
9. Trubetskoy, V. S., Loomis, A., Hagstrom, J. E., Budker, V. G., and Wolff, J. A. (1999) *Nucleic Acids Research* 27, 3090-3095.
10. de Fructos, M., Raspaud, E., Leforstier, A., and Livolant, F. (2001) *Biophysical Journal* 81, 1127-1132.
11. Nguyen, T. T., and Shklovskii, B. I. (2002) *Physical Review E* 65, 031409-1-031409-7.
12. Levin, Y., and Arenzon, J. J. (2003) *Journal of Physics A: Mathematical and General* 36, 5857-5863.
13. Ha, B.-Y., and Liu, A. J. (1998) *Physical Review Letters* 81, 1011-1014.

14. Stevens, M. J. (1999) *Physical Review Letters* 82, 101-104.
15. Conwell, C. C., Vilfan, I. D., and Hud, N. V. (2003) *Proceedings of the National Academy of Sciences of the United States of America* 100, 9296-9301.
16. Arscott, P. G., Li, A.-Z., and Bloomfield, V. A. (1990) *Biopolymers* 30, 619-630.
17. Dahlgren, P. R., and Lyubchenko, Y. L. (2002) *Biochemistry* 41, 11372-11378.
18. Revet, B., and Fourcade, A. (1998) *Nucleic Acids Research* 26, 2092-2097.
19. Hud, N. V., Downing, K. H., and Balhorn, R. (1995) *Proceedings of the National Academy of Sciences of the United States of America* 92, 3581-3585.
20. Yoshikawa, K., and Matsuzawa, Y. (1996) *Journal of the American Chemical Society* 118, 929-930.
21. LaMer, V. K., and Dinegar, R. H. (1950) *Journal of the American Chemical Society* 72, 4847-4854.
22. Mateescu, E. M., Jeppensen, C., and Pincus, P. (1999) *Europhysics Letters* 46, 493-498.
23. Grosberg, A. Y., Nguyen, T. T., and Shklovskii, B. I. (2002) *Reviews of Modern Physics* 74, 329-345.
24. Bloomfield, V. A. (1991) *Biopolymers* 31, 1471-1481.
25. Rouzina, I., and Bloomfield, V. A. (1996) *Journal of Physical Chemistry* 100, 4292-4304.
26. Rouzina, I., and Bloomfield, V. A. (1997) *Biophysical Chemistry* 64, 139-155.
27. Porschke, D. (1984) *Biochemistry* 23, 4821-4828.
28. He, S., Arscott, P. G., and Bloomfield, V. A. (2000) *Biopolymers* 53, 329-341.

29. Adrian, M., Heggeler-Bordier, B., Wahli, W., Stasiak, A. Z., Stasiak, A., and Dubochet, J. (1990) *EMBO Journal* 9, 4551-4554.
30. Bednar, J., Furrer, P., Stasiak, A., Dubochet, J., Egelman, E. H., and Bates, A. D. (1994) *Journal of Molecular Biology* 235, 825-847.
31. Kornyshev, A. A. (1999) *Physical Review Letters* 82, 4138-4141.
32. Safinya, C. R. (2001) *Current Opinion in Structural Biology* 11, 440-448.
33. Cherny, D. I., and Jovin, T. M. (2001) *Journal of Molecular Biology* 313, 295-307.
34. Shen, M., Downing, K., Balhorn, R., and Hud, N. (2000) *Journal of the American Chemical Society* 122, 4833-4834.
35. Rouzina, I., and Bloomfield, V. (1996) *Journal of Physical Chemistry* 100, 9977-9989.
36. Gronbech-Jensen, N., Mashl, R. J., Bruinsma, R. F., and Gelbart, W. M. (1997) *Physical Review Letters* 78, 2477-2480.
37. Ha, B.-Y., and Liu, A. J. (1997) *Physical Review Letters* 79, 1289-1292.
38. Ha, B.-Y., and Liu, A. J. (1999) *Physical Review E* 60, 803-813.
39. Hansma, H. G., Golan, R., Hsieh, W., Lollo, C. P., Mullen-Ley, P., and Kwoh, D. (1998) *Nucleic Acids Research* 26, 2481-2487.
40. Böttcher, C., Endisch, C., Fuhrhop, J. H., Catterall, C., and Eaton, M. (1998) *Journal of the American Chemical Society* 120, 12-17.

CHAPTER 5

CHARACTERIZATION OF ssDNA CONDENSATION

Investigations of DNA condensation *in vitro* have revealed a variety of factors that influence the size and morphology of DNA condensates. In particular, DNA persistence length has been proven to be a major determinant of condensate morphology (1). Double-stranded DNA (dsDNA) has a persistence length of approximately 150 bp in length, which largely governs the size of toroids (2, 3). By decreasing the persistence length of the DNA, it may be possible to form smaller condensate structures due to the reduced bending energy required during condensation.

To directly investigate the effects of persistence length on DNA condensation, single-stranded plasmid DNA was condensed under a variety of conditions and compared to double-stranded condensates under the same conditions. Single-stranded DNA (ssDNA) has a much smaller persistence length (~3 bases) than dsDNA (4, 5). ssDNA was condensed with a variety of condensing agents, including hexamine cobalt chloride, poly-L-lysine (50), salmon protamine and bull protamine, as well as several divalent cations. By using a variety of condensing agents, our comparison of double- and single-stranded condensates provides a means to investigate the potential effects of variations in the manner in which condensing agents interact with the dsDNA versus ssDNA. Additionally, by varying the solution conditions, we were able to alter the size and morphology of the condensates substantially as has been shown in previous studies

(3, 6). Studies described in this chapter illustrate the variation between double- and single-stranded condensates and further emphasize the effects of persistence length and condensing agent on the size and morphology of the condensates.

5.1 Experimental Procedures

Bacteriophage Growth and Titering: To produce a large quantity of ssDNA, it was necessary to use bacteriophage to replicate the plasmid DNA of interest. The bacteriophage, R408 was purchased from Promega and a new bacteriophage stock was grown. This allowed us to create a large stock of the bacteriophage as well as re-estimate the rate of bacteriophage infection. The protocol followed is an adaptation of the Promega instructions on bacteriophage propagation and infection. JM109 cells were grown on a M9 plate containing no antibiotic for approximately 30 hours at 37°C. No antibiotic was used because the JM109 cells contained no plasmids to provide antibiotic resistance. The use of careful sterile techniques is extremely important in maintaining an uncontaminated culture, particularly in the absence of antibiotic. An individual colony of JM109 was used to inoculate an overnight starter culture of sterile Luria Bertani (LB) broth (Fisher Scientific). Colonies may be picked from the plate for up to one week after streaking.

The starter culture was incubated at 37°C for 12-16 hours, while agitating in a shaker at 225 rpm. After the 12-16 hour growth, one milliliter of culture was added to 10 ml of fresh LB and incubated at 37°C in the shaker for another 60 minutes, or until the culture had a log phase OD reading. If the overnight culture was very turbid, it was

necessary to dilute the solution with 2-3 more milliliters of fresh LB media to achieve log phase growth approximately one hour after dilution.

Serial dilutions of the bacteriophage, R408 (Promega, Madison WI) were made by adding 10 μ l of phage stock solution to 990 μ l of LB broth (1:100 dilutions). From the first dilution, 10 μ l was added to the next 990 μ l of LB, and so on. A total of 6 dilutions were made, giving a 10^{12} final dilution. Approximately 100 μ l of each phage dilution was added to 200 μ l of log phase JM109, and the solution was briefly vortexed to mix, then allowed to incubate for 5 minutes. During this incubation, the bacteriophage is expected to begin infection of the cells. In the meantime, LB agar plates were warmed to $\sim 50^{\circ}\text{C}$ and 3.5 ml of LB top agar was aliquoted into culture tubes and heated in a beaker of boiling water. After the 5 minute incubation period, a 300 μ l phage/JM109 dilution was added to the warm top agar, vortexed lightly (Vortex machine at a setting of $\sim 4-5$) for 2 seconds, then poured onto the plate marked with the respective dilution. To spread the top agar mixture evenly, the plates were gently swirled in a circular motion. After the top agar solidified, the plates were inverted and incubated at room temperature for several hours. The plates were incubated at 37°C for 12-14 hours. Exceeding this incubation time makes plaques difficult to identify. It should be noted that pre-warming the LB agar plates and keeping the LB top agar very warm until they are used is very important for success with this protocol. The LB top agar will solidify quickly and cause the surface of the plates to become uneven, making identification of plaques extremely difficult.

After overnight incubation, single plaques were isolated by stabbing the agar with a sterile 1000 ml pipette tip. Plaques are usually clear spherical spots visible on the surface of the agar. This is the area in which bacterial growth is slowed or completely

stopped as a result of phage infection. A pipette was used to eject the agar plug into 50 ml of sterile LB broth in a 300 to 500 ml flask. The culture was incubated for 8-12 hours at 37°C while agitating at 270 rpm. The culture becomes slightly turbid in appearance, but bacterial growth is slowed due to infection. The cells were pelleted by centrifuging in a RC-5Bplus Sorvall centrifuge at 12,000 x g for 15 minutes. The supernatant was removed and spun again for 15 minutes further pellet cells remaining in the supernatant. In a fresh tube, the supernatant containing the phage was incubated for 30 minutes at 55°C to kill any remaining cells. The phage preparation was stored overnight at 4°C.

To obtain a multiplicity of infection (m. o. i.) for the bacteriophage preparation, an overnight culture of JM109 was diluted as described above and grown to log phase. Serial dilutions of phage (1:100) into LB broth were performed as described above. Additional dilutions were made between 10^6 and 10^{10} to allow for increased accuracy in calculating the m.o.i. values. The phage was mixed with log phase JM109 as described above, allowed to incubate 5 minutes, mixed with LB top agar, and poured onto warm LB plates. The plates were incubated at room temperature for several hours, then at 37°C overnight (12-14 hours). Plaque forming units were determined for the multiple dilutions. The number of plaques is multiplied times the dilution factor for the particular plate. This value is multiplied times another factor of 10, which accounts for the 1:10 dilution introduced when only 0.1 ml of phage was plated with the top agar. Variations in the protocol include, the media used (LB instead of TYP) and some incubation times.

Single-Stranded DNA Preparation and Purification: pBluescript II SK- plasmid (2961 bp) was transformed into the *E. coli* strain DH12S (ElectroMAX, Life Technologies,

Carlsbad, CA) by electroporation according to the manufacturers protocols. This particular cell line was recommended to increase the probability of bacteriophage infection. A culture of pBluescript II SK- was grown overnight in LB broth containing 100 µg/ml of ampicillin. PBluescript II SK- is technically classified as a phagemid, meaning that the plasmid is engineered to contain information that is recognized by the bacteriophage transcription mechanism. This promotes the rolling circle replication of the plasmid DNA, leading to single-stranded DNA copies of the plasmid. After 12-16 hours, 5 ml of LB in a 50 ml tube was inoculated with 100 µl of the overnight culture and incubated for another 30 minutes at 37°C. It is important to allow for thorough aeration to get maximum infection and growth. Single-stranded DNA was propagated by infecting the bacteria with the M13 derivative helper phage, R408, at an m.o.i. of 10-100. Stocks of R408 were prepared and titered as described above. The mixture of bacteria and bacteriophage were incubated at 37°C and agitated 270 rpm for approximately 24 hours to achieve optimal growth. Bacteriophage was separated from the cellular components by centrifugation and then precipitated from the supernatant using 0.25x volume of 40% (w/v) polyethylene glycol 8,000 MW/ 2.5 M NaCl and incubating on ice. After 30 minutes to several hours, the precipitated phage particles were collected by centrifugation and resuspended in a small volume (~1 ml) of 1× TE (10 mM Tris, 1mM EDTA, pH 8.0). Repeated chloroform: isoamyl alcohol (24:1 v/v) extractions were performed to lyse the phage particles and to remove proteinaceous materials and excess PEG. The extractions were repeated until no solid extract was visible between the phases. The DNA was precipitated from the aqueous layer by ethanol precipitation. The ssDNA was resuspended in dH₂O. S1 Nuclease (New England Biolabs) digestion was used to verify

that the isolation contained only ssDNA with no double-stranded contamination. The nuclease digestion is specific for dsDNA fragments. After exposure to the nuclease, the sample was compared to the untreated ssDNA by agarose gel electrophoresis and no observable differences were noted between the preparations. The purified sample contained a mixture of single-stranded pBluescript II SK- plasmid DNA and R408 phage DNA (~6.4 kb), as both were replicated during this process.

The pBluescript II SK- ssDNA was separated from the R408 ssDNA by electrophoresis in a 0.8 % agarose gel with a running buffer of 1× TBE (90 mM Tris-borate, 2 mM EDTA), and 0.5 µg/mL ethidium bromide. The Eppendorf (Hamburg, Germany) Perfectprep Gel Cleanup kit was used to extract the pBluescript II SK- ssDNA from the gel slice. The kit was used according to manufacturer's protocol with a slight modification to the elution step. The water used for elution was heated to 80°C and incubated on spin column for five minutes in an 80°C water bath before the final centrifugation step to increase recovery of ssDNA. Residual buffer and salts from the isolation and extraction procedures were removed by rinsing the ssDNA at least five times with dH₂O using a Microcon YM-30 spin column (Millipore). The de-ionized H₂O was filtered with a 0.2 µm syringe filter to remove any particulates from the solution. The pBluescript II SK- ssDNA was eluted from the spin column membrane and subsequently diluted to a final concentration of 10 µg/mL in dH₂O. ssDNA concentrations were verified spectrophotometrically. The purified single-stranded pBluescript II SK- preparation will be referred to as ultra-low salt ssDNA.

To examine the interactions of different cationic species at approximately equal ionic strength, three additional stock solutions of 10 µg/mL ssDNA were prepared for

condensation: 1) ssDNA in 1× TE (10 mM Tris-HCl, 1 mM EDTA, pH 8.0), 2) ssDNA in 13 mM NaCl, and 3) ssDNA in 4.5 mM MgCl₂.

Double-Stranded DNA Preparation and Purification: Double-stranded pBluescript II SK- plasmid DNA was grown in the *E. coli* strain DH5 α . The plasmid was isolated and purified using the Qiagen Maxi-prep kit (Valencia, CA). The DNA was linearized with the endonuclease *Hind* III (New England Biolabs, Beverly, MA), then purified using the Microcon-YM30 spin columns (Millipore, Billerica, MA). At least five rinses were performed with deionized H₂O to ensure complete exchange of the buffers and removal of excess salts from the digest reaction. The linear DNA was eluted from the spin column and diluted to a concentration of 10 μ g/ml. The concentrations were verified spectrophotometrically. This purified double-stranded pBluescript II SK- sample will be referred to as ultra-low salt dsDNA.

DNA Condensate Preparation and Transmission Electron Microscopy (TEM). DNA condensates were prepared by mixing equal volumes of ssDNA or linear dsDNA with a hexamine cobalt chloride (Sigma, St. Louis, MO) or poly-L-lysine (pLL₅₀, ~ 50 lysines/molecule) (Sigma) stock solution. The final concentrations in the condensation reaction mixture were 5 μ g/mL DNA and either 100 μ M hexamine cobalt chloride or 6.25 μ g/mL pLL₅₀ unless otherwise noted. The DNA condensation reaction mixture was thoroughly mixed by repeated pipetting, allowed to equilibrate for five minutes at room temperature, and then deposited on carbon-coated grids (Ted Pella, Redding, CA). After 10 minutes on the grid, 2% (w/v) uranyl acetate (Ted Pella) was added momentarily to

the condensate mixture. The grids were rinsed in 95% ethanol and air-dried. The DNA condensates were recorded on film with a JEOL-100C transmission electron microscope (TEM) at 100,000× magnification. The TEM negatives were scanned at 300 pixels/inch, and a graphics program was used to measure the diameters of individual spheres. Each DNA condensate mixture was prepared and imaged several times for repeatability. The same condensation protocol was repeated using ssDNA under various solution conditions in the presence of pLL₅₀. A final study to observe the dependence of ssDNA condensation on the condensing agent concentration was performed using the same concentrations of ssDNA but varying the concentration of pLL₅₀ to 3 µg/ml and 9 µg/ml. These variations in pLL₅₀ concentration provide a 1:1 and a 3:1 lysine to phosphate charge ratio, respectively.

5.2 Results

Single-stranded pBluescript II SK- (ssDNA) was propagated by the bacteriophage R408. This plasmid was chosen because it has been studied previously in DNA condensation experiments and is relatively well characterized. Moreover, it was optimal for phage replication as it is a phagemid, meaning it contains the necessary genes to be recognized and replicated by bacteriophage. Replication by this method produces a single-stranded plasmid DNA as well as single-stranded copies of the phage DNA. After isolation of the DNA from the phage, these single-stranded DNA molecules had to be separated from each other by gel electrophoresis to acquire purified single-stranded pBluescript II SK- DNA.

Single-stranded DNA can be distinguished from any double stranded contaminants by agarose gel electrophoresis. Figure 5.1 depicts the electrophoretic mobilities of both double- and single-stranded pBluescript II SK-. A sample of dsDNA from a bacterial isolation was run in lane 2 of the gel as a control. This lane contains 2 distinct bands, a supercoiled band that is shown at approximately 1.8 kb and a relaxed circle band that is visible slightly below 4 kb, as compared to the ladder. No distinct band of linear DNA is observed from the isolation procedure. Linearized dsDNA was run in lane 3, where a single band of approximately 3 kb is present. DNA from the single-stranded preparation was run in lane 4. Two bands are observed from the isolation. The bacteriophage DNA is approximately 6.4 kb in length, which was observed at approximately 4 kb as compared to the double-stranded marker. The lower band at approximately 1.4 kb represents the single-stranded plasmid DNA. Single-stranded DNA typically exhibits an electrophoretic mobility of approximately one half the size of the dsDNA, as was observed here. The easily distinguishable single-stranded structures allow for the plasmid DNA to be isolated from the phage DNA by gel extraction after electrophoresis. Lane 5 contains the gel extracted single-stranded plasmid DNA. One distinct band of DNA was observed, indicating that the gel extraction procedure successfully purified the plasmid from the phage ssDNA. The purified single-stranded plasmid DNA (ssDNA) was used for all further studies.

Condensation of ssDNA. Very few studies have reported the morphology of particles produced by the condensation of ssDNA. Thus, we began our studies by investigating the condensation of ssDNA with several different condensing agents, so that any condensing

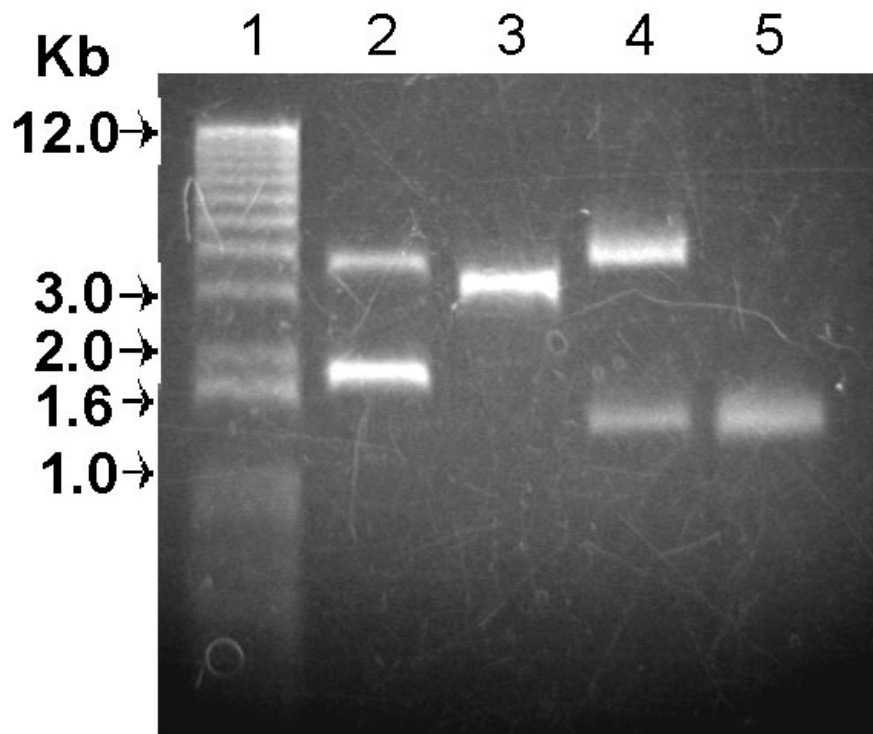


Figure 5.1. Verification of ssDNA isolation by gel electrophoresis. An electrophoretic agarose gel stained with ethidium bromide comparing the migration of double strand and phage-produced single-strand forms of pBluescript SK II (ssDNA). 1 kb+ dsDNA ladder (lane 1), supercoiled dsDNA (lane 2), dsDNA linearized with Hind III (lane 3), isolated R408 helper bacteriophage ssDNA and circular ssDNA (lane 4), and gel extracted and purified circular ssDNA (lane 5).

agent-specific effects would be revealed. Poly-L-lysine (pLL₅₀) and hexamine cobalt chloride were primarily studied, along with several other polyvalent condensing agents. In the presence of pLL₅₀, ssDNA condensed into small, single spherical particles. While some variation in the particle sizes was observed, the majority of the particles were less than 40 nm in diameter (Figure 5.2A). Condensates formed in the presence of hexamine cobalt(III) were also spherical in shape, but ranged from 2-4 fold larger in diameter than the condensates formed by pLL₅₀ (Figure 5.2B). Additionally, when hexamine cobalt(III) was used as the condensing agent, an appreciable amount of the particles were not as well defined as the condensates observed in the pLL₅₀ sample. For example, the middle-most sphere shown in Figure 5.2B, does not have a well defined outside edge like the particle to its immediate left. No similar ill-defined condensates were produced with pLL₅₀. Condensation with spermine and salmon protamine produced spherical condensates resembling those produced in the presence of hexamine cobalt(III).

Both pLL₅₀ and hexamine cobalt chloride have been frequently used to condense double-stranded DNA (2, 3, 6-12). Under ultra-low salt conditions, linear dsDNA condensed with pLL₅₀ produced a heterogeneous mixture of condensates (Figure 3A). The majority of the condensates were rods, although both toroids and spherical particles were observed. While the condensates are small and well dispersed, the dsDNA condensates lack the uniformity of the ssDNA condensates formed by under identical reaction conditions. The ssDNA favored the formation of a specific morphology, whereas the dsDNA had at least three different condensate morphologies produced.

Previous studies have demonstrated that linear dsDNA condensed by hexamine cobalt(III) produce predominantly toroidal structures (3, 7, 12). Under our ultra-low salt

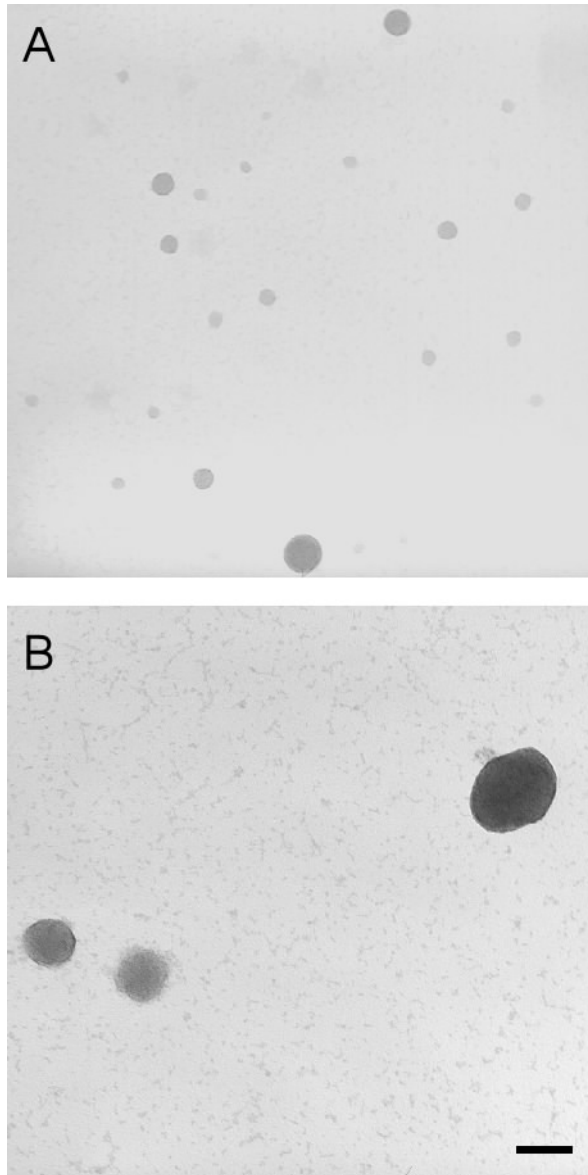


Figure 5.2. Transmission electron microscopy (TEM) images of ssDNA condensates produced with various condensing agents. The single-stranded DNA pBluescript SK II- plasmid (3kb) is at a final concentration of 5 $\mu\text{g/ml}$ in dH_2O . (A) Small spherical particles formed when ssDNA was condensed in the presence of 6.25 $\mu\text{g/ml}$ pLL₅₀. (B) Large spherical particles produced when ssDNA was condensed in the presence of 100 μM hexamine cobalt chloride. The scale bar is 100 nm.

conditions, the condensates observed were also toroids. However, the individual toroids were difficult to distinguish from each other, as the vast majority of condensates were clustered into large aggregates (Figure 5.3B). The toroids appear to be relatively small, approximately 40 nm in outer diameter. The nature of the aggregation, however, made a quantitative assessment difficult, as the condensates were very tightly packed making their boundaries nearly indiscernible. In comparison to the spherical structures produced by ssDNA condensation with hexammine cobalt(III), the dsDNA condensates are smaller in size. The dsDNA condensates are also of a different morphology than the spherical particles formed when ssDNA is condensed (Figures 5.2B and 5.3B). Furthermore, the ssDNA condensates were observed primarily as single particles, whereas the dsDNA toroids were seldom seen outside of groups containing less than three toroids.

Counterion Interactions with ssDNA Affect Condensation. In chapter 2, it was shown that the addition of counterions to a condensation reaction greatly influences the size of the resulting condensates (3). To determine the possible effects of various counterions on ssDNA condensates, the ssDNA was condensed under three different solution conditions with pLL₅₀. This condensing agent was chosen for these experiments because it was found to produce condensates that were relatively monodispersed in size and of well defined morphology. First, the ssDNA was prepared in a solution of 1× TE (10 mM Tris, 1 mM EDTA), and then condensed with pLL₅₀ (12.5 µg/ml). The resulting condensates were spherical but distinctly different in size and degree of aggregation from those observed under ultra-low salt conditions. While a few smaller condensates were observed, the majority of those present were at least 50 nm in diameter. Clusters of

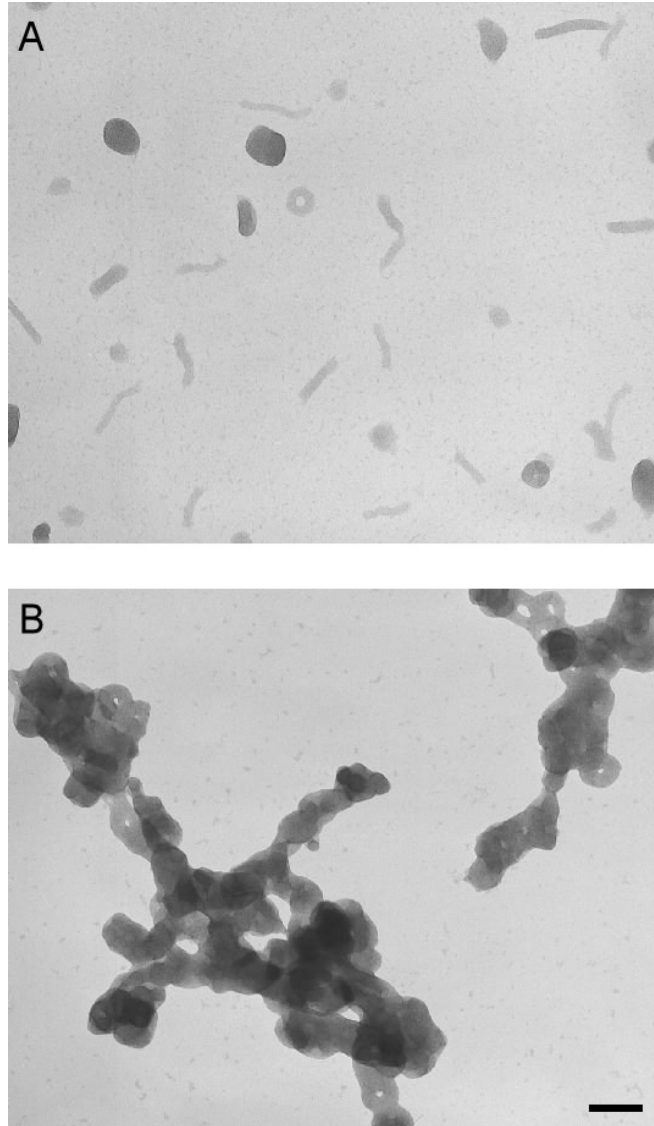


Figure 5.3. TEM images of dsDNA condensates produced with various condensing agents. Linear double-stranded pBluescript SK II- was prepared in dH₂O to a final concentration of 5 $\mu\text{g/ml}$. (A) Several morphologies of DNA condensates including rods, spheres and toroids observed when dsDNA was condensed with 6.25 $\mu\text{g/ml}$ pLL₅₀. (B) Small toroids produced by condensation of dsDNA with 100 μM hexammine cobalt chloride aggregate into large complex structures. Single toroids were rarely observed in this preparation. The scale bar is 100 nm.

condensed particles were frequently observed. Association of the clusters resulted to the formation of aggregates as large as several hundred nanometers in diameter. Additionally, it appeared that some of the ssDNA may not have been completely condensed as some of the clustered spheres have a fibril-like strand linking several spheres together (Figure 5.4A). The addition of 1× TE to the ssDNA resulted in the produced of structures distinctly different from the single, well defined spheres formed under ultra-low salt conditions.

The monovalent salt NaCl was also added to the ultra-low salt ssDNA prior to condensation. Comparison between the TE and a sample containing NaCl allows the examination of two monovalent cations that differ in terms of structure and mode of interaction with the DNA molecules (13). A solution containing ssDNA with NaCl was prepared such that the sample would be approximately equal ionic strength to that of the 1× TE (13 mM NaCl). The condensates produced in the presence of NaCl were very similar to those observed under ultra-low salt conditions (Figure 5.2A and 5.4B). Spherical particles were the predominant morphology and little aggregation was observed. It was noted that in the presence of NaCl, the background of the TEM images contained irregular circular structures. These low contrast particles do not contain distinct boundaries and are difficult to characterize with any certainty, as they are barely visible against the background (Figure 5.4B).

Finally, the ssDNA was prepared in 4.5 mM MgCl₂, which is approximately equal in ionic strength to the TE and NaCl preparations described above. Upon condensation with pLL₅₀, the ssDNA condensed into spherical particles of intermediate size (i.e., slightly larger than those produced under ultra-low salt conditions, but smaller than those

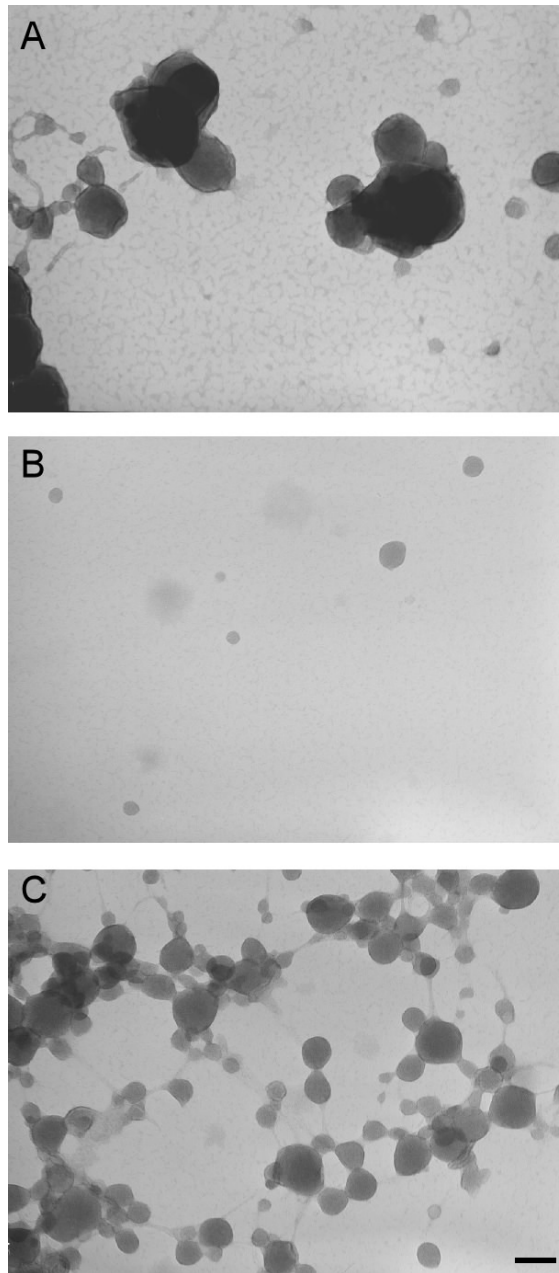


Figure 5.4. TEM images of ssDNA condensate with pLL₅₀ under several solution conditions. The solutions were prepared such that they are of approximately equal ionic strength. All condensates were produced in the presence of 6.25 $\mu\text{g/ml}$ pLL₅₀. (A) Large spherical condensates and aggregates resulted from ssDNA prepared in 1 \times TE. (B) Small spherical condensates are observed from ssDNA prepared in 13 mM NaCl. (C) Spherical condensates observed from ssDNA prepared in 4.5 mM MgCl₂ display increased propensity to form aggregates. The scale bar is 100 nm.

observed in the presence of $1\times$ TE) (Figure 5.4C). The condensates were well formed, although some fibril-like structures protruded from spheres, frequently linking particles together. TEM imaging revealed that the condensates were generally part of a larger aggregate, as opposed to the single spheres that dominated the ultra-low salt preparations. In the presence of MgCl_2 , the condensates have a combination of characteristics similar to both the TE and NaCl preparations, suggesting although the ionic strengths are approximately equal, the nature of the cation greatly influences the final structure and morphology of the condensate.

The Condensation of ssDNA is Concentration Dependent. The pLL₅₀ concentration used to perform the experiments described above was approximately 2:1 (poly-L-lysine: DNA phosphate), which provides a sufficient excess of positive lysine charge available to neutralize the negative phosphate charge. At this concentration, the condensates formed were well defined and appeared to be fully condensed, as no fibrils or structures resembling uncondensed DNA were observed in these preparations, indicating that the lysine: phosphate interactions were sufficient for condensation. pLL₅₀ has been shown to condense dsDNA at slightly less than a 1:1 charge ratio (14, 15). The ssDNA was condensed at a ratio of 1:1 with pLL₅₀ under ultra-low salt conditions. Under these conditions, uncondensed DNA was observed protruding from the spherical particles (Figure 5.5A). Spheres were the dominant morphology, however the condensates are larger in diameter than those produced in an excess of pLL₅₀. Quantitative measurements were not performed, as the boundaries of many of the particles are difficult to distinguish. These images suggest that at a 1:1 charge ratio, the condensation of ssDNA was not

complete. Incomplete condensation of the ssDNA is consistent with observations of condensates resulting from hexamine cobalt(III) induced condensation (Figure 5.2B). This incomplete collapse of ssDNA at concentrations of condensing agent known to completely condense dsDNA, implies that condensation of single-stranded DNA requires higher concentrations of condensing agent for efficient condensation.

ssDNA condensation was also performed using a charge ratio of 3:1 pLL₅₀:phosphate. A greater excess of positive charge in solution did not significantly change the outcome of the condensation reaction. As observed in the 2:1 charge ratio (Figure 5.2A), the condensates were small, spherical and well distributed. No aggregation of the condensates was obvious. Quantitative measurements were performed on the spheres to determine if having a further excess of the cationic condensing agent significantly changes the size of the particles. Diameters of the particles were measured and compared (Figure 5.6). The overall distribution of sphere diameter is very similar for the two preparations and is dominated by spheres of approximately 15 nm in diameter in both cases. In order to estimate the number of ssDNA molecules in the smallest condensates, approximate volume calculations were performed. These estimations assumed hexagonal-close packing of the strands within the condensates, as would be expected in dsDNA condensates. The particles observed were found to be primarily monomolecular under both conditions.

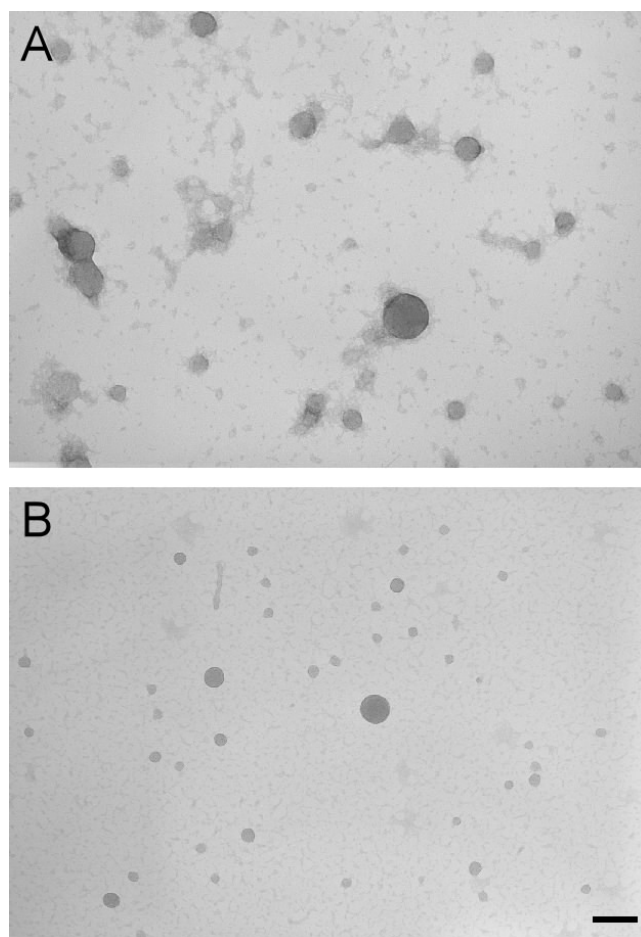


Figure 5.5. TEM images of ssDNA condensed with various concentrations of poly-L-lysine. All ssDNA concentrations are 5 $\mu\text{g/ml}$ in dH_2O . (A) DNA condensates formed with 3 $\mu\text{g/ml}$ pLL₅₀ form spherical particles; however, the particles are only partially condensed as DNA can be seen protruding from the surface of the spheres. (B) At higher concentrations of pLL₅₀ (9 $\mu\text{g/ml}$), spheres are small and tightly packed, closely resembling those formed with 6.25 $\mu\text{g/ml}$ pLL₅₀. The scale bar is 100nm.

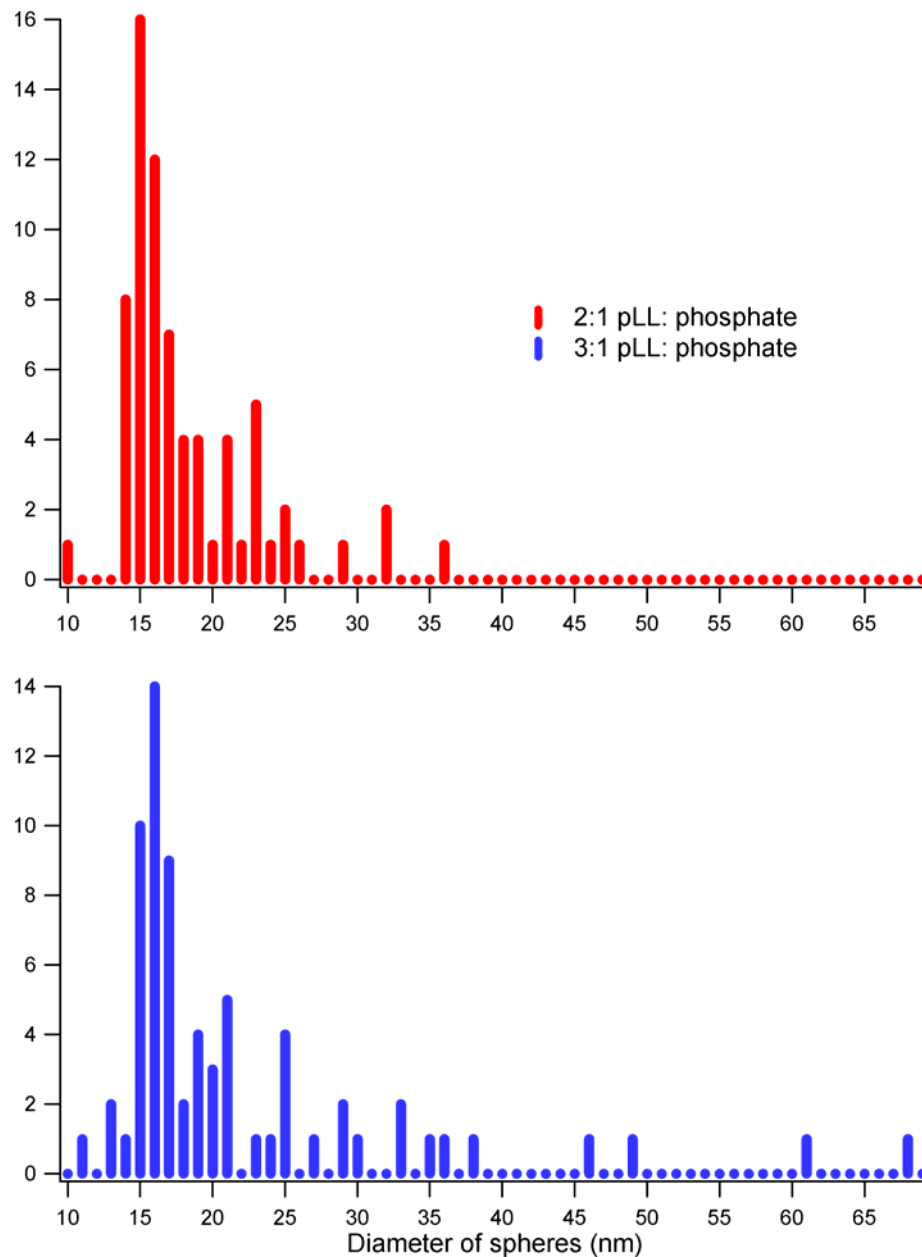


Figure 5.6. Histogram of particle diameters from ssDNA condensed with poly-L-lysine. ssDNA spheres were measured from TEM images and the distribution of particle diameters was plotted. Both the 6.25 $\mu\text{g/ml}$ and 9 $\mu\text{g/ml}$ pLL₅₀ predominantly contained particles of approximately 15 nm in diameter, which is consistent with monomolecular collapse, assuming hexagonal-close packing.

5.3 Discussion

The condensation of dsDNA has been studied for nearly three decades. Based upon both experimental data and theoretical calculations, many theories have been developed regarding what energetic constraints determine the size and morphology of these condensates. The energetic contribution of DNA bending on condensate formation has been widely appreciated (*1, 11, 16*). By increasing the inherent flexibility of the DNA, the bending energy required for DNA collapse should decrease significantly, allowing for the formation of smaller, more compact particles (*2, 17*). As a means to study the effects of increased DNA flexibility on condensation, single-stranded DNA condensation was examined. Very few studies have been performed on single-stranded DNA and the factors that govern its condensation (*9, 18*). In the present study, we have examined the effects of varying condensing agents and salt conditions on ssDNA.

The initial state of the ssDNA used in this study was briefly examined by AFM (data not shown). The ssDNA in ultra-low salt solution conditions appears to take on a significant amount of secondary structure. The small clusters of spherical particles observed are likely to consist of varying degrees of inter- and intrastrand interactions between neighboring particles. These contacts between particles would provide opportunity for additional stabilizing interactions (e.g., basepairing or base-stacking) to occur between ssDNA strands, potentially locking them into a complex secondary structure.

While persistence length constraints were reduced with ssDNA, it is difficult to quantitatively assess actual persistence length of the DNA under these specific conditions. Bustamante and colleagues investigated ssDNA flexibility in single molecule

studies using optical tweezers (4). They proposed that the persistence length of ssDNA is approximately 0.75 nm or ~3 basepairs, which is about a 75-fold reduction from the persistence length of double-stranded DNA (4). It is likely that some secondary structure interactions occur within the random sequence of the ssDNA. The additional secondary structure would create regions of double-stranded DNA, thereby increasing the persistence length of those areas of the DNA. Thus, it is expected that the DNA studied is more flexible than standard dsDNA but not as flexible as the ssDNA molecules examined in previous single molecule studies of ssDNA (4, 19-21).

The secondary structure interactions observed in the ssDNA preparations are expected result from one or more of the following factors: electrostatics, basepairing and base-stacking (20). Basepairing is expected to occur in DNA with random sequences, when complimentary regions interact with each other in solution. Base-stacking interactions are formed as a result of interactions between several neighboring regions of basepairing along the length of the DNA. In random DNA sequences, the effects of base-stacking have been found to be negligible, as the distance between stable regions of duplex are infrequent (22). Infrequent basepairing in random sequences promotes the formation of many complex looped and branched structures within the ssDNA (20). However, due to the instability of the ssDNA with minimal basepairing, it is possible to remove the secondary structure elements with much less force than has been observed for sequences with high complementarity. Since the pBluescript plasmid is a quasi-random sequence, it can be presumed that the base-stacking interactions have only a small contribution to the stability of the secondary loop structures within the ssDNA. The lack of base-stacking interactions within these structures allows for rearrangement of the DNA

(i.e. condensation) have a smaller energetic barrier to overcome to break apart the secondary structures components in the ssDNA.

Condensation of ssDNA by pLL₅₀ Produces Small Spherical Particles. ssDNA condensed by the cationic condensing agent, pLL₅₀ produced small, spherical particles (Figure 5.2A). Condensing the ssDNA with hexammine cobalt chloride also produced spherical particles (Figure 5.2B), however, the particles were larger and less defined than those observed with pLL₅₀. Since the ssDNA and the solution conditions were identical in these preparations, the difference observed in the size of the particles must be due to the difference in condensing agents. Both condensing agents were added in excess of the DNA phosphate charge in the solution. The structures and charge distributions of the condensing agents are quite different. Hexammine cobalt(III) is a small inorganic cation resembling a hexa-hydrated Mg²⁺ that carries a point charge of 3+, whereas, the pLL₅₀ is a long chain polymer consisting of approximately 50 lysines/chain. Each lysine carries a charge of 1+ and this charge is evenly distributed along the polymer. Since the pLL₅₀ carries approximately 15× greater charge/molecule than the hexammine cobalt(III), it is expected to have a higher binding affinity for DNA.

It is evident from the dsDNA condensation reactions that pLL₅₀ interacts with DNA in a different manner than the hexammine cobalt(III), as condensates of different morphologies and sizes were observed. The predominance of rods produced by pLL₅₀ condensation suggests that the pLL₅₀ is able to induce kinking in the helical structure, possibly by distorting the helix (16). In the presence of hexammine cobalt(III) the predominant structures are toroidal condensates, which are largely influenced by

persistence and bending constraints. It is hypothesized that the pLL₅₀ interacts nonspecifically with the DNA such that local bending constraints are reduced and it becomes energetically favorable to allow the DNA polymers to bend freely. The difference in the condensates may result from the charge density and distribution of charge on the condensing agent.

Condensation of ssDNA Requires an Excess of Condensing Agent. The data presented in Figure 5.4 shows the concentration effect of decreasing and increasing the concentration of condensing agent by half, from a 2:1 lysine to phosphate charge ratios to 1:1 and 3:1, respectively. While previously reported studies condensed dsDNA with less than 1:1 charge ratios of poly-L-lysine, an excess of positive charge is apparently required to condense the ssDNA (14, 15). Although the concentration of hexamine cobalt chloride was not varied, the concentration used for these studies (100 mM) has been shown to completely condense dsDNA under several conditions (3, 6, 8). A spherical particle formed by condensation of ssDNA with hexamine cobalt(III) does not appear to be completely condensed, as it does not have a well-defined outer diameter (Figure 5.2B). Even with an excess of condensing agent, these ill-defined particles may be a result of inefficient interactions of the condensing agent with the anionic charge of the DNA molecules. Possible explanations for this occurrence may be related to the structure of the DNA. Foremost, for condensing agents that have specific binding pockets on the DNA (i.e., hexamine cobalt ions may occupy Mg²⁺ sites in the major groove) may have reduced associations with the DNA due to these alterations in the helical structure. The lack of stable helical structure would also affect other condensing agents that are DNA

groove binders (e.g., spermine, protamine) (24). The local anionic charge density of the DNA is also reduced in ssDNA as compared to dsDNA, as there is only one phosphate charge every 0.34 nm as opposed to the two charges found in dsDNA. Hexamine cobalt(III) ions are expected to neutralize the charge of phosphates in a basepair of dsDNA; however, in ssDNA, the charge of the cationic condensing agent would only be able to neutralize one phosphate charge as a result of the secondary structure of the DNA. One or both of these effects may account for the incomplete condensation of the ssDNA observed when a 1:1 lysine to phosphate charge ratio was used for condensation (Figure 5.5B).

Condensation of ssDNA with poly-L-lysine Results in Predominantly Monomolecular Spheres. ssDNA condensation by pLL₅₀ favors the production of monomolecular condensates as shown by the histogram in Figure 5.6. Several hundred particles were examined and estimated to consist of a single DNA molecule. Monomolecular collapse is seldom observed in condensation experiments and may be a result of the flexibility of the single-stranded polymer as well as an effect of the tightly binding pLL₅₀. Although, the persistence length of the ssDNA molecule examined here is likely to be greater than that calculated by Smith et al. due to random basepairing, the ssDNA is expected to be much more flexible than dsDNA (4). The formation of hairpins and looped structures within the ssDNA molecules due to their inherent flexibility, would provide optimal nucleation sites for the initiation of condensation. Additionally, due to the flexibility and secondary structural elements of the ssDNA, condensate morphology may favor spheres over toroids as the persistence length would not be limiting, as expected in the

condensation of dsDNA into toroids (2). Increased nucleation of stable condensates and strong binding of the condensing agent allow for kinetic factors to govern the ssDNA condensate formation.

Salt Conditions Cause Variations in ssDNA Condensate Size and Aggregation. Under ultra-low salt conditions (i.e., deionized H₂O), the condensing agent would be able to freely associate with the ssDNA to neutralize charge and condense the polymer. Previous studies have shown that increasing the ionic strength of a DNA solution can appreciably alter condensation, and eventually reach a concentration where condensation more condensing agent is necessary for condensation to occur (3, 6, 8, 25-28). Furthermore, studies of ionic strength affects on ssDNA indicated that at very low ionic strengths (i.e., < 2 mM NaCl), ssDNA forms less self structure as a result of reduced screening of repulsion between the phosphates (19, 22). Thus, under our ultra-low salt conditions, it is likely that the ssDNA forms a minimal amount of secondary structure as a result of increased electrostatic repulsions (21).

To investigate the effects of increased ionic strength on the condensation of ssDNA, three solution conditions of approximately the same ionic strength (~13 mM) were examined. The presence of the monovalent cation Na⁺ did not significantly alter the condensation reaction, as the particles formed closely resembled those produced under ultra-low salt conditions (Figure 5.2A and 5.4B). However, when the ssDNA was in solution with the organic monovalent Tris (i.e., 1× TE; 10 mM Tris, 1 mM EDTA, pH 8.0), the resulting condensates had much larger size distribution and increased aggregation as compared to the ultra-low salt condensates (Figure 5.4A). Tris molecules

have been shown to interact with bases via salt bridges and hydrogen bonding, in addition to electrostatic interactions (13). These modes of interaction may with the DNA provide additional stability compared to the lone electrostatic interactions expected from an inorganic monovalent cation such as Na^+ , and may account for the variations in the condensates observed by TEM.

The introduction of the divalent cation, Mg^{2+} , to solution also caused condensate size to vary from the ultra-low salt preparation. Spherical condensates increased in size, but did not exhibit the same increase in size observed for the condensate reaction containing TE buffer. Furthermore, spherical condensates showed a marked increase in aggregation, as DNA fibers were observed linking particles. Mg^{2+} has been shown to increase the interactions between strands of DNA due to the association of the divalent cation with the polyanionic polymer (29, 30). In Chapters 3 and 4, we have shown that the preassociation of Mg^{2+} with DNA prior to condensation increases the degree of aggregation among condensate particles. These studies also revealed that in the presence of Mg^{2+} condensates tend to favor a larger size particle, which also may explain the larger spheres observed in the present study (Figure 5.4C).

5.4 Concluding Remarks

Comparisons between ssDNA and dsDNA particles reveal that the increased flexibility allows the DNA to compact into various morphologies, with increased propensity to form spherical structures. Monomolecular spheres were predominantly observed in condensation reactions with pLL₅₀. Achieving such a consistent production of small monomolecular condensates has been a goal of many studying DNA condensation

and gene delivery for years. Even though we are achieving this level of compaction, there are several factors influencing the compaction of ssDNA that are currently unclear. Poly-L-lysine is a powerful DNA condensing agent. From the data presented above, we are unable to differentiate between the condensing agent effects and the effects of increased flexibility in the ssDNA. Therefore, we cannot attribute the small spherical condensates observed here solely to the flexibility of the ssDNA. To differentiate between the effects of poly-L-lysine and the flexibility of the DNA on condensation, further studies must be performed. Two approaches to gaining understanding of this system include, examining condensates produced by various condensing agents with properties in between hexamine cobalt(III) and poly-L-lysine and/or examining a chimeric DNA that contains a length of both single- and double-stranded DNA. Further experimentation is necessary to determine the exact nature of the effects explored in this study.

References

1. Vasilevskaya, V. V., Khokhlov, A. R., Kidoaki, S., and Yoshikawa, K. (1997) *Biopolymers* 41, 51-60.
2. Hud, N. V., Downing, K. H., and Balhorn, R. (1995) *Proceedings of the National Academy of Science USA* 92, 3581-3585.
3. Conwell, C. C., Vilfan, I. D., and Hud, N. V. (2003) *Proceedings of the National Academy of Science USA* 100, 9296-9301.
4. Smith, S. B., Cui, Y., and Bustamante, C. (1996) *Science* 271, 795-799.
5. Hagerman, P. J. (1988) *Annual Review of Biophysical Chemistry* 17, 265-286.
6. Conwell, C. C., and Hud, N. V. (2004) *Biochemistry*.
7. Hud, N. V. and Downing, K. H. (2001) *Proceedings of the National Academy of Science USA* 98, 14925-14930.
8. Widom, J., and Baldwin, R. L. (1980) *Journal of Molecular Biology* 144, 431-453.
9. Davidson, B., and Fasman, G. D. (1969) *Biochemistry* 8, 4116-4126.
10. Pelta, J., Livolant, F., and Sikorav, J.-L. (1996) *Journal of Biological Chemistry* 271, 5656-5662.
11. Bloomfield, V. (1996) *Current Opinion in Structural Biology*. 6, 334-341.
12. Arscott, P. G., Li, A.-Z., and Bloomfield, V. A. (1990) *Biopolymers* 30, 619-630.
13. Righetti, P. G., Magnusdottir, S., Gelfi, C., and Perduca, M. (2001) *Journal of Chromatography A* 920, 309-316.
14. Trubetskoy, V. S., Loomis, A., Hagstrom, J. E., Budker, V. G., and Wolff, J. A. (1999) *Nucleic Acids Research* 27, 3090-3095.

15. Lee, R. J., and Huang, L. (1996) *Journal of Biological Chemistry* 271, 8481-8487.
16. Bloomfield, V. (1998) *Biopolymers* 44, 269-282.
17. Shen, M., Downing, K., Balhorn, R., and Hud, N. (2000) *Journal of the American Chemical Society* 122, 4833-4834.
18. Molas, M., Bartrons, J. C., and Perales, J. C. (2002) *Biochimica et Biophysica Acta* 1572, 37-44.
19. Bustamante, C., Smith, S. B., Liphardt, J., and Smith, D. (2000) *Current Opinion in Structural Biology* 10, 279-285.
20. Zhang, Y., Zhou, H., and Ou-Yang, Z. C. (2001) *Biophysical Journal* 81, 1133-1143.
21. Montanari, A., and Mezard, M. (2001) *Physical Review Letters* 86, 2178-2181.
22. Maier, B., Bensimon, D., and Croquette, V. (2000) *Proceedings of the National Academy of Science* 97, 12002-12007.
23. Hud, N. V., and Polak, M. (2001) *Current Opinion in Structural Biology* 11, 293-301.
24. Hud, N. V., Milanovich, F. P., and Balhorn, R. (1994) *Biochemistry* 34, 7528-7535.
25. Rouzina, I., and Bloomfield, V. A. (1996) *Journal of Physical Chemistry* 100, 4292-4304.
26. Rouzina, I., and Bloomfield, V. A. (1997) *Biophysical Chemistry* 64, 139-155.
27. Raspaud, E., Olvera de la Cruz, M., Sikorav, J.-L., and Livolant, F. (1998) *Biophysical Journal* 74, 381-393.
28. Raspaud, E., Chaperon, I., Leforstier, A., and Livolant, F. (1999) *Biophysical Journal* 77, 1547-1555.

29. Dahlgren, P. R., and Lyubchenko, Y. L. (2002) *Biochemistry* 41, 11372-11378.
30. Revet, B., and Fourcade, A. (1998) *Nucleic Acids Research* 26, 2092-2097.

CHAPTER 6

HIGH MOBILITY GROUP PROTEINS ALTER THE PATH OF DNA CONDENSATION

It is widely recognized that chromatin packing is regulated by histones and proteins that interaction with DNA. It has been known for many years that histones bend DNA to a radius of curvature that is well below the persistence length of free DNA in solution (1, 2). However, more recently it has been observed that other proteins present in the cell during replication may actively bend DNA, and further reduce the unfavorable energetic cost of DNA bending to allow for efficient packing (1).

High mobility group proteins are currently of great interest for their role in many cellular processes. While their exact purpose remains to be determined, HMG proteins have been found to be active during replication, recombination and transcription (3-5). HMG proteins have dynamic interactions with DNA and have been shown to bend DNA at a single location from 65-120°, based on the system investigated (6-8). Furthermore, it has been shown that HMG proteins do not display sequence specificity or specificity for particular secondary structure, allowing them to interact freely at a genomic level. The ability of HMG proteins to induce DNA bending in a nonspecific manner was recently examined using ligation circularization studies (5). In these studies, a short oligonucleotide of random sequence and a similar oligonucleotide containing a single A-tract, which introduced approximately 18° of bend into the DNA helical axis, were independently ligated to form monomers of the sequences. The DNA was exposed to a

nuclease that digested all linear fragments in the solutions, and the circular ligation products were run on an agarose gel so the size could be determined. The study revealed that when ligated, the sequence containing the A-tract formed smaller circular structures than the similar oligonucleotide of the same length but with random sequence. However, upon the addition of a nuclear extract containing HMG proteins, or pure HMG protein alone, both the random sequence oligonucleotide and the A-tract containing oligonucleotide favored the formation of the same size small circular structures, providing strong evidence that HMG proteins bend DNA substantially and overwhelm the effects of inherent DNA bending.

In this study, we will examine the effects of HeLa cell nuclear extract (NE), which contain HMG proteins, on the size and morphology of DNA condensates. By examining various topologies (i.e., supercoiled and linear) of plasmid DNA, we observed that in the presence of NE, DNA condensates strongly favor the rod morphology. To investigate the effects of inherent bending on HMG interactions further, plasmid DNA containing either 15 or 30 A-tract repeats was condensed in the presence of NE. Condensates formed by the A-tract containing DNA did not display a change in morphology; however, an increase in the size of the condensates was observed. Concentration studies were also performed to determine if higher concentrations of NE could eliminate the A-tract effect and to determine at lower concentrations of NE the point at which the NE ceases to affect condensate morphology.

6.1 Experimental Procedures

DNA Preparation: pBluescript II SK- (Stratagene) was isolated from the *E. coli* cell line, DH5- α (Life Technologies) using the Qiagen maxi-prep kit. The pBluescript II SK- plasmid will be referred to as *3kbDNA* in this chapter. DNA was eluted in 1 \times TE (10 mM Tris, 1 mM EDTA, pH 7.8). Several micrograms of the isolated DNA were linearized with the restriction endonuclease, *HindIII* (New England Biolabs), which singly cuts the plasmid. DNA after digestion was purified using a Microcon-YM 30 spin column (Millipore). The column was rinsed at least 5 times with 1 \times TE to ensure all remaining salts were removed from the DNA solution. Supercoiled DNA was used directly from the plasmid isolation procedure, as greater than 90% of the plasmid was estimated to be supercoiled based upon analysis by gel electrophoresis. The supercoiled DNA was also rinsed at least 5 times with 1 \times TE to remove any additional impurities and ensure the solution conditions of the DNA samples were identical. The DNA was diluted with 1 \times TE to a concentration of 20 μ g/ml. All concentrations were verified spectrophotometrically at A_{260} .

Plasmid DNA containing the A-tract repeats was designed by Shen et al. (9). The parent plasmid was pBluescript II SK-, with repeats of the following sequence inserted: 5' ATCCATCGACC(AAAAAACGGGCAAAAAACGGC)₇AAAAAAGCAGTGGAAG-3'.

Plasmid with one copy of the insert will be referred to as *Atract15*, and with two copies, *Atract30*, as the plasmids contain 15 and 30 A-tract repeats, respectively. Each A-tract is estimated to contribute approximately 13.5° of bend to structure of the plasmid (10). *Atract15* and *Atract30* were isolated from the *E. coli* cell line, Sure 2 (Stratagene). This cell line was specifically chosen because it has been engineered to tolerate sequence

repeats and structural anomalies in a plasmid with minimal recombination. After the DNA was isolated using the Qiagen maxi-prep kit, several micrograms of the plasmids were linearized as described above. Following the restriction digest, the DNA was purified, and diluted to 20 $\mu\text{g/ml}$ in 1 \times TE, as described above. Complete plasmid digestion was verified by agarose gel electrophoresis.

Nuclear Extract Preparation. HeLa cell nuclear extract (NE) was obtained from the Maher group as part of a collaboration (Mayo Clinic, MI). Isolation of the extract was performed as described by Dignam et al. (11). Prior to use, the nuclear extract was removed from a -80°C freezer and allowed to thaw on ice. The sample was then incubated for 5 minutes at 95°C , placed on ice for 2 minutes, then centrifuged for 50 seconds at $20,800\times g$. The supernatant was extracted from the tube by pipetting. The centrifugation step was repeated with the precipitate, and any additional supernatant was removed by pipetting away from the precipitate pellet. The supernatant was divided into ~ 3 μl aliquots of soluble NE. Aliquots not used immediately were returned to -80°C . The NE was diluted three fold with 1 \times TE prior to preparation of condensate reactions. This dilution was always performed on a new aliquot of heat-treated NE immediately before the condensation reaction was initiated. Tubes of NE were not refrozen, to avoid any possible changes induced by repeated freeze-thawing of the proteins. One microliter of the diluted NE was added to 9 μl of DNA (20 $\mu\text{g/ml}$), mixed by repeated pipetting, and allowed to equilibrate for 5 minutes prior to the addition of condensing agent.

Control experiments were performed to investigate potential effects of sample buffer in which the NE is stored on the condensation reaction. The buffer was prepared as

described by Dignam and contained 20 mM Hepes buffer, 20% v/v glycerol, 0.1 M KCl, 0.2 M EDTA, 0.5 M PMSF, and 0.5 M DTT (11). The buffer was diluted three fold with 1× TE, to mimic the buffer conditions of the reactions described above. One microliter of the diluted buffer was added to 9 μl of *3kbDNA*. One microliter of undiluted buffer was also added to 9 μl of *3kbDNA* to determine potential buffer effects induced by the addition of undilute NE to DNA.

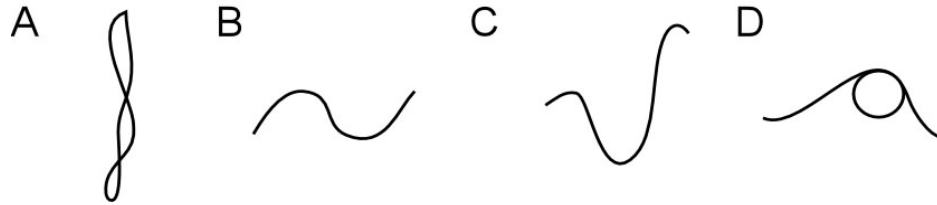
Concentration Studies of Nuclear Extract (NE): To examine the effects of decreasing the concentration of NE on DNA condensation, the following serial dilutions of NE were made: 1:3, 1:6, 1:12, and 1:24 in 1× TE. The solutions were mixed by repeated pipetting and 1μl was added to 9 μl of *3kbDNA*, as described above. The effects of increasing the concentration of NE on DNA condensation were examined by diluting the concentrated NE stock either 2 or 3-fold in 1× TE. One microliter of the 1:2 and 1:3 dilutions and 1 μl of the stock NE were added to *Atract30* DNA, so that three concentration could be compared.

Preparation of DNA Condensates: DNA solutions were mixed with an equal volume of 200 μM hexamine cobalt chloride (Sigma) and allowed to condense for 5 minutes. 5 μl of the reaction was then removed and placed on a carbon-coated electron microscopy grid (Ted Pella). After allowing 10 minutes for condensates to settle onto the grid an equal volume of 2% uranyl acetate was added to the grid momentarily, then the grid was rinsed in 95% ethanol and air dried.

Transmission Electron Microscopy (TEM) of DNA Condensates: The size and morphology of the DNA condensates were examined by TEM using the JEOL-100C. Images were taken at 100,000× magnification and scanned at 300 pixels/inch. Size measurements were performed by examining the images in Canvas software and analyzing size data using the “Read Coordinates” program written by Nick Hud. To obtain a statistical distribution of condensate morphologies, the grid surfaces were randomly scanned and the number of toroids and rods visible on the viewing screen were tallied. Several hundred structures were examined for each preparation.

6.2 Results

We have studied the condensation of two common topologies (i.e., supercoiled and linear) of the plasmid pBluescript II SK- DNA as well as two similar sequences containing varying amounts of A-tract repeats. The supercoiled plasmid DNA, referred to as supercoiled *3kbDNA*, was obtained directly from the plasmid isolation procedure; the linear DNA was prepared by digestion with a restriction endonuclease specific to a single site on the plasmid. The A-tract containing sequences were prepared by inserting repeats of phased A-tracts, the first containing 15 repeats (*Atract15*), and the second containing 30 repeats (*Atract30*), as described in the Experimental Procedures. The plasmids were estimated to contain approximately 195° and 390° of bend, respectively. Upon linearization, the A-tract sequences are located near one end of the linear DNA.



Scheme 6.1. Schematic representation of the topologies of plasmid DNA used for condensation experiments. A) Supercoiled *3kbDNA*; B) Linear *3kbDNA*; C) Linear *Atract15* containing approximately 180° of static bend; D) Linear *Atract30* containing approximately 360° of static bend.

Nuclear Extract Induces Changes in Supercoiled and Linear DNA Condensate Morphology. The condensation of linear and supercoiled DNA by hexamine cobalt chloride produced two distinctly different populations of condensate morphologies. When supercoiled *3kbDNA* was condensed, the resulting particles favored a mixed population of rods and toroids, with slightly over half the condensates observed in the rod morphology (Figure 6.1A). The linear *3kbDNA* condensates, on the other hand, were predominantly toroidal in morphology (Figure 6.1B). Similar results have been previously reported in the literature (12, 13).

Nuclear extract (NE) was added to the DNA solutions and allowed to interact with the DNA for 5 minutes prior to condensation. Supercoiled *3kbDNA* condensate morphologies were altered by the presence of NE such that approximately 20% of the population converted from toroids to rods, resulting in $> 80\%$ of the condensates existing as rods (Figure 6.1C). The change in condensate morphology in the linear *3kbDNA* preparation was greater than that of the supercoiled sample (Figure 6.2). The population of rods increased by approximately 50%, from having a vast majority of toroidal structures and a few scattered rods in the absence of NE, to a having nearly an equal proportion of the two structures when the NE was allowed to interact with the DNA prior

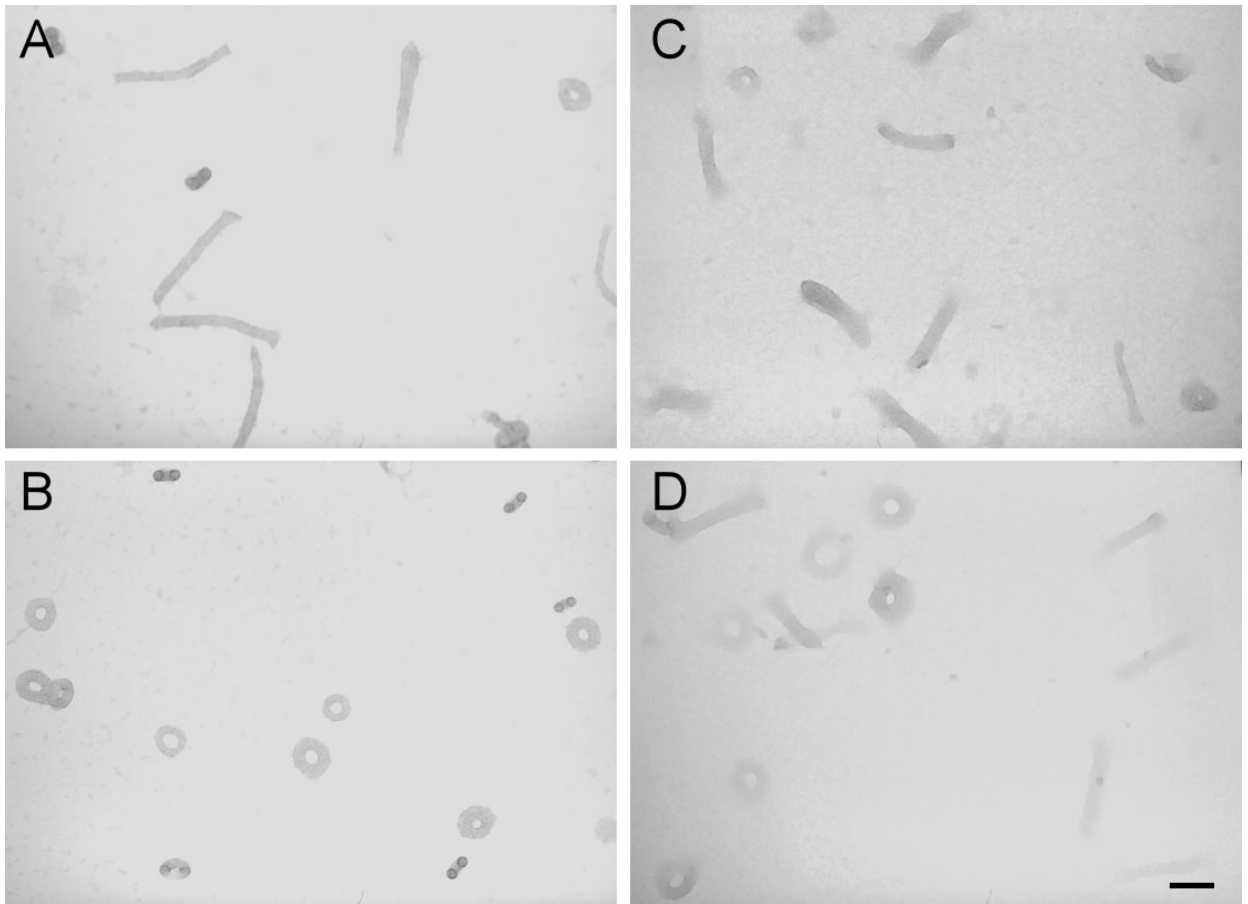


Figure 6.1. Transmission electron microscopy (TEM) images of supercoiled and linear pBluescript SK II- (*3kbDNA*) DNA condensates. (A) Rods and toroids produced by the addition of hexamine cobalt chloride to supercoiled *3kbDNA*. (B) Toroids produced by the addition of hexamine cobalt chloride to linear *3kbDNA*. (C) Rods and toroids produced by supercoiled *3kbDNA* in the presence of nuclear extract (NE), condensed with hexamine cobalt chloride. (D) Rods and toroids produced by linear *3kbDNA* in the presence of NE, condensed with hexamine cobalt chloride. The final solution conditions are 10 $\mu\text{g/ml}$ DNA and 100 μM hexamine cobalt chloride in 0.5 \times TE. Scale bar is 100 nm.

to condensation (Figure 6.1D). The presence of NE in both the supercoiled and linear *3kbDNA* samples increased the quantity of rods produced upon condensation. It is clear that in the presence of the nuclear extract the toroid diameters increased for the linear *3kbDNA*, whereas a similar effect was not obvious in the supercoiled *3kbDNA* sample.

Nuclear Extract Effects on Condensate Morphology Are Less Prominent on DNA Containing A-tract Sequences. As previously reported, the presence of multiple phased A-tract repeats decreases the size of toroidal DNA condensates (9, 12). *Atract15* is estimated to induce approximately 180° of bend into the plasmid secondary structure, creating a static horseshoe-like structure. Condensates produced when *Atract15* DNA is condensed with hexamine cobalt (III) are predominantly toroids, as was observed in the linear *3kbDNA* reaction (Figure 6.3A). Many of the toroids were also similar in size to those observed with the linear *3kbDNA* (Figure 6.1B), however, some toroids were noticeably smaller in diameter. The A-tract effect was greater in the *Atract30* preparations as this DNA is estimated to contain over 360° of intrinsic bending from the A-tract sequences, which forms a static loop in the linear DNA. The *Atract30* preparation was also found to contain a population of greater than 90% toroids (Figure 6.3B). Toroids observed appeared smaller than those seen in the linear *3kbDNA* sample (i.e. diameter of *Atract30* toroids = 64.4 nm (n=134), diameter of *3kbDNA* toroids = 73.6 nm (n=106)).

The addition of NE to the *Atract15* sample resulted in a notable alteration of the condensate morphologies (Figure 6.2). The condensate population was composed of greater than 90% toroids in the absence of NE, which decreased to approximately 65%

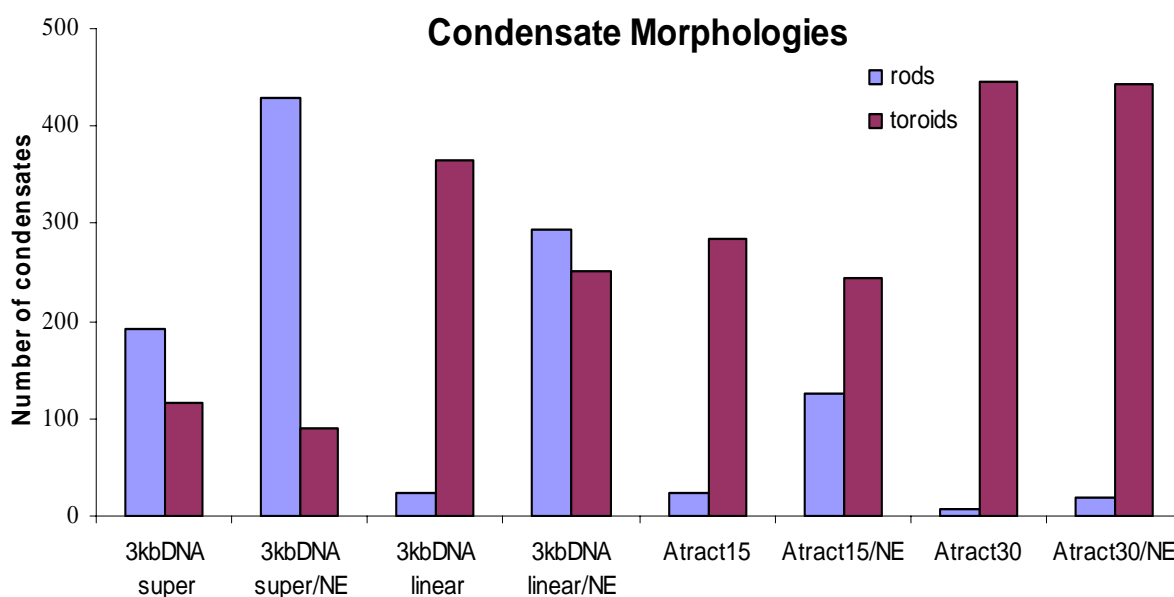


Figure 6.2. Histogram of DNA condensate morphologies (rod vs. toroid) for various DNA samples and condensation conditions. TEM grids of the four DNA samples (including supercoiled and linear *3kbDNA*, *Atract15*, and *Atract30*) were randomly sampled to assess the condensate population. The distributions of condensate morphologies were also compared in the presence of NE, to determine affects of NE and the proteins therein on condensate morphology.

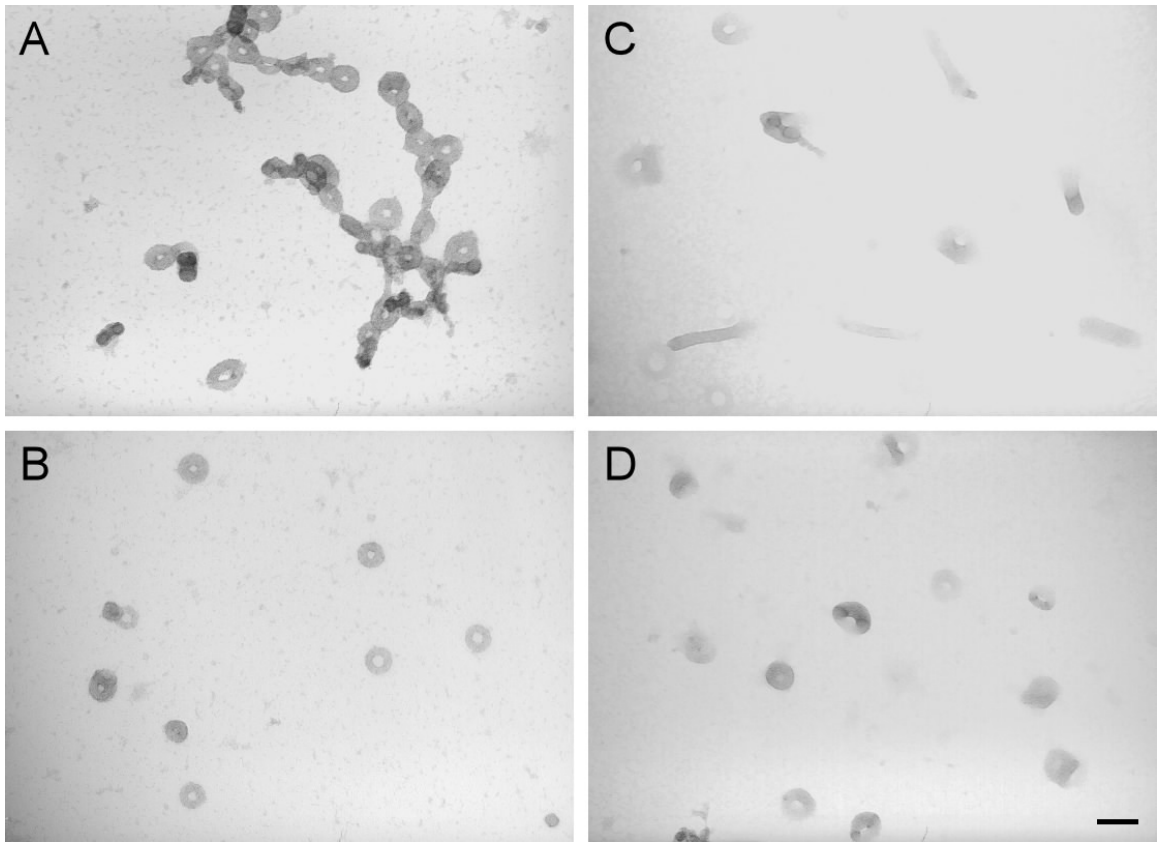


Figure 6.3. TEM images of DNA condensates formed by the condensation of linear plasmid DNA containing varying amounts of static curvature (*Atract15* and *Atract30*). (A) Toroids produced upon the addition of hexamine cobalt chloride to *Atract15*. (B) Toroids produced upon the addition of hexamine cobalt chloride to *Atract30*. (C) Rods and toroids produced by *Atract15* in the presence of nuclear extract (NE), condensed with hexamine cobalt chloride. (D) Toroids produced by *Atract30* in the presence of nuclear extract (NE), condensed with hexamine cobalt chloride. The final solution conditions are 10 $\mu\text{g/ml}$ DNA and 100 μM hexamine cobalt chloride in 0.5 \times TE. Scale bar is 100 nm.

toroids in the presence of NE (Figure 6.3C). *Atract30* condensate morphology was less affected by the presence of the NE. Greater than 90% of the condensates remained as toroids, similar to the condensation of *Atract30* in the absence of NE (Figure 6.3D). Although the toroid to rod ratio varied between the A-tract containing samples, both samples showed an increase in toroid size in the presence of NE. Toroid diameters of the *Atract30* sample were measured to quantify the difference in toroid size in the presence of NE. This

particular DNA was chosen for size quantification because the majority of condensates formed with and without NE present were toroids. Toroids formed in the absence of NE had a mean outer diameter of 64.4 nm, and a mean thickness of 23.4 nm, while toroids formed in the presence of NE had a mean outer diameter of 88.2 nm and a mean thickness of 35.1 nm (n=66) (Figure 6.3B and D).

Nuclear Extract Effects on DNA Condensation Are Concentration Dependent. To further investigate the effect of NE on the morphology of the condensates, studies were performed at both increasing and decreasing concentrations of nuclear extract. Due to the large alteration in condensate morphology observed in the presence of NE, the linear *3kbDNA* sample was chosen as the optimal system to determine the sensitivity of condensation to the concentration of NE in the condensation reaction. Under the conditions examined above, the concentration of NE was diluted three fold prior to mixing with the DNA solution. As described in the Experimental Procedures, one microliter of dilute NE was added to 9 μ l of DNA, which accounts for an additional ten fold decrease in the NE concentration. Dilutions of the NE stock were performed such

that NE concentrations were 1:3, 1:6, 1:12, and 1:24 dilutions of the stock prior to addition to the DNA. These dilute NE solutions were added to the *3kbDNA* and then condensed with hexamine cobalt (III). The 1:3 dilution, as shown in Figure 6.1D, contained nearly equal quantities of toroids and rods. However, a two fold further dilution of the NE lead to a reversion of the condensates to the toroid morphology (Figure 6.4B). Nearly 95% of the condensates were toroids, much closer to the morphology of the *3kbDNA* condensates formed in the absence of NE. Although the morphology of the condensates reverted to toroids, the toroidal condensates produced in the presence of NE were larger in diameter than those observed in the absence of NE (Figure 6.4B and 6.1B), similar to toroids formed in all other preparations containing NE. Further dilutions of NE yielded results similar those for the 1:6 dilution (i.e. no observable NE affect on morphology).

Nuclear Extract Dialysis Buffer Also Affects Condensate Morphology. The concentration of NE was also increased to determine if the observable effects of NE would be more pronounced at higher concentrations. *Atract30*, whose condensate morphology was least unaffected by the 1:3 concentration of NE in the initial set of experiments, was used to study the effect of increased NE concentration. We hypothesized that increased concentrations of NE may at some point dominate the A-tract effect, and lead to increased rod formation. Concentrated nuclear extract was added without dilution from the isolate, and also was diluted two fold in 1× TE as described above (Figure 6.5). These concentrations are higher than the three fold dilution of NE that was used for the initial experiments. In both cases the NE was added to the DNA as described earlier. A

detectable change in the morphologies of the condensates was observed when the isolated stock of NE was added to the DNA. The quantity of rods increased approximately 10% and a mix of toroidal and spherical condensates were observed. Spherical particles were not observed in other preparations at lower NE concentrations. The higher concentration of NE introduces the possibility that the NE storage buffer may also affect the condensate size and morphology, as this buffer contains 100 mM KCl and 20% v/v glycerol, both of which can affect condensation (12, 14). Control experiments using only the stock buffer containing no NE produced condensates that were predominantly spherical or ellipitical in shape (Figure 6.6A). Thus, it is evident that the storage buffer alone can alter DNA condensation. However, at a three fold dilution of the storage buffer containing no NE, these effects are reduced as compared to the more concentrated buffer. The spherical structures were not as well defined and had an increased tendency to aggregate. Additionally, some free DNA was observed on the EM grids, indicating incomplete condensation (Figure 6.6B). No further experiments to adjust the buffer conditions for the NE stock were attempted at this time, because it is unknown if variations in the NE storage buffer would alter the efficiency of the proteins in the NE.

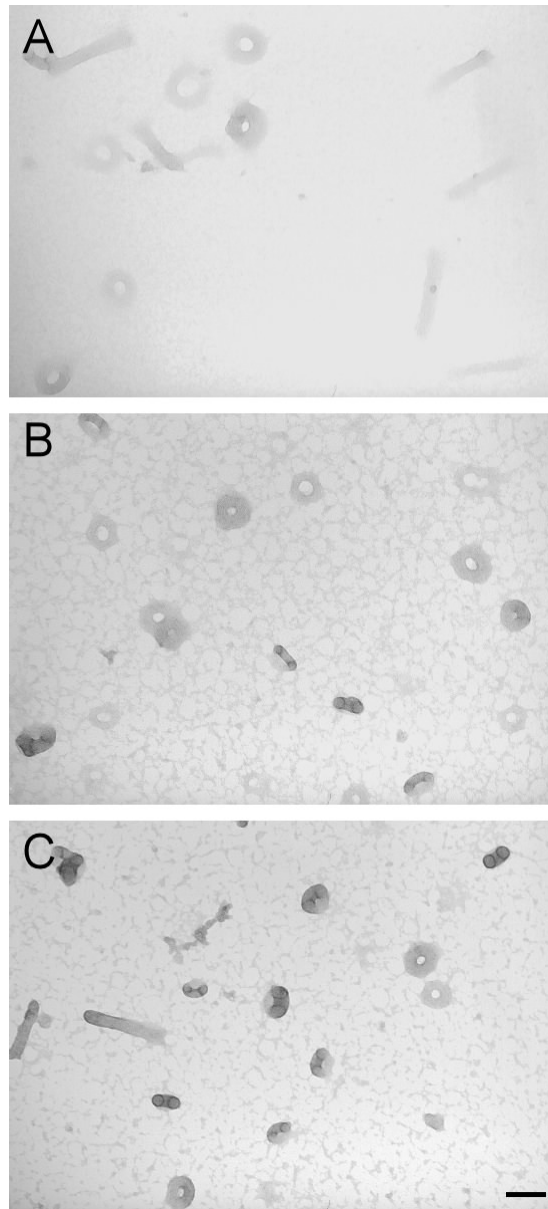


Figure 6.4. TEM images of *3kbDNA* condensed with hexamine cobalt chloride in the presence of varying concentrations of nuclear extract. (A) Typical condensates produced when *3kbDNA* mixed with a 1:3 dilution of NE is condensed. (B) Typical condensates produced when *3kbDNA* mixed with a 1:6 dilution is condensed. (C) Typical condensates produced when *3kbDNA* mixed with a 1: 12 dilution of NE is condensed. The concentration of NE in the DNA solution is 10× greater than the dilution factor. The DNA concentration is 10 $\mu\text{g/ml}$ and hexamine cobalt chloride is at 100 μM . The scale bar is 100 nm.

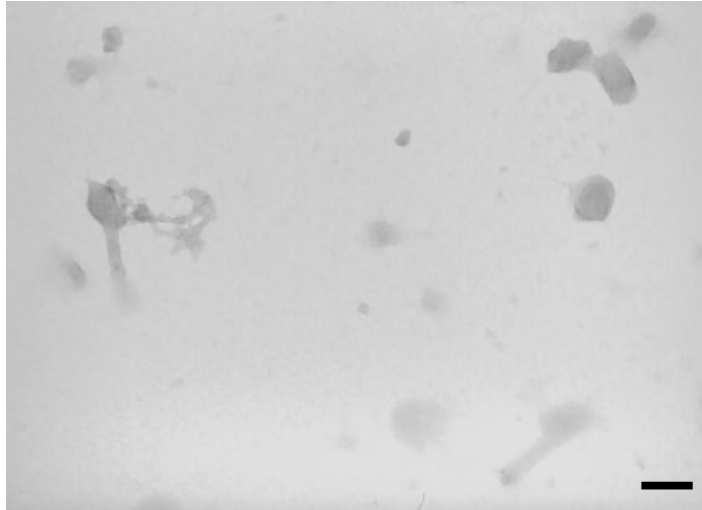


Figure 6.5. TEM image of *Atract30* condensed with hexamine cobalt chloride in the presence of undiluted nuclear extract. Condensates formed in the presence of undiluted (1:1) NE. The final DNA concentration is 10 $\mu\text{g/ml}$ and hexamine cobalt chloride is 100 μM . Scale bar is 100 nm.

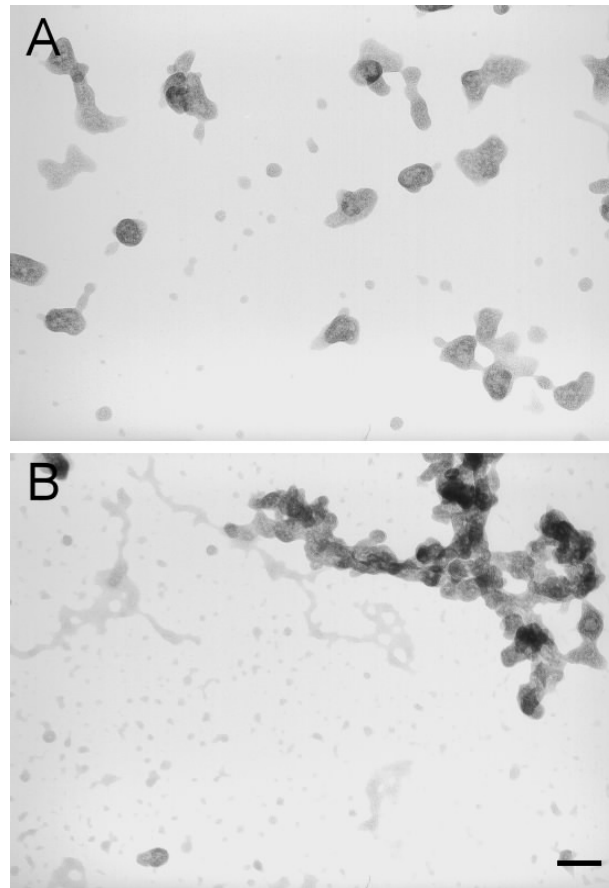


Figure 6.6. TEM images of linear *3kbDNA* condensed with hexamine cobalt chloride with increasing concentrations of sample buffer. (A) Condensates formed by *3kbDNA* condensed in the presence of undiluted storage buffer. (B) Condensates formed by *3kbDNA* condensed in the presence of a 1:3 dilution the storage buffer. The final DNA concentration is 10 $\mu\text{g/ml}$ and hexamine cobalt chloride is 100 μM . Scale bar is 100 nm.

6.3 Discussion

Chapters 2, 3 and 4 have shown that altering the structure of DNA, ionic strength, temperature and the order in which components are added to a reaction, can significantly affect the size and morphology of condensates (9, 12, 13). In this study, we further examine the effects of DNA topology and bending on DNA condensation by condensing DNA in the presence of proteins known to bend DNA *in vivo*. The condensates that resulted from the dynamic bending induced by the proteins were compared to condensates formed by DNA containing static curvature, both in the presence and absence of the DNA bending proteins. We have examined the contributions of the dynamic and static bending individually, and then collectively to determine, under the conditions of condensation, which factor primarily controls the size and morphology of the condensates.

Nuclear Extract Greatly Alters the Condensation of 3kbDNA. Supercoiled 3kbDNA condensed with hexamine cobalt (III) produced a mixed population of condensate morphologies. Supercoiled plasmid DNA has topological constraints that restrict the ability of the DNA to condense into certain compact structures (e.g. toroids and spheroids). The tertiary structure of supercoiled DNA (i.e., cross-over contacts) may provide potential nucleation sites for the initiation of condensation. However, these same crossovers within the plasmid may also limit the path of plasmid collapse (Figure 6.7A). As was shown in Figure 6.1A, supercoiled 3kbDNA produces both rods and toroids. The formation of rods indicates that there are additional factors (e.g. tertiary structural

constraints) influencing the supercoiled DNA to bend over short distances that are less than the persistence length of DNA.

The addition of NE, which contains several proteins that are known to increase DNA bending (e.g., HMG proteins), was expected to introduce additional conformational freedom to the DNA (i.e. reduce the persistence length) (1). The energy necessary for the kinks in the DNA required to form rod morphologies, is reduced by the binding of proteins that induce bends and twists into the DNA structure (Figure 6.7A). The HMG proteins present in the NE are expected to contribute to this effect. There was a 20% increase in the quantity of rods produced in the supercoiled condensation reaction (Figure 6.2). Previous studies of DNA condensation have suggested that the reduction of persistence length allows for the formation of structures such as rods, which require DNA to have reduced bending constraints for formation to be favorable (Stevens ??). The ability of the proteins in the nuclear extract to increase the bending of the DNA reduces energetic constraints to be overcome, allowing the formation of rods.

The effects of reduced persistence length provided by the addition of nuclear extract are the most evident in the linear *3kbDNA* sample. *3kbDNA* condensed with hexamine cobalt (III) produced primarily toroidal structures (Figures 6.1B and 6.2). Toroids produced under these conditions have been estimated to be at the minimum size allowed by persistence length limitation (12, 15). The addition of NE to the linear *3kbDNA* condensation reaction decreased the concentration of toroids significantly so that the toroids and rods were present in nearly equal proportions (Figure 6.7B). Since there were no other factors to influence the secondary structure of the DNA, this increase in the quantity of rods, indicating a reduction in persistence length limitations, must be

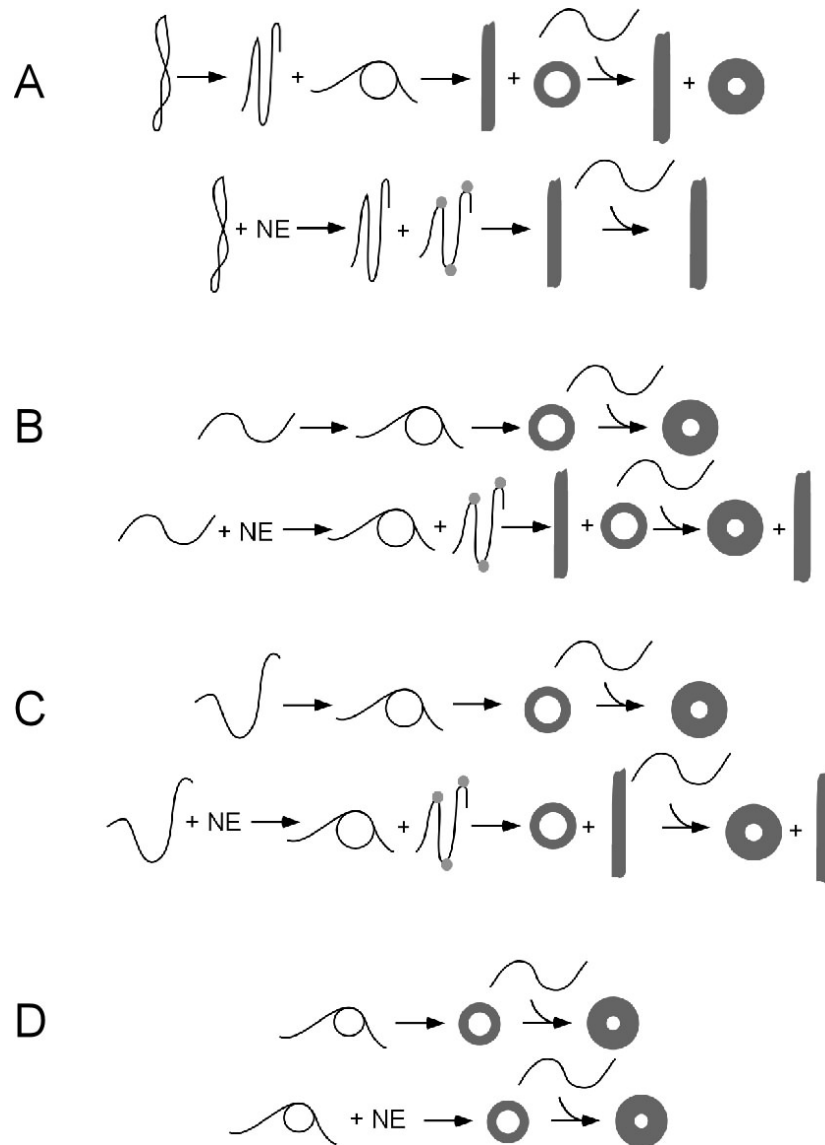


Figure 6.7. Schematic diagrams of DNA condensation in the presence and absence of nuclear extract. Free DNA in solution nucleates condensates upon the addition of hexamine cobalt chloride. These proto-condensates grow larger by the addition of remaining free DNA to the stable proto-condensate. The gray circles represent the nuclear extract proteins binding the DNA. (A) Condensation of supercoiled *3kbDNA* without NE (top) and with NE (bottom). (B) Condensation of linear *3kbDNA* in the presence of NE (top) and absence of NE (bottom). (C) Condensation of *Atract15* without NE (top) and with NE (bottom). (D) Condensation of *Atract30* without NE (top) and with NE (bottom).

attributed solely to the components of the NE. It should be noted that it is known that HMG proteins are present in the nuclear extract used in these experiments (5). However, other proteins isolated in the nuclear extract and components of the storage buffer may also contribute to the effects observed as a result of the presence of nuclear extract.

Intrinsic Bending of DNA Can Reduce the Effects of NE on Condensation. Condensation of *Atract15* with hexamine cobalt (III) produced primarily toroidal condensates (Figure 6.2). The size of toroids observed in this preparation varied somewhat, showing similarity to both the *3kbDNA* and *Atract30* toroids. While the A-tracts present in the *Atract15* plasmid do not form a static nucleation loop, like the *Atract30* DNA, a substantial amount of bending exists in the DNA structure (Figure 6.7C). This horseshoe-like bending may increase the probability of toroid nucleation by decreasing the end to end distance of the DNA. The condensates observed included a mixed population with several smaller toroids, similar in diameter to those observed in plasmid containing greater numbers of A-tracts (9, 12). The variation in toroid size may be attributed to the occasional nucleation of smaller toroids as a result of the static bend in the DNA structure. This effect was examined in Chapter 2.

Morphologies of *Atract15* condensates were also significantly affected by the addition of NE to the DNA solution. While the increase in the rod to toroid ratio was not as significant as in the *3kbDNA* preparation (Figure 6.2), there was nearly a 30% increase in the rod population. This transition in the rod population is significantly less than the 50% increase in rods observed for the *3kbDNA* condensates. Thus, it is apparent that the static horseshoe-like bend in the DNA secondary structure, from the A-tract sequence,

apparently influences the morphology of condensates. This result was somewhat unexpected because the A-tract bend in *Atract15* does provide a nucleation loop in the manner we have previously described. The static bend seems to provide enough bend to make the spontaneous formation of a nucleation loop more favorable, thereby increasing the successful nucleation of toroids in the presence of the nuclear extract, as compared to *3kbDNA* (Figure 6.7C).

In *Atract30* condensation reactions, toroids accounted for greater than 90% of the population in the absence of NE (Figure 6.2). The toroids formed by *Atract30* were 10 nm smaller than those formed by *3kbDNA* under the same conditions (Figure 6.7D). The *Atract30* toroids were similar in size to toroids formed by the same plasmid DNA containing 60 phased A-tract repeats as described previously (9, 12), indicating that the presence of one static nucleation loop formed by the A-tract bending can effectively decrease the size of toroids by more than 10%. The presence of the static nucleation loop is expected to reduce the energetic barrier of toroid formation by eliminating the rate limiting step of spontaneous nucleation loop formation (15). Thus, the nucleation of toroids with *Atract30* DNA is clearly more favorable than in the *Atract15* or *3kbDNA* samples.

Bending effects induced by NE did not significantly affect the *Atract30* condensate morphology (Figure 6.2). Toroids remained as the dominant structure, thus, it is apparent that the presence of the static nucleation loop contributes substantially to the path of condensation. Increasing the quantity of A-tract repeats from 15 to 30 enhanced the A-tract effect as compared to the *Atract15* data described above (Figure 6.7D). In this case, the nucleation loop provides stability to the DNA that allows nucleation and

growth of the toroids, regardless of reduction of the bending energies due to protein interactions. It is also possible that the presence of the nucleation loop favors toroid formation to occur so quickly that minimal sampling can occur and the DNA becomes trapped in the toroidal structures.

Toroid Size Increases in the Presence of NE. An increase in the diameter of toroids produced in the presence of NE was consistently observed for linear *3kbDNA*, *Atract 15*, and *Atract30* condensation reactions. One possible explanation for this observation involves protein-DNA interactions. The proteins in NE, particularly HMG1 and 2 proteins, have been found to bind non-specifically to DNA sequences and secondary structures (5). This suggests that the bending of DNA by the proteins is completely random, which may reduce the intrinsic bending of the A-tract inserts. By binding within the A-tract rich regions of the plasmid, the proteins could either enhance the degree of bending substantially or counteract the A-tract bends, depending on if the dynamic bending is in phase with the A-tract bend. If the protein is out of phase with the A-tract bend, the nucleation loop may increase in size.

Furthermore, the increase in toroid diameter was observed even at lower concentrations of NE; the toroid sizes increase even though the concentration of proteins present is not enough to significantly alter the morphology of the particles. Thus, the increase in toroid size may be attributed to some extent to the increased conformational freedom of the plasmid DNA in the presence of NE, even at concentrations where the morphology is not obviously altered.

Buffer contributions must also be considered when examining the increasing size of toroidal structures in the presence of NE. As described above, the sample buffer for the NE contains multiple components that may affect the interactions of the condensing agent with the DNA. The high concentration of the monovalent salt, KCl, in the buffer could lead to increased toroid size (12). It has been proposed that increased ionic strength of condensation reactions leads to decreased interactions of the condensing agent with the DNA, making the formation of a stable nucleation loop more difficult (13, 16, 17). This reduced stability allows the DNA to sample more nucleation loop sizes prior to the formation of a stable proto-toroid structure. The less frequent nucleation of stable proto-toroids leads to free DNA being present in solution for a longer time, causing the toroids to grow to larger sizes which are ultimately limited by the concentration of free DNA in solution or a net undercharging of the condensates (18-20).

The high percentage of the crowding agent, 20 % v/v glycerol in the buffer may also affect the condensate size and morphology. Previous studies have shown that crowding agents such as polyethylene glycol (PEG) can aid in the condensation of DNA (14). The crowding agent enhances the interactions of DNA strands, favoring the formation of condensates. The effects of buffer on condensation indicate that one or both of these factors contribute to the variations in condensate size and morphology observed by TEM (Figure 6.6A and B). Comparison of the condensates formed by condensation in the control buffer with the condensates formed in the presence of the nuclear extract indicate that effects of the proteins in the nuclear extract are greater than the effects of the buffer.

A Minimal Amount of NE Must Be Present to Affect Condensation. Condensation of linear *3kbDNA* with decreasing concentrations of nuclear extract revealed a substantial concentration affect (Figure 6.4). By decreasing the concentration of NE two-fold, the morphologies of the condensates reverted back to approximately the same rod to toroid ratio observed for linear *3kbDNA* condensed in the absence of NE (i.e., > 90% toroids). It was somewhat surprising that the effects of decreased persistence length were reduced to this extent over such a small change in NE concentration. However, recent studies have revealed that HMG proteins bind cooperatively to DNA (7, 21-23). Decreasing concentrations of the HMG proteins has been shown to lead to a non-linear decrease in protein binding (21). Under the conditions examined here, it is possible that the protein concentration in the solution was reduced to an extent at which the cooperative binding of the HMG proteins was essentially eliminated. We hypothesize that the dramatic reversion in condensate morphologies over such a small change in concentration may be attributed to this cooperative binding effect. By dropping below the NE concentrations that favored the cooperative binding of HMG proteins, bending energy constraints resurfaced as a determining factor in condensate morphology, favoring the formation of toroidal condensates at low NE concentrations.

Although at lower concentrations, the morphologies of the condensates were not altered by the presence of NE, the sizes of the toroids observed were noticeably larger than those formed in the absence of NE (Figures 6.1 and 6.4). The toroids produced at low concentrations of NE (e.g., 1:6 and 1:12 dilutions) were larger in diameter. While this effect may to some extent be attributed to the buffer composition, it may also result from the non-cooperative binding of HMG protein molecules. At low concentrations,

HMG proteins, although not cooperatively binding DNA, still formed a distinct structure that was observable on gel retardation assays (21). Bending can still be induced in the DNA structure, which reduces bending constraints for DNA toroid formation. Such an effect may allow for toroids to sample more nucleation loop sizes and settle on a slightly larger loop size (with less bending energy) prior to the formation of a stable proto-toroid. Further studies are necessary to determine to what extent this increase in toroid size resulted from the protein-DNA interactions as opposed to buffer conditions.

References

1. Travers, A. A., Ner, S. S., and Churchill, M. E. (1994) *Cell* 77, 167-169.
2. Hagerman, P. J. (1988) *Annual Reviews in Biophysical Chemistry* 17, 265-286.
3. Paull, T. T., Haykinson, M. J., and Johnson, R. C. (1993) *Genes and Development* 7, 1521-1534.
4. MacAlpine, D. M., Perlman, P. S., and Butow, R. A. (1998) *Proceedings of the National Academy of Sciences of the United States of America* 95, 6739-6743.
5. Ross, E. D., Hardwidge, P. R., and Maher, L. J. (2001) *Molecular and Cellular Biology* 21, 6598-6605.
6. Love, J. J., Li, X., Case, D. A., Giese, K., Grosschedl, R., and Wright, P. E. (1995) *Nature (London)* 376, 791-795.
7. Werner, M. H., Huth, J. R., Gronenborn, A. M., and Clore, G. M. (1995) *Cell* 81, 705-714.
8. Tang, L., J., L., Katz, D. S., and Feng, J. (2000) *Biochemistry* 39, 3052-3060.
9. Shen, M., Downing, K., Balhorn, R., and Hud, N. (2000) *Journal of the American Chemical Society* 122, 4833-4834.
10. Rivetti, C., Walker, C., and Bustamante, C. (1998) *Journal of Molecular Biology* 280, 41-59.
11. Dignam, J. D., Lebovitz, R. M., and Roeder, R. G. (1983) *Nucleic Acids Research* 11, 1475-1489.
12. Conwell, C. C., Vilfan, I. D., and Hud, N. V. (2003) *Proceedings of the National Academy of Sciences of the United States of America* 100, 9296-9301.
13. Conwell, C. C., and Hud, N. V. (2004) *Biochemistry*, in press.

14. Bloomfield, V. (1996) *Current Opinion in Structural Biology* 6, 334-341.
15. Hud, N. V., Downing, K. H., and Balhorn, R. (1995) *Proceedings of the National Academy of Sciences of the United States of America* 92, 3581-3585.
16. Rouzina, I., and Bloomfield, V. A. (1996) *Journal of Physical Chemistry* 100, 4292-4304.
17. Rouzina, I., and Bloomfield, V. A. (1997) *Biophysical Chemistry* 64, 139-155.
18. Park, S. Y., Bruinsma, R. F., and Gelbart, W. M. (1999) *Europhysics Letters* 46, 454-460.
19. Nguyen, T. T., and Shklovskii, B. I. (2002) *Physical Review E* 65, 031409-1-031409-7.
20. Gelbart, W. M., Bruinsma, R. F., Pincus, P. A., and Parsegian, V. A. (2000) *Physics Today* 53, 38-44.
21. Webb, M., Payet, D., Lee, K. B., Travers, A. A., and Thomas, J. O. (2001) *Journal of Molecular Biology* 309, 79-88.
22. Schlierf, B., Ludwig, A., Klenovsek, K., and Wegner, M. (2002) *Nucleic Acids Research* 30, 5509-5516.
23. Ellwood, K. B., Yen, Y. M., Johnson, R. C., and Carey, M. (2000) *Molecular and Cellular Biology* 20, 4359-4370.

CHAPTER 7

BRIEF DISCUSSIONS OF TEMPERATURE, TOPOLOGY AND MIXED DNA POPULATIONS ON DNA CONDENSATION

Minute changes in the conditions of DNA condensation can have significant effects on the size and morphology of DNA condensates. As shown in previous chapters, variations in ionic strength, the order of counterion addition, static curvature, and increased DNA flexibility were investigated to determine the effects on DNA condensate formation. In addition to these factors, several other reaction conditions have been found to influence the size and morphology of DNA condensates. This chapter briefly addresses the variations in condensate size and morphology introduced by changing the temperature of the reactions, the topology of the plasmid DNA, mixing DNA containing static structures with DNA lacking additional secondary structure, and condensing fragments plasmid DNA.

7.1 Temperature Effects on DNA Toroid Size

The condensation of DNA into toroids is a nucleation and growth process that is dependent upon the spontaneous bending of the DNA into a nucleation loop. The persistence length of DNA significantly influences the size of the nucleation loop. Studies have shown that persistence length of DNA may vary with ionic strength of the solution as well as temperature (1, 2). In Chapter 2, the effects of ionic strength on persistence length were addressed. As the ionic strength was increased, no obvious change in nucleation loop size was observed. The effects of temperature on toroid formation were not incorporated into that discussion.

Previous investigations of DNA persistence length have indicated that a maximum in persistence length occurs at approximately 20-30°C (1, 2). The persistence length of DNA was shown to decrease between ~10-15% from the maximum with both increasing and decreasing temperature (1). DNA was condensed at three temperatures to determine if variations in temperature altered the size or morphology of DNA toroids.

7.1.2 Experimental Procedures

DNA Preparation. Bluescript II SK- plasmid DNA (Stratagene) was grown in DH5a (Life Technologies) and isolated using the Qiagen Maxi Prep kit. The DNA was eluted in 1× TE (10 mM Tris, pH 7.8, 1 mM EDTA) and linearized by digestion with the restriction enzyme Hind III (New England Biolabs). Buffer and salts introduced for the restriction digest reaction were removed by rinsing the DNA three times with 0.25× TE using a Microcon YM-30 spin column (Millipore). After the final rinse, DNA was resuspended from the spin column membrane to a final concentration of 20 µg/ml in

0.25× TE. DNA concentrations were verified spectrophotometrically. The sample was brought back to a buffer concentration of 1× TE by adding a small volume of concentrated TE to the sample.

DNA Condensate Preparation and Imaging. DNA condensates were prepared by mixing a DNA sample solution with an equal volume of a hexamine cobalt chloride (Sigma) solution to yield a condensation reaction mixture 8.5 µg/ml in DNA, 100 µM in hexamine cobalt chloride and 0.5× in buffer. Condensate reaction mixtures were allowed to equilibrate for 5 minutes and then deposited on carbon-coated grids (Ted Pella). After 10 minutes on the grids, 2% uranyl acetate (Ted Pella) was added momentarily to the condensate mixtures, the grids were then rinsed in 95% ethanol and air-dried. The condensation reactions were performed at ~22°C (room temperature), 4°C (cold room) and 38°C (warm room). All of the individual solutions were allowed to equilibrate to the room temperature for 10 minutes prior to mixing.

The DNA condensates were recorded on film using a JEOL-100C transmission electron microscope (TEM) at 100,000× magnification. The TEM negatives were scanned at 300 pixels/inch and Canvas graphics program was used to measure the outer diameter and thickness of individual DNA toroids. The lines representing the toroid diameters and thicknesses were copied to a new Canvas file and saved in .eps format. This file was read using the “*Read Coordinates*” program written by Nick Hud, which allowed the data to be opened and analyzed in Microsoft Excel.

7.1.3 Results

Linear Bluescript DNA (abbreviated *3kbDNA*) was condensed with hexamine cobalt chloride at three temperatures to determine the effects of temperature on condensate size. DNA was condensed at 22°C (room temperature) in the presence of hexamine cobalt chloride. The resulting toroidal condensates had a mean *toroid diameter* of 70 nm (Figure 7.1B). (Toroid diameter was defined in Chapter 2 as the average of the inner and outer diameter of the toroid.) The mean toroid thickness was approximately 42 nm.

3kbDNA condensed with hexamine cobalt chloride at 4°C formed well dispersed toroidal condensates. The mean *toroid diameter* of condensates formed at 4°C was 66 nm, which is approximately the same as the toroids formed at 22°C. The mean toroid thickness, however, decreased significantly to 29 nm.

Toroidal condensates formed when *3kbDNA* was condensed with hexamine cobalt chloride at 38°C were also observed to be smaller than those formed at 22°C. The condensates had a mean toroid diameter of 49 nm and a mean thickness of 30 nm. These toroids were smaller in both toroid diameter and mean thickness than the toroids prepared at 22°C. Additionally, the toroids were significantly smaller in toroid diameter than those formed at 4°C, however, the mean thicknesses of the condensates were approximately equal. These differences in condensate size are shown in Figure 7.2. The graph shows a tight distribution of toroids formed at 38°C as compared to the other data sets, indicating that the increased temperature is limiting toroid size to some extent.

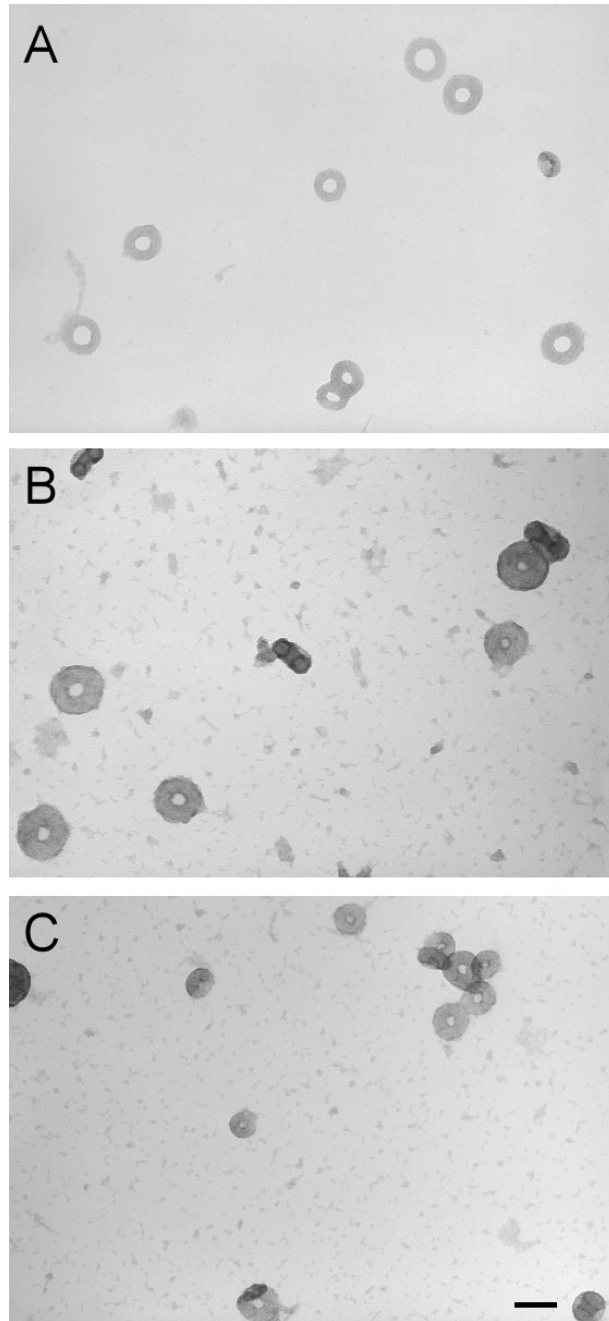


Figure 7.1. Transmission electron microscopy images of *3kbDNA* condensed at 4, 22, and 38°C with hexamine cobalt chloride. (A) Toroidal condensates formed when *3kbDNA* was condensed at 4°C. (B) Toroidal condensates formed when *3kbDNA* was condensed at 22°C (room temperature). (C) Toroidal condensates formed when *3kbDNA* was condensed at 38°C. The final concentration of DNA was 10 $\mu\text{g/ml}$ and hexamine cobalt chloride was 100 μM . The scale bar is 100 nm.

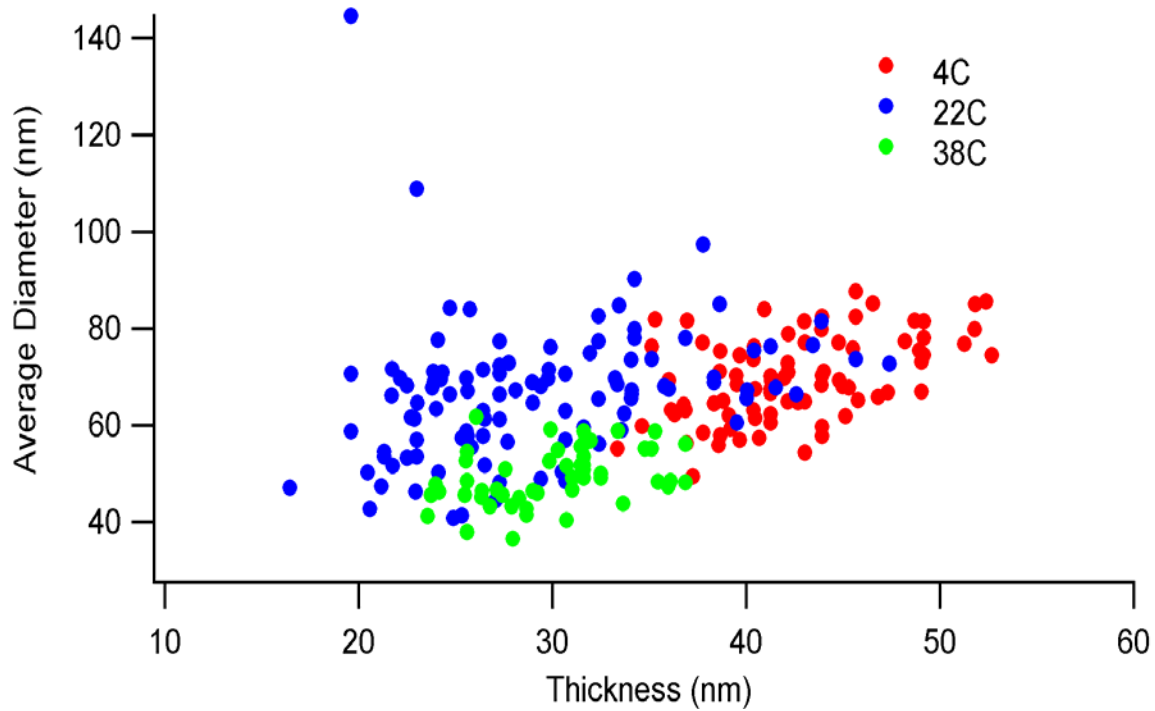


Figure 7.2. Scatter plot of toroid diameter and thickness for DNA condensed at 4, 22, and 38°C.

7.1.4 Discussion

It should be noted that the DNA(s) used to prepare the toroids for these experiments were not under “low salt” conditions (i.e., $1\times$ TE). This was determined when the DNA stock used for these experiments was exhausted and new Bluescript was linearized. The buffers were exchanged by rinsing through the Microcon YM-30 spin columns. The toroids formed from this DNA purification were substantially smaller in size than those shown in Figure 7.1B. The decrease in toroid size was found to be resulting from residual salt in the DNA from the restriction digest. The concentration of monovalent and divalent counterions in solution was increased by adding millimolar quantities of NaCl and MgCl₂, respectively. These incremental increases in the ionic strength of the solution resulted in increased toroid dimensions, eventually comparable to those observed at 22°C in this study. The changes in toroid size introduced by changing the ionic strength of the solution were discussed in Chapter 2.

Based on the systematic investigation of increasing ionic strength on toroid size, it was determined that the DNA contained approximately 1/6- 1/8 the concentration of New England Biolabs Buffer #2 (50 mM NaCl, 10 mM Tris, 10 mM MgCl₂ and 1 mM DTT). According to studies of DNA persistence length, these concentrations of monovalent and divalent counterions should *minimize* the persistence length of DNA for these specific solution conditions, and should not differ significantly from the persistence length of DNA in TE buffer. Thus, it is expected that the influence of ionic strength on persistence length has been optimized for all the conditions investigated.

As discussed previously, temperature can also alter the persistence length of DNA. Studies have found that persistence length reaches a maximum value at approximately 20-30°C, or close to room temperature. Both increasing and decreasing the

temperature from the maximum resulted in a decreased persistence length of the DNA (1, 2). It is evident from the variations in the size of toroidal condensates is a direct result of the temperature of the reactions, as all other conditions remained identical between preparations. Both increasing and decreasing the temperature at which condensation occurs decreased the size of the condensates.

It has been proposed that the spontaneous formation of a nucleation loop along the length of a strand of DNA is necessary to initiate condensation into toroidal structures (3). Since the persistence length of DNA plays a role in determining the loop size, it is expected that variations in the persistence length may affect the size of toroidal condensates. As described in Chapter 2, the nucleation loop size is directly correlated to the toroid diameter and inner diameter. If the size of the nucleation loop were to decrease based on decreased persistence length, we would expect that the size of the toroids would also decrease. The results of this study indicated that the toroids produced at 4 and 38°C were smaller in dimensions than those produced at 22°C, which supports the conclusion that persistence length decreases around these temperatures (1, 2, 4). Decreased persistence length should allow for the favorable formation of smaller nucleation loops which would yield results similar to those observed when DNA containing static nucleation loops was condensed into small toroidal condensates (Chapter 2). The increased thickness observed at 22°C is most likely a result of the increased counterion concentration in the solution.

These results provide evidence that decreasing the persistence length of DNA by altering the temperature of the reaction may allow for the formation of smaller condensates. Further investigations are necessary to determine if this temperature effect is only the result of decreased persistence length of the DNA or if other factors (i.e., ionic

strength) are also influencing the toroid diameter and thickness of these condensates. It is necessary to also consider that successful nucleation and ion interactions with DNA will vary at increasing and decreasing temperatures.

7.2 DNA Topology Influences Condensate Size and Morphology

The topology of plasmid DNA has been reported to influence the morphology of DNA condensates. Supercoiled DNA has more topological constraints as compared to linear and relaxed circular DNA, due to the writhe of the DNA (5, 6). Böttcher and colleagues reported that relaxed circle DNA condensed with spermine formed better toroidal structures than supercoiled and linear DNA. We performed a similar study on the three topologies of plasmid DNA by condensing it in the presence of hexamine cobalt chloride to determine which form of DNA produced *optimal* condensate structures. These studies were performed to further investigate the effects of topological constraints on DNA condensation and also to investigate factors that lead to the production of *optimal* condensates (i.e., small, single, well defined particles).

7.2.1 Experimental Procedures

DNA Preparation: Bluescript II SK- plasmid DNA (Stratagene) was grown in the *E. coli* cell line, DH5 α (Life Technologies) and isolated using the Qiagen Maxi Prep kit. The DNA was isolated in 1 \times TE (10 mM Tris, 1 mM EDTA, pH 7.8). The topology of the DNA was examined by agarose gel electrophoresis and it was determined that greater than 90% of the DNA in the isolation was in the supercoiled topology. Linear DNA was prepared by digestion with the restriction endonuclease HindIII (NEB). Relaxed circular DNA was prepared by digestion with the DNase, DNaseI. This DNase completely

degrades DNA at the recommended concentrations, however it was demonstrated that at reduced concentrations, the enzyme introduced multiple single-stranded nicks into the DNA but did not degrade it. Several 10-fold serial dilutions of the enzyme were performed to optimize the relaxing of the DNA and a dilution of 1:1000 was found to be the optimal DNaseI concentration to produce relaxed DNA without degradation. The DNA was allowed to digest with the diluted DNaseI for 15 minutes at room temperature and the nuclease was degraded by heating to 65°C for 10 minutes in the presence of 1 mM EDTA. The linearization and relaxation were verified by gel electrophoresis. Each preparation was estimated from the gel to be at greater than 90% in the specific topology. The digested DNA samples were cleaned by rinsing through the Microcon YM-30 with 0.25× TE at least 5 times to ensure that all residual salts from the digestion were removed. All DNA concentrations were diluted to 20 µg/ml in 0.25× TE. Concentrations were verified spectrophotometrically at A_{260} . The buffer concentration was then brought to 1× TE by the addition of a small volume of concentrated TE. The final DNA concentration was ~18 µg/ml in 1× TE.

DNA Condensation. DNA was mixed with 200 µM hexamine cobalt chloride and allowed to condense for 5 minutes in an Eppendorf tube. Several microliters of the sample was then applied to a carbon coated grid (Ted Pella) and allowed to settle for 10 minutes. The grid was stained with 2% uranyl acetate momentarily then rinsed with 95% ethanol and airdried.

The grids were imaged on a JEOL-100C electron microscope at 100,000×. The TEM negatives were scanned at 300 pixels/inch and Canvas graphics program was used

to measure the outer diameter and thickness of individual DNA toroids. No statistical measurements were performed on these samples.

7.2.2 Results and Discussion

Three topologies of Bluescript plasmid DNA (*3kbDNA*) were condensed with hexamine cobalt chloride. Linearized *3kbDNA* condensed into toroidal structures as shown in Figure 7.3A. The condensates were primarily toroidal in morphology with occasional rod structures. The toroid diameter and thickness of these condensates is on average much larger in this data set than in most showing linear *3kbDNA*, as a result of increased salt in the linear DNA stock solution (discussed above).

Relaxed circle DNA condensed into predominantly toroidal particles, with occasional rod structures. Condensation of the plasmid DNA in this topology did not result in *optimal* particle formation as the condensate size and morphology are strikingly similar to those formed by linearized plasmid as shown in Chapters 2, 3, and 6 (Figure 7.2B). Therefore, this data does not support the conclusions by Böttcher and colleagues, which suggested relaxed circle plasmid DNA produced toroidal condensates that were superior to those formed by linear and supercoiled DNA. The differences between the linear and relaxed circle DNA topology does not seem to significantly affect the condensation of the DNA into toroidal condensates.

Supercoiled DNA condensed with hexamine cobalt chloride, unlike linear and relaxed *3kbDNA*, did not form primarily toroidal structures. In these reactions, the condensates were predominantly rod structures, with a few toroids throughout the sample (Figure 7.3C). The increased propensity for supercoiled DNA to form rods was discussed in Chapter 6, where a study with similar results was described. Briefly, it has been

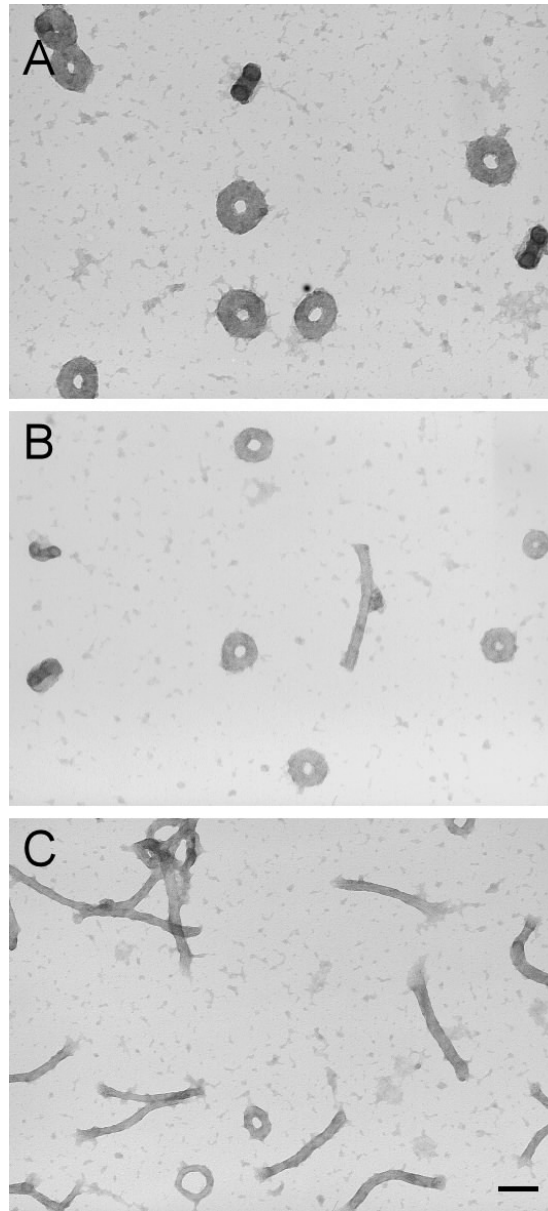


Figure 7.3. TEM images of linear, relaxed circle and supercoiled *3kbDNA* condensed with hexamine cobalt chloride. (A) Toroids formed by the condensation of linear *3kbDNA*. (B) Toroids formed by the condensation of relaxed circular *3kbDNA*. (C) Rods and toroids formed by the condensation of supercoiled *3kbDNA*. The final concentrations in solution are 10 $\mu\text{g/ml}$ DNA and 100 μM hexamine cobalt chloride. The scale bar is 100 nm.

suggested that the increased topological constraints in the supercoiled DNA favors the kinking of the DNA to form rods rather than the constant bending to form the loops within the toroidal structures.

7.3 Condensation of Mixtures of DNA With and Without Static Curvature

Condensation of DNA containing static curvature (i.e., loops) favors the production of toroidal structures smaller in diameter than those formed by plasmid DNA without the static curvature as discussed in Chapter 2 and Chapter 6. It was proposed that the static loops act as nucleation sites, making proto-toroid formation and toroid growth more favorable by eliminating the need for the spontaneous formation of a nucleation loop (3, 7). We have hypothesized that by mixing the DNA containing the static loop structures with plasmid DNA, smaller toroids will be produced upon condensation with hexamine cobalt chloride.

7.3.1 Experimental Procedures

DNA Preparations. Bluescript II SK- plasmid DNA (Stratagene) was grown in DH5a (Life Technologies) and isolated using the Qiagen Maxi Prep kit. The DNA was eluted in 1× TE (10 mM Tris, pH 7.8, 1 mM EDTA) and linearized by digestion with the restriction enzyme Hind III (New England Biolabs). Buffer and salts introduced for the restriction digest reaction were removed by rinsing the DNA at least five times with 0.25× TE using a Microcon YM-30 spin column (Millipore). Between rinses and before elution, the buffer was mixed by pipetting on the column. After the final rinse, DNA was resuspended from the spin column membrane to a final concentration of 20 µg/ml in

0.25× TE. DNA concentrations were verified spectrophotometrically. A modified Bluescript II SK- containing extensive sequence-directed curvature was also used in this study. This plasmid contains two tandem repeats of the following A-tract sequence: 5'-ATCCATCGACC(AAAAAACGGGCAAAAAACGGC)₇AAAAAAGCAGTGGAAG-3'. This plasmid (*Atract30*) was grown in Sure2 Supercompetent cells (Stratagene), then isolated and prepared as described above.

DNA Condensate Preparation and Imaging. DNA condensates were prepared by mixing a DNA sample solution with an equal volume of a hexamine cobalt chloride (Sigma) solution to yield a condensation reaction mixture 10 µg/ml in DNA, 100 µM in hexamine cobalt chloride and 0.5× in the salt/buffer of the DNA sample. Three reaction conditions were prepared: 2:1, 1:1 and 1:2 *Atract30*: *3kbDNA*. Condensate reaction mixtures were allowed to equilibrate for 5 minutes and then deposited on carbon-coated grids (Ted Pella). After 10 minutes on the grids, 2% uranyl acetate (Ted Pella) was added momentarily to the condensate mixtures, the grids were then rinsed in 95% ethanol and air-dried. The DNA condensates were recorded on film using a JEOL-100C transmission electron microscope (TEM) at 100,000× magnification. The TEM negatives were scanned at 300 pixels/inch and Canvas graphics program was used to measure the outer diameter and thickness of individual DNA toroids. The lines representing the toroid diameters and thicknesses were copied to a new Canvas file and saved in .eps format. This file was read using the “*Read Coordinates*” program written by Nick Hud, which allowed the data to be opened and analyzed in Microsoft Excel.

7.3.2 Results and Discussion

Condensation of the DNA mixtures resulted in the formation of toroidal condensates under all reaction conditions. The 2:1 *Atract30: 3kbDNA* and 1:2 *Atract30: 3kbDNA* condensates will be discussed, as the grid of the 1:1 preparation was not representative of the data set. (The reactions conditions were only examined once, not multiple times to acquire a representative sampling of the various conditions). Toroids produced by the 2:1 and 1:2 *Atract30: 3kbDNA* samples looked very similar by TEM analysis, however statistical examination of the toroid outer diameters and thicknesses revealed a difference between the preparations (Figure 7.4). Toroids formed with a 2:1 *Atract30: 3kbDNA* ratio had a mean outer diameter of 66 nm (n = 39), while toroids formed by 1:2 *Atract30: 3kbDNA* had a mean outer diameter of 75 nm (n = 44). The mean outer diameter of the toroids formed by the 2:1 mixture of DNA is very similar to that of toroids formed by *Atract60 (3kbDNA* containing 4 phased A-tract repeats, Chapter 2). The increased number of static nucleation loops in the reaction (i.e., increased [*Atract30*]) will allow for faster toroid formation than in preparations with lower concentrations of *Atract30* or with *3kbDNA* alone since spontaneous nucleation loop formation is the rate limiting step in toroid formation (3).

These results suggest that the presence of pre-formed nucleation structures in a solution linear DNA can influence the diameter of the toroidal structures. It should also be noted that toroids from both the 2:1 and 1:2 mixtures of *Atract30: 3kbDNA* had mean thicknesses of 25 nm, which further supports the conclusion in Chapter 2 that toroid thickness is independent of toroid diameter (and nucleation loop size) under these conditions. While it is interesting that a decrease in toroid size is observed at a 2:1 ratio of *Atract30: 3kbDNA*, the effects of the static loops in solution with linear plasmid DNA

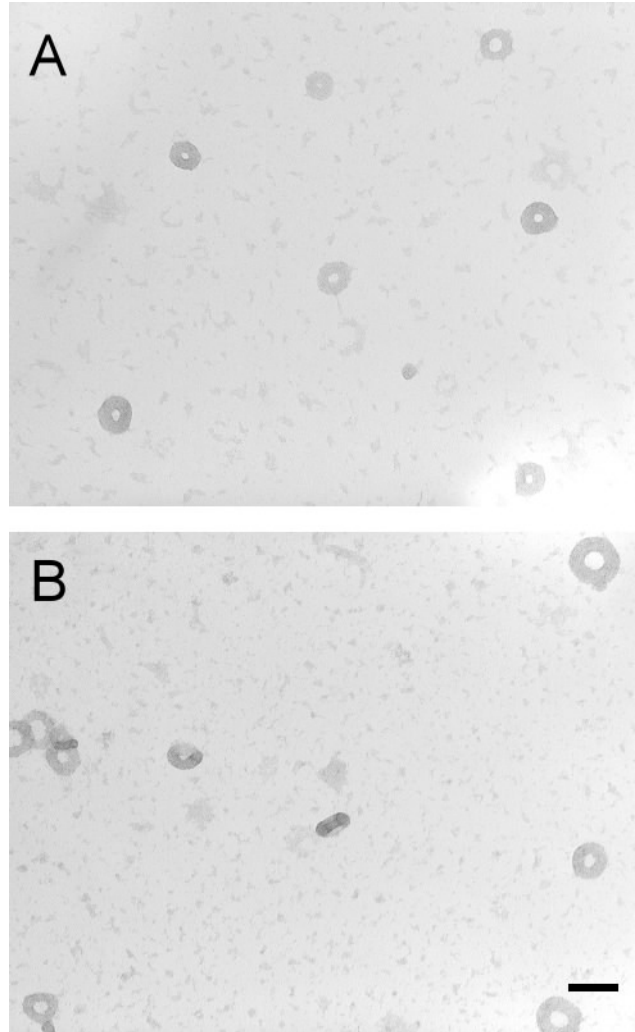


Figure 7.4. TEM images of *Atract30*: *3kbDNA* mixtures condensed with hexamine cobalt chloride. (A) Toroidal condensates produced by a mixture of 2:1 *Atract30*: *3kbDNA*. (B) Toroidal condensates produced by a mixture of 1:2 *Atract30*: *3kbDNA*. Final concentrations are 10 $\mu\text{g/ml}$ DNA and 100 μM hexamine cobalt chloride. Scale bar is 100 nm.

should also be explored. To further explore this effect, *Atract30* or *Atract60* DNA may be digested at various points along the length of DNA to isolate several lengths of DNA containing the A-tract repeats. By doing this, it is possible to observe the A-tract effects while considering the effect of shortening the overall length of DNA attached to the loops.

7.4 Condensation of Fragmented Plasmid DNA

Early studies of DNA condensation found that DNA under 400 bp in length did not condense into toroidal structures (5, 8). At this length of DNA it is difficult to bend over a constant radius of curvature without encountering limitations by the persistence length of DNA. Additionally, since the DNA is short in length, it would be unable to wrap around a loop more than one time to make the DNA-DNA contacts necessary for stable proto-toroid formation. Increasing the length of the DNA to greater than 500 bp would increase the probability of loop formation; however, the length of the DNA would still make the formation of multiple intrastrand loops difficult. Although the shortened length of DNA may hinder toroid formation, these lengths of DNA may be able to easily attach to toroidal structures initiated and stabilized by longer DNA sequences. To investigate the potential effect of mixing short DNA with longer sequences, *3kbDNA* was double digested in two reactions to get a variety of DNA fragment sizes. These fragments were condensed alone, and then with the intact plasmid DNA to see the effect on condensate formation.

7.4.1 Experimental Procedures

DNA Preparation. Bluescript SK II- was grown in DH5 α cells and isolated using the Qiagen Maxi Prep kit as described above. The DNA was digested with two enzymes to form 3 fragments. The first digest performed sequentially using the restriction endonuclease DrdI and then ScaI. This digest produced fragments of 1271, 980 and 710 bp. A second double digest was performed with the restriction endonucleases PvuII and ScaI yielding fragments of 1549, 964 and 448 bp in length. Excess salts and buffer from the digestion were removed from the reaction by rinsing the DNA through a Microcon YM-30 five times with 1 \times TE (10 mM Tris, 1 mM EDTA, pH 7.8). The DNA concentration of 20 μ g/ml was verified spectrophotometrically at A₂₆₀. Digests were verified by agarose gel electrophoresis.

DNA Condensate Preparation and Imaging. The digested DNA was condensed with 200 μ M hexamine cobalt chloride and allowed to react for 5 minutes. Several microliters were placed on a carbon coated grid (Ted Pella) and allowed to settle for 10 minutes before staining with 2% uranyl acetate. The grids were rinsed with 95% ethanol and air-dried. Several condensate mixtures were examined: DrdI/ScaI *3kbDNA*, PvuII/ScaI *3kbDNA*, DrdI/ScaI *3kbDNA*+ intact *3kbDNA* (1:1 in concentration), and DrdI/ScaI *3kbDNA* + intact *Atract30* (1:1 in concentration).

The condensates were imaged on a JEOL-100C transmission electron microscope. All grids were imaged at a magnification of 100,000 \times . The ratio of rods to toroids was quantified for the samples containing the DrdI/ScaI *3kbDNA*. The data shown here was not examined in multiple preparations.

7.4.2 Results and Discussion

The condensates produced when the *3kbDNA* was digested with *DrdI/ScaI* were of mixed morphology. Approximately 35% of the condensates were in rods, which is a significant increase from less than 10% rods observed in the linear *3kbDNA* discussed in Chapter 6. When the digested DNA was mixed with intact *3kbDNA* and then condensed, the rod to toroid ratio did not change significantly. Although little variation was observed when the fragments were condensed with intact *3kbDNA*, mixing *Atract30* with the DNA fragments resulted in the formation of primarily toroidal structures (i.e., less than 10% rods).

This data suggests that DNA fragments of 1271, 980, and 710 have an increased propensity to nucleate rod structures. Kinking of the DNA to nucleate a condensate may be preferred in the shorter DNA fragments over bending into loop structures. The observation that this rod to toroid ratio only slightly decreased in the presence of intact *3kbDNA* suggests that the nucleation of rods is faster than the nucleation of stable toroids. This result was unexpected as spontaneous nucleation loop formation is expected to occur frequently in *3kbDNA*, so it was hypothesized that the presence of intact *3kbDNA* mixed with the fragments would increase the successful formation of toroids. The presence of static nucleation loops in the *Atract30* had an obvious effect on the morphology of the condensates. Since it was not necessary to spontaneously form a nucleation site, it is likely that many of the fragments attached to stable proto-toroid structures formed by *Atract30*. This is supported by the decrease in the rod population when the *3kbDNA* fragments mixed with *Atract30* and condensed.

The fragment size was varied by the double-digestion of *3kbDNA* with *PvuII/ScaI*. The resulting condensates were predominantly toroids and were similar in

size to those observed in the studies of *DrdI/ScaI* digested *3kbDNA*. The increase in toroidal condensates as compared to the *DrdI/ScaI* fragments described above may be attributed to several factors. If the 1549 bp fragment was spontaneously nucleating loop structures, it is possible that the other fragments would attach to the stable proto-toroid structure and allow those structures to grow. There is a high probability that the 448 bp fragment did not condense on its own into toroids or into rods as a result of the short length of the DNA, but is likely that it could attach to a structure nucleated by the other fragments. Although these results imply that rod formation is reduced under these conditions, it is necessary to repeat this experiment before analyzing the results further, since these results are dissimilar from the results of the *DrdI/ScaI* fragments. It is possible that the DNA fragments studied in this preparation were only single digested by *PvuII* due to a mix up in the sample, which would most likely favor toroid formation by the 2513 bp fragment.

References

1. Lu, Y., Weers, B., and Stellwagen, N. C. (2002) *Biopolymers* 61, 261-275.
2. Porschke, D. (1986) *Journal of Biomolecular Structure and Dynamics* 4, 373-389.
3. Hud, N. V., Downing, K. H., and Balhorn, R. (1995) *Proceedings of the National Academy of Sciences of the United States of America* 92, 3581-3585.
4. Schurr, J. M., and Schmitz, K. M. (1986) *Annual Review of Physical Chemistry* 37, 271-305.
5. Bloomfield, V. A. (1991) *Biopolymers* 31, 1471-1481.
6. Bloomfield, V. (1997) *Biopolymers* 44, 269-282.
7. Shen, M., Downing, K., Balhorn, R., and Hud, N. (2000) *Journal of the American Chemical Society* 122, 4833-4834.
8. Widom, J., and Baldwin, R. L. (1980) *J. Mol. Biol.* 144, 431-453.

CHAPTER 8

IMPLICATIONS OF DNA CONDENSATION ON THE DEVELOPMENT OF GENE DELIVERY SYSTEMS

Gene therapy holds great promise for the treatment of genetic and acquired diseases and as a means to vaccinate against viral and bacterial pathogens. However, gene delivery remains as a bottleneck in the development of genetic medicines. Gene therapy techniques can be divided into viral or nonviral delivery systems. The development of nonviral delivery systems is the focus of much current research because unlike viral delivery systems, nonviral delivery systems can be designed not to elicit a strong and potentially harmful immune response. A current limitation of nonviral delivery systems is the decreased transgene expression as compared to viral methods. This decreased efficiency can be attributed to one or several of the following factors: instability of the complex containing DNA and the delivery agent, poor uptake by the cell, inability to release DNA from the endosome into the cytoplasm, degradation of the DNA, and inefficient penetration of the nucleus, among others. Efforts to overcome these barriers to nonviral gene delivery have led to the incremental improvements of established systems, as well as the proposal of completely new approaches to delivery.

The condensation of DNA into compact particles is essential to optimizing the uptake of DNA into the cell by endocytosis. The efficiency of cellular uptake and transgene expression is increased significantly for condensates less than 100 nm in diameter. Thus, it is of interest to create condensates that are single, well-defined

particles of less than 100 nm in diameter. By understanding the factors that govern the size and morphology of DNA condensates, it is possible to optimize the particle size, thereby increasing the efficiency of vector uptake and gene expression.

This dissertation has provided evidence that the size of DNA condensates can be controlled by temperature, ionic strength, static curvature and by increasing the flexibility of the DNA. Furthermore, small variations in the conditions of condensation can lead to dramatic changes in the size, morphology and degree of aggregation of the particles. In these studies, the smallest single double-stranded DNA condensates resulted from the compaction of DNA containing static curvature. By introducing phased A-tract repeats onto a sequence of interest, it should be possible to collapse the DNA, regardless of the length, into compact particles. The condensation of plasmid DNA containing A-tract curvature also provided a tight distribution of toroid sizes, leading to a population of small, well-defined condensates. Single-stranded DNA produced primarily unimolecular condensates; however, it is unclear how efficiently ssDNA would be expressed in the cell.

The condensation solution conditions also may alter the size of the condensates substantially. Optimizing the ionic strength of the solution is crucial to producing small single particles. If DNA is condensed in dH₂O or MgCl₂, the condensates have an increased propensity to aggregate. While it is necessary to have some buffer present (~10 mM in ionic strength), increasing the ionic strength much beyond this concentration leads to larger condensates, and eventually reaches a point where condensation into discrete particles does not occur. Thus, condensing DNA in serum or under physiological conditions (> 150 mM ionic strength) would not be likely to produce small, well-defined

particles. Condensation of DNA under *low salt* conditions (~ 10 mM) would be optimal for producing small condensates. Additionally, performing the reaction at 4°C may also decrease the size of the condensates further.

While these variations in condensation conditions are effective in condensing DNA *in vitro*, the effects of condensation *in vivo* or the environment of delivery can not be inferred from these results. The systems described here are not salt stable, so it is necessary to find a non-toxic cationic polymer to condense the DNA that does not dissociate from the DNA at high salt concentrations in solution. A possible alternative condensing agent is a naturally occurring condensing agent such as protamine.

This study has provided a large quantity of experimental data on the factors that govern DNA size and morphology *in vitro* and have made major contributions to understanding and optimizing DNA condensation. The conclusions resulting from these investigations will be valuable in determining conditions for DNA condensation and encapsulation for gene delivery.

Vita

Christine Carole Conwell was born in Pittsburgh, Pennsylvania on August 12, 1977. She attended East Allegheny Jr./Sr. Highschool in North Versailles, Pennsylvania and graduated in the top of her class in June of 1995. From there, she enrolled at Westminster College in New Wilmington, Pennsylvania. She graduated in May of 1999 with Bachelor of Science degree in both Chemistry and Molecular Biology. Christine pursued her graduate studies in the School of Chemistry and Biochemistry at Georgia Institute of Technology in Atlanta, Georgia.